

**CATALYTIC HYDROGENATION OF AN AROMATIC SULFONYL
CHLORIDE INTO THIOPHENOL**

A Dissertation

by

NICOLAS JULIEN ROUCKOUT

Submitted to the Office of Graduate Studies of
Texas A&M University
in partial fulfillment of the requirements for the degree of

DOCTOR OF PHILOSOPHY

May 2008

Major Subject: Chemical Engineering

**CATALYTIC HYDROGENATION OF AN AROMATIC SULFONYL
CHLORIDE INTO THIOPHENOL**

A Dissertation

by

NICOLAS JULIEN ROUCKOUT

Submitted to the Office of Graduate Studies of
Texas A&M University
in partial fulfillment of the requirements for the degree of

DOCTOR OF PHILOSOPHY

Approved by:

Co-Chairs of Committee,	Rayford G. Anthony
	Gilbert F. Froment
Committee Members,	Marcetta Y. Darensbourg
	Daniel F. Shantz
Head of Department,	Michael V. Pishko

May 2008

Major Subject: Chemical Engineering

ABSTRACT

Catalytic Hydrogenation of an Aromatic Sulfonyl Chloride
into Thiophenol. (May 2008)

Nicolas Julien Rouckout, B.S., Universite Pierre et Marie Curie, Paris VI;

M.S., Universite Pierre et Marie Curie, Paris VI

Co-Chairs of Advisory Committee: Dr. Rayford G. Anthony
Dr. Gilbert F. Froment

The catalytic hydrogenation of an aromatic sulfonyl chloride was investigated in continuous and semi-batch mode processes using a Robinson-Mahoney stationary basket reactor. A complete experimental unit was designed and built. The operating and analytical procedures have been developed and the methodologies to gather the kinetic data have been described. Hydrogenation reactions were conducted at a reaction pressure of 364.7 psia, at three different reaction temperatures: 85 °C, 97 °C and 110 °C, at five different residence times: 0.6 (only at 110 °C), 1.0, 1.5, 2.0, 3.1 hr, with the hydrogen to the aromatic sulfonyl chloride molar ratio: 8.0 mol/mol and hydrogen to argon molar ratio: 3.0 mol/mol. Intrinsic reaction rates of the reacting species were obtained on the surface of a commercial 1 wt% palladium on charcoal catalyst.

The conversion and molar yield profiles of the reacting species with respect to process time suggest a deactivation of the 1 wt % palladium on charcoal catalyst. Kinetic data collected in a continuous process mode show that the catalyst is deactivated during an experiment when the process time equal to two to three times the residence time of the liquid within the reactor. XRD analysis shows that the active sites are blocked and an amorphous layer was formed on the surface of the palladium catalyst. Semi-Batch mode experimental data were obtained at 110 °C after 8 hours of reaction time for several aromatic sulfonyl chlorides.

A kinetic model has been developed, which includes adsorption of individual components and surface reactions as well as rate equations of the Hougen-Watson type. A hyperbolic deactivation function expressed in term of process time is implemented in the Hougen-Watson equation rates. The mathematical model consists of non-linear and simultaneous differential equations with multiple variables. The kinetic parameters were estimated from the minimization of a multi-response objective function by means of a sequential quadratic program, which includes a quasi-Newton algorithm. The statistical analysis was based on the t- and F-tests and the simulated results were compared to the experimental data.

DEDICATION

Dedicated to

Odette Rouckout and Jeanne Slezak

Daniele and Dany Rouckout

Sandrine Caillaud and Thomas Rouckout

Elaine Suerte

ACKNOWLEDGEMENTS

I would like to thank my committee chairs, Dr. Rayford G. Anthony and Dr. Gilbert F. Froment, for their guidance and support throughout the course of this research. I am also grateful to my committee members, Dr. Marcetta Y. Darensbourg and Dr. Daniel F. Shantz, for their suggestions and assistance.

Thanks also to my friends, the Galindo family, colleagues and the department faculty and staff for making my time at Texas A&M University a great experience. I also want to extend my gratitude to DuPont, which provided the financial support for this research.

I would like to express my deepest gratitude to my parents and my brother, Thomas, for their trust, constant help and support throughout my studies in France and in Texas.

TABLE OF CONTENTS

	Page
ABSTRACT	iii
DEDICATION	v
ACKNOWLEDGEMENTS	vi
TABLE OF CONTENTS	vii
LIST OF FIGURES	ix
LIST OF TABLES	xix
 CHAPTER	
I INTRODUCTION.....	1
II LITERATURE REVIEW.....	4
2.1 Reduction Methods	4
2.2 Mass Transfer Resistances in Catalytic Hydrogenation Reactions	7
2.3 Catalytic Gradientless Reactor	18
2.4 Material Selection	19
2.5 Chemistry of the Catalytic Hydrogenation of 2,5-Dimethylbenzene Sulfonyl Chloride.....	22
2.6 Catalyst Deactivation	28
III DESCRIPTION OF THE EXPERIMENTAL UNIT.....	32
3.1 Experimental Unit	32
3.2 Experimental Procedure and Gathering of Kinetic Data.....	43
3.2.1 Continuous Mode	43
3.2.2 Semi-batch Mode	46
3.3 Analytical Procedure	48
3.3.1 On-line Gas Analysis	48

CHAPTER	Page
3.3.2 Off-line Liquid Analysis	49
3.4 Calculation Methods	53
3.4.1 Liquid Phase	53
3.4.2 Gas Phase	63
IV EXPERIMENTAL RESULTS	69
4.1 Hydrogenation of Toluene	69
4.2 Catalytic Hydrogenation of 2,5-Dimethylbenzene Sulfonyl Chloride into Thiophenol in Continuous Process Mode	73
4.3 Catalytic Hydrogenation of Several Aromatic Sulfonyl Chlorides in Semi-batch Mode Reaction	94
V KINETIC MODELING AND PARAMETER ESTIMATION	97
5.1 Introduction	97
5.2 Catalyst Deactivation	99
5.3 Formulation of the Kinetic Model for the Catalytic Hydrogenation of an Aromatic Sulfonyl Chloride	101
5.4 Continuity Equations and Initial Conditions for the Reacting Species	111
5.5 Parameter Estimation Technique and Statistical Analysis	113
5.6 Results and Discussion	120
5.6.1 Parameter Estimation per Process Temperature	120
5.6.2 Comparison Between Experimental and Calculated Values	128
VI CONCLUSION AND RECOMMENDATION	155
NOMENCLATURE	157
LITERATURE CITED	163
APPENDIX A	171
VITA	174

LIST OF FIGURES

FIGURE	Page
2.1 Yields of the products of the conversion of toluene 1) into methylcyclohexane 2) and cyclohexane 3)	6
2.2 Estimated solubility of hydrogen in toluene	7
2.3 Concentration profile of hydrogen in a three-phase reactor	8
2.4 Hydrogenation sequence for the aromatic sulfonyl chloride.....	22
2.5 Tautomer forms for the aromatic sulfenic acid	23
2.6 Intermolecular hydrogen bonding in the formation of thiosulfinate	25
2.7 Disproportionation of thiosulfinate	25
2.8 Dehydrative disproportionation mechanism of the aromatic sulfinic acid proposed by J.L Kice.....	26
2.9 Temperature-composition PdS phase diagram.....	30
3.1 Robinson-Mahoney stationary basket reactor design. Property of, and used with the permission of Snap-Tite, Inc	33
3.2 Flow pattern of the fluid around the basket within the reactor. Property of, and used with the permission of Snap-Tite, Inc	35
3.3 Simplified flow diagram of the hydrogenation unit in continuous mode ..	36
3.4 Detailed flow diagram of the hydrogenation unit in continuous mode.....	37
3.5 Simplified flow diagram of the hydrogenation unit in semi-batch mode ..	38
3.6 Design of the gas-liquid cyclonic separator	41
3.7 Overall hydrogenation reaction of the aromatic sulfonyl chloride.....	53

FIGURE	Page
3.8 Reaction scheme of the catalytic hydrogenation of the aromatic sulfonyl chloride.....	53
3.9 Reaction scheme of the dehydration of the aromatic sulfinic acid	54
3.10 Material balance applied to the liquid collector	58
4.1 Thermodynamic equilibrium between toluene and methylcyclohexane in the presence of hydrogen.....	69
4.2 Hydrogen outlet molar flow rate during the hydrogenation of toluene. T = 110 °C, P = 364.7 psia and liquid residence time of 0.62 hr	72
4.3 Overall conversion of the aromatic sulfonyl chloride (SC) X with respect to process time at residence times θ : 1.0, 1.5, 2.0 and 3.1 hr, process temperature: 85 °C, process pressure: 364.7 psia, $F_{H_2}^0 / F_{sulfonyl}^0 = 8.0 \text{ mol/mol}$, $F_{H_2}^0 / F_{Ar}^0 = 3.0 \text{ mol/mol}$	74
4.4 Overall conversion of hydrogen XH ₂ with respect to process time at residence times θ : 1.0, 1.5, 2.0 and 3.1 hr, process temperature: 85 °C, process pressure: 364.7 psia, $F_{H_2}^0 / F_{sulfonyl}^0 = 8.0 \text{ mol/mol}$, $F_{H_2}^0 / F_{Ar}^0 = 3.0 \text{ mol/mol}$	75
4.5 Molar yield of the aromatic disulfide (DS) Y ₁ from the aromatic sulfonyl chloride (SC) with respect to process time at residence times θ : 1.0, 1.5, 2.0 and 3.1 hr, process temperature: 85 °C, process pressure: 364.7 psia, $F_{H_2}^0 / F_{sulfonyl}^0 = 8.0 \text{ mol/mol}$, $F_{H_2}^0 / F_{Ar}^0 = 3.0 \text{ mol/mol}$	76

FIGURE

Page

- 4.6 Molar yield of the aromatic thiol (THIOL) Y_2 from the aromatic sulfonyl chloride (SC) with respect to process time at residence times θ : 1.0, 1.5, 2.0 and 3.1 hr, process temperature: 85 °C, process pressure: 364.7 psia, $F_{H_2}^0 / F_{sulfonyl}^0 = 8.0 \text{ mol/mol}$,
 $F_{H_2}^0 / F_{Ar}^0 = 3.0 \text{ mol/mol}$ 77
- 4.7 Molar yield of the aromatic thiosulfone (TS) Y_3 from the aromatic sulfonyl chloride (SC) with respect to process time at residence times θ : 1.0, 1.5, 2.0 and 3.1 hr, process temperature: 85 °C, process pressure: 364.7 psia,
 $F_{H_2}^0 / F_{sulfonyl}^0 = 8.0 \text{ mol/mol}$, $F_{H_2}^0 / F_{Ar}^0 = 3.0 \text{ mol/mol}$ 78
- 4.8 Overall conversion of the aromatic sulfonyl chloride (SC) X with respect to process time at residence times θ : 1.0, 1.5, 2.0 and 3.1 hr, process temperature: 97 °C, process pressure: 364.7 psia,
 $F_{H_2}^0 / F_{sulfonyl}^0 = 8.0 \text{ mol/mol}$, $F_{H_2}^0 / F_{Ar}^0 = 3.0 \text{ mol/mol}$ 79
- 4.9 Overall conversion of hydrogen XH_2 with respect to process time at residence times θ : 1.0, 1.5, 2.0 and 3.1 hr, process temperature: 97 °C, process pressure: 364.7 psia,
 $F_{H_2}^0 / F_{sulfonyl}^0 = 8.0 \text{ mol/mol}$, $F_{H_2}^0 / F_{Ar}^0 = 3.0 \text{ mol/mol}$ 80
- 4.10 Molar yield of the aromatic disulfide (DS) Y_1 from the aromatic sulfonyl chloride (SC) with respect to process time at residence times θ : 1.0, 1.5, 2.0 and 3.1 hr, process temperature: 97 °C, process pressure: 364.7 psia,
 $F_{H_2}^0 / F_{sulfonyl}^0 = 8.0 \text{ mol/mol}$, $F_{H_2}^0 / F_{Ar}^0 = 3.0 \text{ mol/mol}$ 81

FIGURE

Page

- 4.11 Molar yield of the aromatic thiol (THIOL) Y_2 from the aromatic sulfonyl chloride (SC) with respect to process time at residence times θ : 1.0, 1.5, 2.0 and 3.1 hr, process temperature: 97 °C, process pressure: 364.7 psia,
 $F_{H_2}^0 / F_{sulfonyl}^0 = 8.0 \text{ mol/mol}$, $F_{H_2}^0 / F_{Ar}^0 = 3.0 \text{ mol/mol}$ 82
- 4.12 Molar yield of the aromatic thiosulfone (TS) Y_3 from the aromatic sulfonyl chloride (SC) with respect to process time at residence times θ : 1.0, 1.5, 2.0 and 3.1 hr, process temperature: 97 °C, process pressure: 364.7 psia,
 $F_{H_2}^0 / F_{sulfonyl}^0 = 8.0 \text{ mol/mol}$, $F_{H_2}^0 / F_{Ar}^0 = 3.0 \text{ mol/mol}$ 83
- 4.13 Overall conversion of the aromatic sulfonyl chloride (SC) X with respect to process time at residence times θ : 0.6, 1.0, 1.5, 2.0 and 3.1 hr, process temperature: 110 °C, process pressure: 364.7 psia, $F_{H_2}^0 / F_{sulfonyl}^0 = 8.0 \text{ mol/mol}$,
 $F_{H_2}^0 / F_{Ar}^0 = 3.0 \text{ mol/mol}$ 84
- 4.14 Overall conversion of hydrogen XH_2 with respect to process time at residence times θ : 0.6, 1.0, 1.5, 2.0 and 3.1 hr, process temperature: 110 °C, process pressure: 364.7 psia,
 $F_{H_2}^0 / F_{sulfonyl}^0 = 8.0 \text{ mol/mol}$, $F_{H_2}^0 / F_{Ar}^0 = 3.0 \text{ mol/mol}$ 85
- 4.15 Molar yield of the aromatic disulfide (DS) Y_1 from the aromatic sulfonyl chloride (SC) with respect to process time at residence times θ : 0.6, 1.0, 1.5, 2.0 and 3.1 hr, process temperature: 110 °C, process pressure: 364.7 psia,
 $F_{H_2}^0 / F_{sulfonyl}^0 = 8.0 \text{ mol/mol}$, $F_{H_2}^0 / F_{Ar}^0 = 3.0 \text{ mol/mol}$ 86

FIGURE	Page
4.16 Molar yield of the aromatic thiol (THIOL) Y_2 from the aromatic sulfonyl chloride (SC) with respect to process time at residence times θ : 0.6, 1.0, 1.5, 2.0 and 3.1 hr, process temperature: 110 °C, process pressure: 364.7 psia, $F_{H_2}^0 / F_{sulfonyl}^0 = 8.0 \text{ mol/mol}$, $F_{H_2}^0 / F_{Ar}^0 = 3.0 \text{ mol/mol}$	87
4.17 Molar yield of the aromatic thiosulfone (TS) Y_3 from the aromatic sulfonyl chloride (SC) with respect to process time at residence times θ : 0.6, 1.0, 1.5, 2.0 and 3.1 hr, process temperature: 110 °C, process pressure: 364.7 psia, $F_{H_2}^0 / F_{sulfonyl}^0 = 8.0 \text{ mol/mol}$, $F_{H_2}^0 / F_{Ar}^0 = 3.0 \text{ mol/mol}$	88
4.18 Saturated solubility of water in pure toluene at different temperatures	89
4.19 Formation of the poison from an adsorbed aromatic sulfonyl chloride and a free metal active site L on the surface of the catalyst.....	92
4.20 XRD analysis of the fresh 1 wt % palladium on charcoal catalyst	93
4.21 XRD analysis of the spent catalyst for the experiment conducted at 110 °C and 1-hour residence time	93
5.1 Steps involved in reactions on a solid catalyst.....	97
5.2 Reaction scheme proposed for the hydrogenation of 2,5-dimethylbenzene sulfonyl chloride	102
5.3 Adsorption of the aromatic sulfonyl chloride and molecular hydrogen on a metal active site L with the corresponding adsorption equilibrium constants	105
5.4 Catalytic rate-determining surface reactions between adsorbed reacting species and molecular adsorbed hydrogen	105
5.5 Desorption of the reacting species from the metal active site L	106

FIGURE

Page

- 5.6 Comparison of simulated and experimental concentration profiles of the aromatic sulfonyl chloride (SC) with respect to process time at residence time θ : 1.0 hr, process temperature: 85 °C, process pressure: 364.7 psia, $F_{H_2}^0 / F_{sulfonyl}^0 = 8.0 \text{ mol/mol}$,
 $F_{H_2}^0 / F_{Ar}^0 = 3.0 \text{ mol/mol}$ 128
- 5.7 Comparison of simulated and experimental concentration profiles of hydrogen with respect to process time at residence time θ : 1.0 hr, process temperature: 85 °C, process pressure: 364.7 psia,
 $F_{H_2}^0 / F_{sulfonyl}^0 = 8.0 \text{ mol/mol}$, $F_{H_2}^0 / F_{Ar}^0 = 3.0 \text{ mol/mol}$ 129
- 5.8 Simulated concentration profile of the aromatic sulfinic acid (SA) with respect to process time at residence time θ : 1.0 hr, process temperature: 85 °C, process pressure: 364.7 psia,
 $F_{H_2}^0 / F_{sulfonyl}^0 = 8.0 \text{ mol/mol}$, $F_{H_2}^0 / F_{Ar}^0 = 3.0 \text{ mol/mol}$ 130
- 5.9 Comparison of simulated and experimental concentration profiles of the aromatic disulfide (DS) with respect to process time at residence time θ : 1.0 hr, process temperature: 85 °C, process pressure: 364.7 psia, $F_{H_2}^0 / F_{sulfonyl}^0 = 8.0 \text{ mol/mol}$,
 $F_{H_2}^0 / F_{Ar}^0 = 3.0 \text{ mol/mol}$ 131
- 5.10 Comparison of simulated and experimental concentration profiles of the aromatic thiol (THIOL) with respect to process time at residence time θ : 1.0 hr, process temperature: 85 °C, process pressure: 364.7 psia, $F_{H_2}^0 / F_{sulfonyl}^0 = 8.0 \text{ mol/mol}$,
 $F_{H_2}^0 / F_{Ar}^0 = 3.0 \text{ mol/mol}$ 132

5.11 Comparison of simulated and experimental concentration profiles of the aromatic thiosulfone (TS) with respect to process time at residence time θ : 1.0 hr, process temperature: 85 °C, process pressure: 364.7 psia, $F_{H_2}^0 / F_{sulfonyl}^0 = 8.0 \text{ mol/mol}$,
 $F_{H_2}^0 / F_{Ar}^0 = 3.0 \text{ mol/mol}$ 133

5.12 Simulated concentration profile of the aromatic sulfonic acid (SULFONIC) with respect to process time at residence time θ : 1.0 hr, process temperature: 85 °C, process pressure: 364.7 psia, $F_{H_2}^0 / F_{sulfonyl}^0 = 8.0 \text{ mol/mol}$, $F_{H_2}^0 / F_{Ar}^0 = 3.0 \text{ mol/mol}$ 134

5.13 Comparison of simulated and experimental concentration profiles of the aromatic sulfonyl chloride (SC) with respect to process time at residence time θ : 1.0 hr, process temperature: 97 °C, process pressure: 364.7 psia, $F_{H_2}^0 / F_{sulfonyl}^0 = 8.0 \text{ mol/mol}$,
 $F_{H_2}^0 / F_{Ar}^0 = 3.0 \text{ mol/mol}$ 135

5.14 Comparison of simulated and experimental concentration profiles of hydrogen with respect to process time at residence time θ : 1.0 hr, process temperature: 97 °C, process pressure: 364.7 psia, $F_{H_2}^0 / F_{sulfonyl}^0 = 8.0 \text{ mol/mol}$, $F_{H_2}^0 / F_{Ar}^0 = 3.0 \text{ mol/mol}$ 136

5.15 Simulated concentration profile of the aromatic sulfinic acid (SA) with respect to process time at residence time θ : 1.0 hr, process temperature: 97 °C, process pressure: 364.7 psia, $F_{H_2}^0 / F_{sulfonyl}^0 = 8.0 \text{ mol/mol}$, $F_{H_2}^0 / F_{Ar}^0 = 3.0 \text{ mol/mol}$ 137

FIGURE

Page

- 5.16 Comparison of simulated and experimental concentration profiles of the aromatic disulfide (DS) with respect to process time at residence time θ : 1.0 hr, process temperature: 97 °C, process pressure: 364.7 psia, $F_{H_2}^0 / F_{sulfonyl}^0 = 8.0 \text{ mol/mol}$,
 $F_{H_2}^0 / F_{Ar}^0 = 3.0 \text{ mol/mol}$ 138
- 5.17 Comparison of simulated and experimental concentration profiles of the aromatic thiol (THIOL) with respect to process time at residence time θ : 1.0 hr, process temperature: 97 °C, process pressure: 364.7 psia, $F_{H_2}^0 / F_{sulfonyl}^0 = 8.0 \text{ mol/mol}$,
 $F_{H_2}^0 / F_{Ar}^0 = 3.0 \text{ mol/mol}$ 139
- 5.18 Comparison of simulated and experimental concentration profiles of the aromatic thiosulfone (TS) with respect to process time at residence time θ : 1.0 hr, process temperature: 97 °C, process pressure: 364.7 psia, $F_{H_2}^0 / F_{sulfonyl}^0 = 8.0 \text{ mol/mol}$,
 $F_{H_2}^0 / F_{Ar}^0 = 3.0 \text{ mol/mol}$ 140
- 5.19 Simulated concentration profile of the aromatic sulfonic acid (SULFONIC) with respect to process time at residence time θ : 1.0 hr, process temperature: 97 °C, process pressure: 364.7 psia,
 $F_{H_2}^0 / F_{sulfonyl}^0 = 8.0 \text{ mol/mol}$, $F_{H_2}^0 / F_{Ar}^0 = 3.0 \text{ mol/mol}$ 141
- 5.20 Comparison of simulated and experimental concentration profiles of the aromatic sulfonyl chloride (SC) with respect to process time at residence time θ : 1.0 hr, process temperature: 110 °C, process pressure: 364.7 psia, $F_{H_2}^0 / F_{sulfonyl}^0 = 8.0 \text{ mol/mol}$,
 $F_{H_2}^0 / F_{Ar}^0 = 3.0 \text{ mol/mol}$ 142

FIGURE	Page
5.21 Comparison of simulated and experimental concentration profiles of hydrogen with respect to process time at residence time θ : 1.0 hr, process temperature: 110 °C, process pressure: 364.7 psia, $F_{H_2}^0 / F_{sulfonyl}^0 = 8.0 \text{ mol/mol}$, $F_{H_2}^0 / F_{Ar}^0 = 3.0 \text{ mol/mol}$	143
5.22 Simulated concentration profile of the aromatic sulfinic acid (SA) with respect to process time at residence time θ : 1.0 hr, process temperature: 110 °C, process pressure: 364.7 psia, $F_{H_2}^0 / F_{sulfonyl}^0 = 8.0 \text{ mol/mol}$, $F_{H_2}^0 / F_{Ar}^0 = 3.0 \text{ mol/mol}$	144
5.23 Comparison of simulated and experimental concentration profiles of the aromatic disulfide (DS) with respect to process time at residence time θ : 1.0 hr, process temperature: 110 °C, process pressure: 364.7 psia, $F_{H_2}^0 / F_{sulfonyl}^0 = 8.0 \text{ mol/mol}$, $F_{H_2}^0 / F_{Ar}^0 = 3.0 \text{ mol/mol}$	145
5.24 Comparison of simulated and experimental concentration profiles of the aromatic thiol (THIOL) with respect to process time at residence time θ : 1.0 hr, process temperature: 110 °C, process pressure: 364.7 psia, $F_{H_2}^0 / F_{sulfonyl}^0 = 8.0 \text{ mol/mol}$, $F_{H_2}^0 / F_{Ar}^0 = 3.0 \text{ mol/mol}$	146
5.25 Comparison of simulated and experimental concentration profiles of the aromatic thiosulfone (TS) with respect to process time at residence time θ : 1.0 hr, process temperature: 110 °C, process pressure: 364.7 psia, $F_{H_2}^0 / F_{sulfonyl}^0 = 8.0 \text{ mol/mol}$, $F_{H_2}^0 / F_{Ar}^0 = 3.0 \text{ mol/mol}$	147

FIGURE	Page
5.26 Simulated concentration profile of the aromatic sulfonic acid (SULFONIC) with respect to process time at residence time θ : 1.0 hr, process temperature: 110 °C, process pressure: 364.7 psia, $F_{H_2}^0 / F_{sulfonyl}^0 = 8.0 \text{ mol/mol}$, $F_{H_2}^0 / F_{Ar}^0 = 3.0 \text{ mol/mol}$	148
5.27 Parity plot for the comparison of experimental and simulated concentrations for the aromatic sulfonyl chloride (SC) at all experimental conditions	149
5.28 Parity plot for the comparison of experimental and simulated concentrations for hydrogen at all experimental conditions	150
5.29 Parity plot for the comparison of experimental and simulated concentrations for the aromatic disulfide (DS) at all experimental conditions	151
5.30 Parity plot for the comparison of experimental and simulated concentrations for the aromatic thiol (THIOL) at all experimental conditions	152
5.31 Parity plot for the comparison of experimental and simulated concentrations for the aromatic thiosulfone (TS) at all experimental conditions	153

LIST OF TABLES

TABLE	Page
2.1 Gas-liquid mass transfer coefficient correlations.....	11
2.2 Changes in variables to determine gas-liquid mass transfer coefficient in Calderbank work	12
2.3 Experimental values of mass transfer, diffusion coefficient and bubble diameter for the dispersion of hydrogen in toluene in a PMFR.....	16
2.4 Solid-liquid mass transfer coefficient correlations.....	17
2.5 Corrosion rates of certain materials in hydrochloric acid and corrosion properties. BP: boiling point, mpy: milli-inch per year	20
2.6 Material of construction cost guide.....	21
2.7 Sulfur-based compounds involved in the hydrogenation of 2,5-dimethylbenzene sulfonyl chloride	24
2.8 Mechanisms of catalyst deactivation.....	29
3.1 Reaction conditions in continuous process for the hydrogenation of 2,5-dimethylbenzene sulfonyl chloride	44
3.2 Calibration constants of the aromatic sulfur-based compounds for the gas chromatograph HP G1800 C.....	51
3.3 Calibration constants of several aromatic sulfur-based compounds for the gas chromatograph HP G1800C	52
3.4 Approximated thermophysical properties of the liquid phase within the reactor at each process temperature.....	61
3.5 Power injected in the liquid, total superficial gas velocity, gas and liquid holdup within the reactor at process temperature of 85 °C.....	61
3.6 Power injected in the liquid, total superficial gas velocity, gas and liquid holdup within the reactor at process temperature of 97 °C.....	62

TABLE	Page
3.7 Power injected in the liquid, total superficial gas velocity, gas and liquid holdup within the reactor at process temperature of 110 °C.....	62
3.8 Solubility constant K of hydrogen dissolved in toluene at process temperatures of 85, 97, 110 °C.....	66
4.1 Reaction conditions for the hydrogenation of toluene	71
4.2. Reaction conditions in semi-batch mode catalytic hydrogenation of several aromatic sulfonyl chlorides.....	94
4.3 Overall conversions of several aromatic sulfonyl chlorides X and yields Y ₂ of several aromatic sulfonyl chlorides into their corresponding aromatic thiols. Semi-batch mode experiments. Reaction conditions: 110 °C, 364.7 psia	95
5.1 Empirical deactivation functions.....	100
5.2 Nomenclature used in the kinetic model of the catalytic hydrogenation of the aromatic sulfonyl chloride	104
5.3 Number of responses in the non-linear regression and tabulated t-value and F-value at the process temperatures of 85, 97 and 110 °C	120
5.4 Estimates of adsorption coefficients, kinetic constants and alpha parameter of the hyperbolic deactivation function with corresponding standard deviations, tc-value and 95 % confidence intervals for the Hougen-Watson kinetic model at process temperature of 85 °C....	121
5.5 Estimates of adsorption coefficients, kinetic constants and alpha parameter of the hyperbolic deactivation function with corresponding standard deviations, tc-value and 95 % confidence intervals for the Hougen-Watson kinetic model at process temperature of 97 °C....	123
5.6 Estimates of adsorption coefficients, kinetic constants and alpha parameter of the hyperbolic deactivation function with corresponding standard deviations, tc-value and 95 % confidence intervals for the Hougen-Watson kinetic model at process temperature of 110 °C..	125

CHAPTER I

INTRODUCTION

Thiols, R-SH, are compounds which contain the functional group composed of a sulfur atom and a hydrogen atom, with R being usually an aliphatic or aromatic group [1]. According to the IUPAC nomenclature, the names of aliphatic or aromatic thiols are constructed by adding the suffix -thiol to the name of the corresponding alkane or phenol [2]. More traditionally, because of the high affinity of the -SH group with the element mercury, the terms mercaptan (from the latin mercurius captans) and mercaptoarenes are often used instead for aliphatic thiols and aromatic thiols, respectively [1].

Many thiols are colorless liquids with a strong and repulsive odor, particularly for those of low molecular weights. Aliphatic thiols are responsible for the aromas of various foods such as cheese, milk, coffee, cabbage and bread [3]. Thiols are also detected in a number of plants and vegetables such as onions, leeks and garlic. Low molecular weight alkanethiol are also formed during the degradation of biological material and they are frequently found in most crude petroleum oil, fossil fuel, natural gas and coal. Arenethiols are found in a very limited extent in natural materials due to the facile oxidation by air into disulfides [3].

Many aliphatic thiols are important starting materials for the synthesis of crop-protection agents, pharmaceuticals, agrochemicals and polysulfides. They are also widely used as polymerization regulators and stabilizers in the manufacturing of plastics and rubber [3].

Aromatic thiols are frequently used as intermediates in reactions for the preparation of pharmaceuticals, agrochemicals, dyes, pigments, rubber, plastics and metal finishing [3]. The current market volume for aromatic thiols was determined to be more than 10 million pounds per year [4].

Aromatic thiols are commonly synthesized from the reduction of the corresponding aromatic sulfonyl chloride using different types of reducing agents or catalysts. Heterogeneous catalysts such as base metals (Ni, Cu, Co and Ca) and precious metals (Pt, Pd, Rh, Ru) dominate commercial practice, especially for large-scale production [5]. However, few heterogeneous kinetic data as well as kinetic models and catalyst activity are available in the literature for the hydrogenation of the aromatic sulfonyl chloride. High importance must be given to the catalyst activity in the case of commercial production of the aromatic thiol since sulfur-based compounds are known to deactivate most of the metal catalysts.

The objectives of this study are to build an experimental apparatus to investigate the catalytic hydrogenation of an aromatic sulfonyl chloride and collect experimental data that is required to develop a kinetic model for the hydrogenation reactions and estimate the parameters of the kinetic model. A particular concern is given to the monitoring of the catalyst activity during the hydrogenation of the aromatic sulfonyl chloride. The Hougen-Watson type of reaction equations are expected to be required to model the system. The rate equations will most likely include adsorption of individual components as well as surface reactions. Parameters of the model will be determined using numerical methods.

Chapter II covers the literature review. The general features of the catalytic hydrogenation of the aromatic sulfonyl chloride are briefly discussed. The theoretical and literature backgrounds are presented. Chapter III explains the experimental methods and calculations used to conduct the catalytic hydrogenation of the aromatic sulfonyl chloride. A description of the experimental unit and quantitative reacting species analysis by gas chromatography is also given. Chapter IV describes the kinetic experimental results for the catalytic hydrogenation of the aromatic sulfonyl chloride obtained at three reaction temperatures: 85, 97 and 110 °C and five different residence times: 0.6 (only at 110 °C), 1.0, 1.5, 2.0 and 3.1 hr. The kinetic data for the reacting species are discussed. A kinetic model and parameter estimations results are presented in chapter V.

CHAPTER II

LITERATURE REVIEW

2.1 Reduction Methods

Several reduction methods have been employed to produce the desired aromatic thiol compound from the corresponding aromatic sulfonyl chloride. One of the reduction methods is the use of zinc and sulfuric acid simultaneously, but it leads to harmful byproducts in the form of metal salts and poor yields (65 %) [6]. Some other methods include the use of reducing agents such as lithium aluminum hydride LiAlH_4 or red phosphorus in the presence of hydrogen iodide in aqueous or glacial acetic acid solution [3]. With LiAlH_4 under heat during four hours, the corresponding thiol is obtained in high yields (89%) [7]. The aromatic sulfinic acid ArSOOH is an intermediate of reaction during the reduction of the aromatic sulfonyl chloride. High yields (80 to 90 %) into the aromatic sulfinic acid are generally obtained when the reduction is conducted at low temperatures (-65 to -20 °C) in ether during approximately two hours with a molar ratio of LiAlH_4 to the aromatic sulfonyl chloride of about 0.5 [8].

One of the most successful methods developed is the catalytic hydrogenation of the corresponding aromatic sulfonyl chloride. In this process, hydrogen, an aromatic sulfonyl chloride (liquid) and a catalyst (solid) are mixed together to lead to the desired aromatic thiol compound [6, 9, 10]. This method limits the production of harmful byproducts of reaction compared to a classic reduction. However, hydrochloric acid, which is a byproduct of the reaction, requires the use of special materials of construction for the reactor and auxiliary equipment.

In the catalytic hydrogenation method, noble metals such as palladium or platinum were used as catalysts under pressurized hydrogen of 400-800 psi and temperatures of 100-110 °C [10]. Hydrogen chloride is formed during the catalytic hydrogenation reaction. Reactors made of tantalum or nickel-based alloys were necessary due to significant corrosion caused by the strong acidic conditions of the hydrogen chloride and the high reaction temperature. An average yield of 83 % for 2,5-dimethylthiophenol was obtained, but expensive reaction equipment was required to perform the reaction properly [9]. Mylroie and Doles reported, respectively, yields of 99%, 95% and 90.5% for the reduction of p-toluenesulfonyl chloride, naphthalene sulfonyl chloride and diisopropylbenzenesulfonyl chloride to the corresponding aromatic thiols [11]. The reduction was conducted during 18 hours at 40 °C and hydrogen pressure of 60 psig with a 5wt% palladium on charcoal catalyst in the presence of an ion exchange Amberlite resin to neutralize the strong hydrochloride acid formed. A yield of 87.4 % was also reported for the reduction of naphthalene disulfide to the corresponding thiol using a Raney cobalt catalyst.

Finally, a method very similar to the one presented previously was proposed using an inorganic base to prevent corrosion of the reactor [10]. However, the selectivity and yield of the aromatic thiol were greatly affected by the nature of the base.

Aprotic solvents such as methylbenzene, dimethylbenzene and chlorobenzene are preferred for the hydrogenation reaction. Toluene (methylbenzene) was the most common solvent used in the experimental methods described previously [6, 9, 10]. Figure 2.1 shows the composition of hydrogenated toluene obtained by using a palladium-zeolite catalyst at several temperatures and a reaction pressure of 40 atm [12].

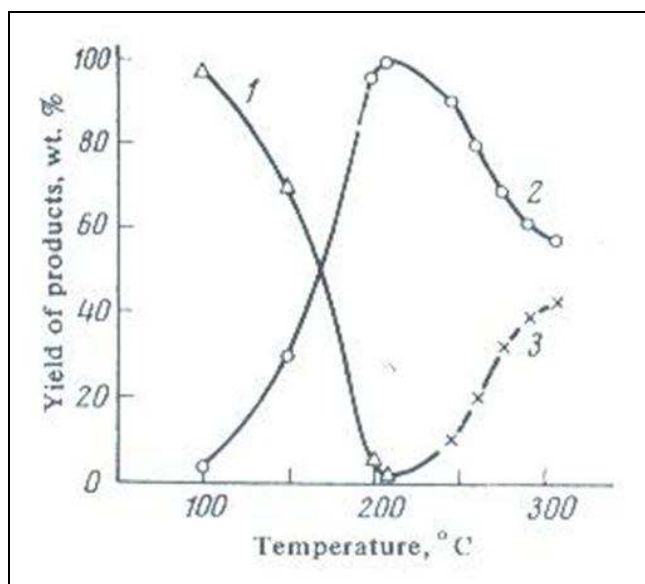


Figure 2.1 Yields of the products of the conversion of toluene 1) into methylcyclohexane 2) and cyclohexane 3) [12]

In the range of temperatures from 100 °C to 200 °C, the formation of methylcyclohexane dominates and no cyclohexane is formed. The formation of cyclohexane from the demethylation of methylcyclohexane is initiated only at temperatures above 200 °C. The hydrogenation of toluene into methylcyclohexane can be assumed negligible at temperatures equal to or less than 110 °C. Goodwin gives the thermophysical properties of toluene at temperature from 178 to 800 K and pressure up to 1000 psi [13]. Measurements of toluene surface tension using surface light scattering technique were also reported by Froba and coworker at different temperatures [14].

Solubility of hydrogen into toluene is a parameter of high importance. Tong estimated the solubility of hydrogen in toluene at different temperatures and pressures as shown in Figure 2.2 [15]. Another useful source is the solubility data series published by the International Union of Pure and Applied Chemistry (IUPAC) which listed solubility data for hydrogen in aqueous solutions as well as different organic compounds including toluene [16]. Bruner listed the solubility of hydrogen in ten different organic solvents including toluene at 298.15, 323.15 and 373.15 K and at different pressures [17].

Solubility data found in the latter for hydrogen in toluene is similar to the values reported by Tong.

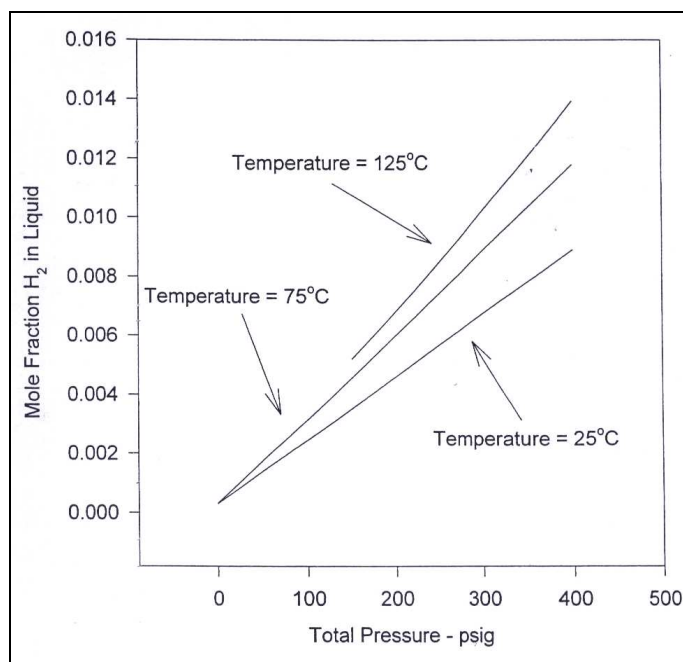


Figure 2.2 Estimated solubility of hydrogen in toluene [15]

2.2 Mass Transfer Resistances in Catalytic Hydrogenation Reactions

Hydrogen has to overcome a number of mass transfer resistances before reacting with aromatic sulfonyl chloride on the surface of a palladium on carbon catalyst as shown in Figure 2.3.

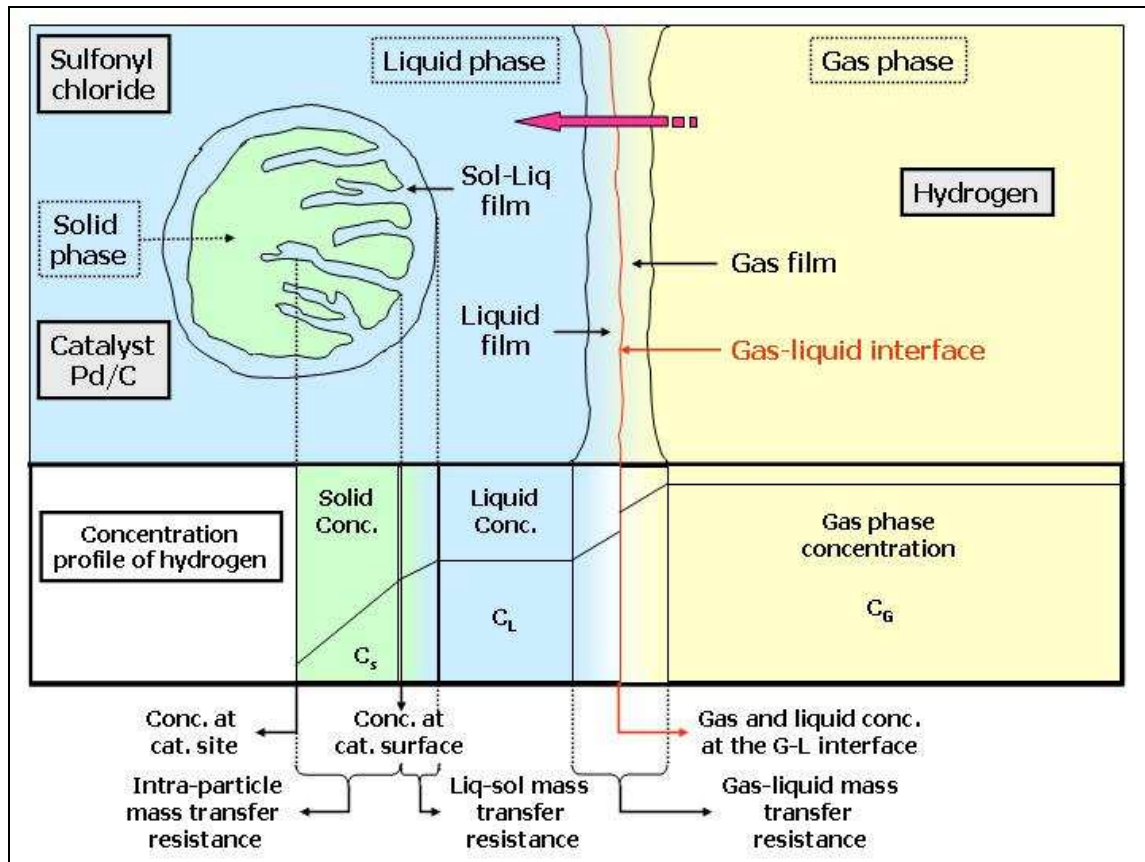


Figure 2.3 Concentration profile of hydrogen in a three-phase reactor

The steps involved are:

- 1) Absorption into the liquid phase by mass transfer
- 2) Diffusion from the gas-liquid interface into the bulk liquid phase
- 3) Diffusion from the bulk liquid phase to the catalyst surface
- 4) Adsorption and diffusion through the pore structure of the catalyst while reacting with the liquid reactant on the active sites of the catalyst

Dispersion of two immiscible phases by mechanical agitation creates not only an increase in the interfacial area between the two contacting phases but also improves the rates of mass transfer. High mass transfer can be achieved due to the fluid motion induced by the agitator. In gas-liquid dispersion, the gas phase is known as the dispersed phase and the liquid phase is called the continuous phase. The gas phase can be seen as a swarm of gas bubbles in free motion. As the gas bubbles rise through the agitated reactor, the surrounding fluid flows around the gas bubbles.

Understanding the mechanics of the dispersion of gases in liquids in an agitated reactor is of high importance for the determination of correlations for interfacial area and gas-liquid mass transfer coefficients. Two types of forces act on a gas bubble:

- The inertial force created by the agitation, which leads to dispersion of gas bubbles in the reactor. This dynamic force is responsible for deformation or eventually break-up of bubbles if it does not act equally over the surface of the bubble. Internal circulation of the fluid within the gas bubble induces internal viscous stress, which opposes the dynamic force. The inertial force mainly affects the gas-liquid interfacial area.
- The static force of surface tension or interfacial force depends mainly on the chemical and physical properties of the continuous phase. Static force mainly affects the gas-liquid mass transfer coefficient.

Theoretical mass transfer correlations, reference or references relating the Sherwood number (Sh) to the Reynolds number (Re) and Schmidt number (Sc) have been given by many workers. These correlations were of the form:

$$Sh = a Re^b Sc^c \quad (2.1)$$

where

$$Sh = \frac{k_L d_b}{D_L} \quad (2.2)$$

$$Sc = \frac{\mu_L}{\rho_L D_L} \quad (2.3)$$

$$Re_{bubble} = \frac{d_b G}{\mu_G} \quad (2.4)$$

with d_b the bubble diameter (m), D_L the gas diffusion coefficient in the liquid phase (m^2/s), ρ_L the density of the liquid (kg/m^3), μ_L the viscosity of the fluid surrounding the gas bubbles ($Pa.s$), μ_G the viscosity of gas ($Pa.s$) and G the superficial gas mass flow velocity ($kg/m^2.s$).

To disperse efficiently gas bubbles into a continuous liquid phase, the inertial force created by the agitator has to overcome the static force of surface tension. Correlations given by several authors are contradictory; the main discrepancy being whether or not the agitation intensities have an influence on the gas-liquid mass transfer coefficient. Some Authors such as Barker [18], Ahmed and Semmens [19] and Griffith [20] found that the mass transfer coefficient is independent of the intensity of agitation. On the other hand, authors such as Yoshida [21], Prasher [22], Davies [23] and Calderbank [24] found that the gas-liquid mass transfer rates are dependent on the agitation intensities. Table 2.1 shows the correlations proposed by these various investigators.

Table 2.1 Gas-liquid mass transfer coefficient correlations

Source	Region of validity	Media	Correlation
Barker and Treybal [18]	Not reported	Benzoic acid pellet/water	$Sh = 0.052 Re_{impeller}^{0.833} Sc^{0.5}$
Ahmed and Semmens [19]	$0.01 \leq Re \leq 100$	Air in water O ₂ in water	$Sh = 0.4911 Re^{0.3824} Sc^{0.33}$
Griffith [20]	$Re > 1$	H ₂ in water	$Sh = 2 + 0.44 Re^{0.5} Sc^{0.35}$
Calderbank and Moo- Young [24]	Transfer due to turbulence in surrounding fluid	CO ₂ in water H ₂ in solvent	$k_L Sc^{2/3} = 0.13 \left(\frac{(P/V) \mu_L}{\rho_L^2} \right)^{1/4}$
Yoshida and Miura [21]	Not reported	O ₂ in water and glycerol solution	$Sh = 0.33 \left(\frac{d_b ND \rho_L}{\mu_L} \right)^{0.6} Sc^{0.5}$
Prasher and Wills [22]	Not reported	CO ₂ in (NaOH)aq	$k_L = 0.592 \left(\frac{8N^3 D^5 \phi}{T^2 H \mu_L} \right)^{1/4} D_L^{1/2}$

In Calderbank's work [25], experiments were conducted in 5-liter and 100-liter tanks with different liquids. Air was spargingly dispersed as a bubble cloud in the reactor and absorbed into the continuous liquid phase. A six flat-blade impeller turbine was used as the agitator. Four radial baffles were symmetrically attached to the internal wall of the tank. Calderbank assumed that a balance exists between interfacial forces and dynamic forces during breakup. The balance between these two forces occurs in the cavities created behind the agitator as the gas is dispersed.

Table 2.2 shows the range in density, surface tension and viscosity of the liquid phase as well as the range in power dissipated in the liquid phase and the superficial gas velocity investigated by Calderbank [25] to find correlations for the gas-liquid mass transfer coefficient and interfacial area.

Table 2.2 Changes in variables to determine gas-liquid mass transfer coefficient in Calderbank work

$\rho_L = (0.79 \text{ to } 1.6)10^3 \text{ kg/m}^3$	Gas used: Hydrogen and CO₂
$\sigma_L = (21.7 \text{ to } 73.5)10^{-3} \text{ N/m}$	
$\mu_L = (0.5 \text{ to } 28)10^{-3} \text{ Pa.s}$	Liquid used: Water, ethyl alcohol, methyl alcohol, isopropyl alcohol, n-butyl alcohol,
$\frac{P}{V} = (0.35 \text{ to } 7.06) \text{ HP/m}^3 \text{ of liquid}$	ethylene alcohol, carbon tetrachloride,
$V_S = (3.04 \text{ to } 18.3)10^{-3} \text{ m}^3/\text{m}^2.\text{s}$	ethyl acetate, nitrobenzene and toluene

Calderbank observed that no variation of k_L occurs with bubble sizes classified as “small bubbles” with diameters less than 2.5 mm and “large bubbles” with diameter greater than 2.5 mm [25]. However, gas bubbles with diameters greater than 2.5 mm have a greater mass transfer coefficients than gas bubbles with diameters less than 2.5 mm.

Small rigid sphere bubbles with diameters less than 2.5 mm experience essentially friction drag when falling or rising through a liquid causing perturbation of the flow within the boundary layer. Calderbank found that the mass transfer coefficient is proportional to $D_L^{2/3}$ and it is independent of the bubble size, degree of agitation and slip velocity v [25]. For large gas bubbles with diameters greater than 2.5 mm, form

drag predominates. Calderbank found that the mass transfer coefficient is proportional to $D_L^{0.86}$ [25].

Calderbank also measured interfacial area by light scattering and investigated the following parameters [26]:

- The power dissipated by the agitator which is primarily dependent upon the agitation speed
- The density of the continuous liquid phase
- The surface tension of the continuous liquid phase
- The superficial gas velocity
- The terminal gas-bubble velocity in free rise

Calderbank gave the following correlations for the gas-liquid interfacial area a (m_i^2 / m_r^3), bubble diameter d_b (m) and gas hold-up ε (m^3 / m_r^3) [26, 27]:

$$a = 1.44 \left(\frac{(P/V)^{0.4} \rho_L^{0.2}}{\sigma_L^{0.6}} \right) \left(\frac{V_S}{V_t} \right)^{1/2} \quad (2.5)$$

$$d_b = 4.15 \left(\frac{\sigma_L^{0.6}}{(P/V)^{0.4} \rho_L^{0.2}} \right) (\varepsilon)^{1/2} + 0.0009 \quad (2.6)$$

$$\varepsilon = \left(\frac{V_S \varepsilon}{V_t} \right) + 0.000216 \left(\frac{(P/V)^{0.4} \rho_L^{0.2}}{\sigma_L^{0.6}} \right) \left(\frac{V_S}{V_t} \right)^{1/2} \quad (2.7)$$

where $\frac{P}{V}$ is the power dissipated by the agitator per unit volume of the liquid (W/m^3), ρ_L the density of the liquid (kg/m^3), σ_L is the surface tension (kg/s^2), V_S is the superficial gas velocity (m^3/m_r^2s) and V_t is the terminal gas-bubble velocity in free rise (m^3/m_r^2s). Calderbank assumed a constant bubble terminal velocity of 26.5 cm/s in his experiments.

Depending on the Reynolds numbers of the bubbles, the free-rising velocity V_t is calculated from the following equations [28]:

$$V_t = \frac{1}{18} \frac{\rho_L g d_b^2}{\mu_L} \text{ (Stokes' law) when } Re_{bubble} < 1 \quad (2.8)$$

$$V_t = \frac{1}{4} d_b \sqrt[3]{\frac{(\rho_L - \rho_G)^2 g^2}{\rho_L \mu_L}} \text{ when } 30 < Re_{bubble} < 10^3 \quad (2.9)$$

$$V_t = 1.76 \sqrt{\frac{(\rho_L - \rho_G) g d_b}{\rho_L}} \text{ when } Re_{bubble} > 10^3 \quad (2.10)$$

where d_b is the bubble diameter (m), ρ_L the density of the liquid (kg/m^3), ρ_G the density of the gas (kg/m^3), μ_L the viscosity of the fluid surrounding the gas bubbles ($Pa.s$) and g is due to the acceleration gravity (m/s^2).

With no agitation, the gas is not dispersed into the liquid phase and $P/V = 0$.

Therefore, the gas hold-up can be expressed as:

$$\varepsilon = \left(\frac{V_S}{V_t} \right) \quad (2.11)$$

With high power dissipation, the first term of Equation 2.7 becomes small. The gas hold-up is proportional to [26]:

$$\varepsilon \propto \left(\frac{P}{V} \right)^{0.4} V_S^{1/2} \quad (2.12)$$

In the absence of stirrer speed, the gas hold-up depends on the superficial gas velocity. With agitation and recirculation of the liquid within the reactor, the gas hold-up should be higher compared to the one obtained with no agitation. Therefore, as the stirrer speed increases, the gas-liquid mass transfer coefficient, gas hold-up and interfacial area should increase.

Calderbank reported McGrea's experimental work [25, 26] on the determination of mass transfer coefficients, diffusion coefficients and bubble diameters during the dispersion of hydrogen in toluene in a Perfectly Mixed Flow Reactor (PMFR) as listed in Table 2.3.

Table 2.3 Experimental values of mass transfer, diffusion coefficient and bubble diameter for the dispersion of hydrogen in toluene in a PMFR

Difference of density between the continuous phase and dispersed phase	0.867 g/cm ³
Continuous phase density	0.867 g/cm ³
Continuous phase viscosity	0.28-0.90 cp
Hydrogen mass transfer coefficient	0.0253-0.048 cm/s
Hydrogen diffusion coefficient	4.75-14.25 10 ⁻⁵ cm ² /s
Hydrogen bubble diameter	0.14 cm

The rate of absorption of small hydrogen bubbles (0 to 16 mm diameter) in toluene obtained experimentally are in close agreement with the correlation given by Calderbank [25, 26] for the gas-liquid mass transfer coefficient proposed for small bubbles.

Sano and coworker [29] and Levins and Glastonbury [30] proposed correlations for the solid-liquid mass transfer coefficient based on Kolmogoroff's theory. Experimental data have been collected in an agitated slurry reactor and correlations are given in Table 2.4.

Table 2.4 Solid-liquid mass transfer coefficient correlations

Sano and coworker [29]	$\frac{k_S d_P}{D_S} = 2 + 0.4 \left(\frac{e d_P^4 \rho_L^3}{\mu_L^3} \right)^{1/4} \left(\frac{\mu_L}{\rho_L D_S} \right)^{1/3}$
Levins and Glastonbury (small density difference between the solid and liquid) [30]	$\frac{k_S d_P}{D_S} = 2 + 0.47 \left(\frac{e^{1/3} d_P^{4/3}}{\mu_L} \right)^{0.62} \left(\frac{D_I}{D_T} \right)^{0.17} \left(\frac{\mu_L}{D_S} \right)^{0.36}$
Levins and Glastonbury (large density difference between the solid and liquid) [30]	$\frac{k_S d_P}{D_S} = 2 + 0.44 \left(\frac{d_P \nu}{\mu_L} \right)^{1/2} \left(\frac{\mu_L}{D_S} \right)^{0.38}$

where d_P is the mean spherical diameter of the catalyst particle (m), D_S the diffusion coefficient into the solid phase (m^2/s), D_I the impeller blade diameter (m), D_T the reactor diameter (m), μ_L the viscosity of the fluid surrounding the solid particles ($Pa.s$), e the energy supplied per unit mass of slurry (m^2/s^3) and ν the slip velocity (m/s).

Goto and Saito evaluated liquid-solid mass transfer coefficients in an agitated vessel with a stationary basket [31]. The experimental data collected was in good agreement with the correlations proposed by Sano [29] and Levins and Glastonbury [30].

2.3 Catalytic Gradientless Reactor

Trickle bed and slurry reactors are the most common catalytic reactors used to obtain intrinsic reaction rates at the surface of a catalyst. In the trickle bed reactor, the gas and the liquid phases flow either co-currently or countercurrently over a stationary bed of catalyst particles whereas in the slurry reactor the catalyst is kept in suspension by mechanical agitation. Weekman [32] and Shah [33] present the advantages and disadvantages for agitated-slurry and trickle-bed reactors. Chaudary and Ramachandran [34] reference some catalytic hydrogenation reactions conducted in three-phase catalytic reactors.

In kinetic investigations, complete mixing of the fluid within the reactor is required in order to achieve a uniform concentration and temperature over the surface of the catalyst. Any transport resistances between phases should be eliminated in order to obtain intrinsic reaction rates at the surface of the catalyst. A gradientless reactor is frequently used to achieve such conditions [35].

In trickle-bed reactors, intrinsic reaction rates over the surface of the catalyst are difficult to obtain because of strong mass and heat transport resistances between the phases as well as fluid dynamics and undefined residence time distributions in the catalyst bed [35]. “Recycle reactors, which approximate continuous-stirred tank reactor (CSTR), by employing either external or internal recirculation, are the most useful for obtaining catalytic kinetic data [36]”. The recirculation of the fluid (backmixing) is ensured by either an external pump or a mechanical agitator. A recycle ratio of more than 50 needs to be attained with a recycle reactor in order to reach the CSTR behavior [37].

Two types of gradientless reactors have been developed in the past [35, 36, 37]. With the spinning basket reactor, the catalyst is placed in the annular section of the

basket and moves in the fluid content of the reactor [35]. The basket serves as a mechanical agitator to achieve complete mixing within the reactor. The initial design was given by Carberry [38] and improvements of this type of reactor were made by Robinson and Mahoney during the kinetic study of the hydrodesulfurization of dibenzothiophene [35].

With the stationary basket reactor, the catalyst is placed in the annular section of the basket but remains fixed in the fluid content of the reactor [36]. It was developed primarily by Robinson and Mahoney as well during the catalyst testing for coal hydroliquefaction. The design of the reactor was inspired from the reactor developed by Berty [39]. Complete mixing is achieved by mechanical agitation.

Mahoney discussed the main advantages and disadvantages of both basket reactors and preference was given to the design of the stationary basket reactor [40]. The main reasons were that the actual temperature over the surface of the catalyst can not be directly measured and the catalyst is not exposed to a uniform concentration of the reactor contents with the rotating basket reactor.

2.4 Material Selection

A good balance between the cost of the material and its performance in corrosive media should be made before selecting any materials for the construction of a chemical production unit. Table 2.5 shows the corrosion rates of different materials and their corrosion properties in oxidizing and reducing media [41, 42, 43, 44, 45, 46, 47].

Table 2.5 Corrosion rates of certain materials in hydrochloric acid and corrosion properties. BP: boiling point, mpy: milli-inch per year

Metals	Maximum corrosion rates in hydrochloride acid (HCl)	Remarks
Hastelloy alloy C-276	50-200 mpy below BP 5 % to 30 % conc in HCl	Good resistance in oxidizing media
Hastelloy alloy B-2	5-20 mpy below BP 5 % to 30 % conc in HCl	Poor resistance in oxidizing media
Hastelloy alloy C-2000	50-200 mpy below BP 2 % to 20 % conc in HCl	Excellent resistance in both oxidizing/reducing media
Hastelloy alloy C-22	<200 mpy below BP 2 % to 25 % conc in HCl	Excellent resistance to crevice/pitting corrosion
Titanium	>50 mpy below BP 20 % to 50 % conc in HCl	Resist only in a mild reducing acid
Zirconium	<2 mpy below BP 10 % to 50 % conc in HCl	Possible pitting/crevice corrosion
Tantalum	<1 mpy below BP 0 % to 50 % conc in HCl	Possible hydrogen embrittlement above BP and 25%conc in HCl

Table 2.6 gives the relative cost of common process items for different materials of construction [48].

Table 2.6 Material of construction cost guide [48]

Material	Relative cost of fabricated item
Carbon steel	0.5
Stainless steel ferritic 430	0.8
Stainless steel austenitic 304	1.0
Stainless steel austenitic	1.1
Stainless steel duplex	2.0
High alloy steel 310	2.2
Titanium (pure grade 2)	2.6
Nickel chromium alloy 400	3.0
Titanium (0.2 Pd grade 7)	4.3
Nickel alloy C-276	4.5
Zirconium	5.5
Nickel alloy 625	6.0
Tantalum	20

Stainless steel austenitic 304 has been taken as the reference material. Special grades of materials may result in a higher price. Table 2.6 gives a rough but realistic idea of material cost. This document is a copyright of the institution of chemical engineers and it should be used by faculty and students in educational institutions for economic calculations [48].

One can notice that tantalum is the most expensive material, which is approximately 5 times more expensive than Hastelloy alloy C-276. Hastelloy C-276 has corrosion rates in hydrochloric acid greater than tantalum. Considering the balance between cost and performance of these materials, Hastelloy C-276 was selected as the material of construction for the experimental unit.

2.5 Chemistry of the Catalytic Hydrogenation of 2,5-Dimethylbenzene Sulfonyl Chloride

The following reaction sequence in Figure 2.4 has been proposed to obtain the aromatic thiol by catalytic hydrogenation of an aromatic sulfonyl chloride [6, 9, 15, 49]. The catalyst employed during hydrogenation is palladium on charcoal. Table 2.7 gives the names and chemical structures of all the compounds involved in the catalytic hydrogenation reaction.

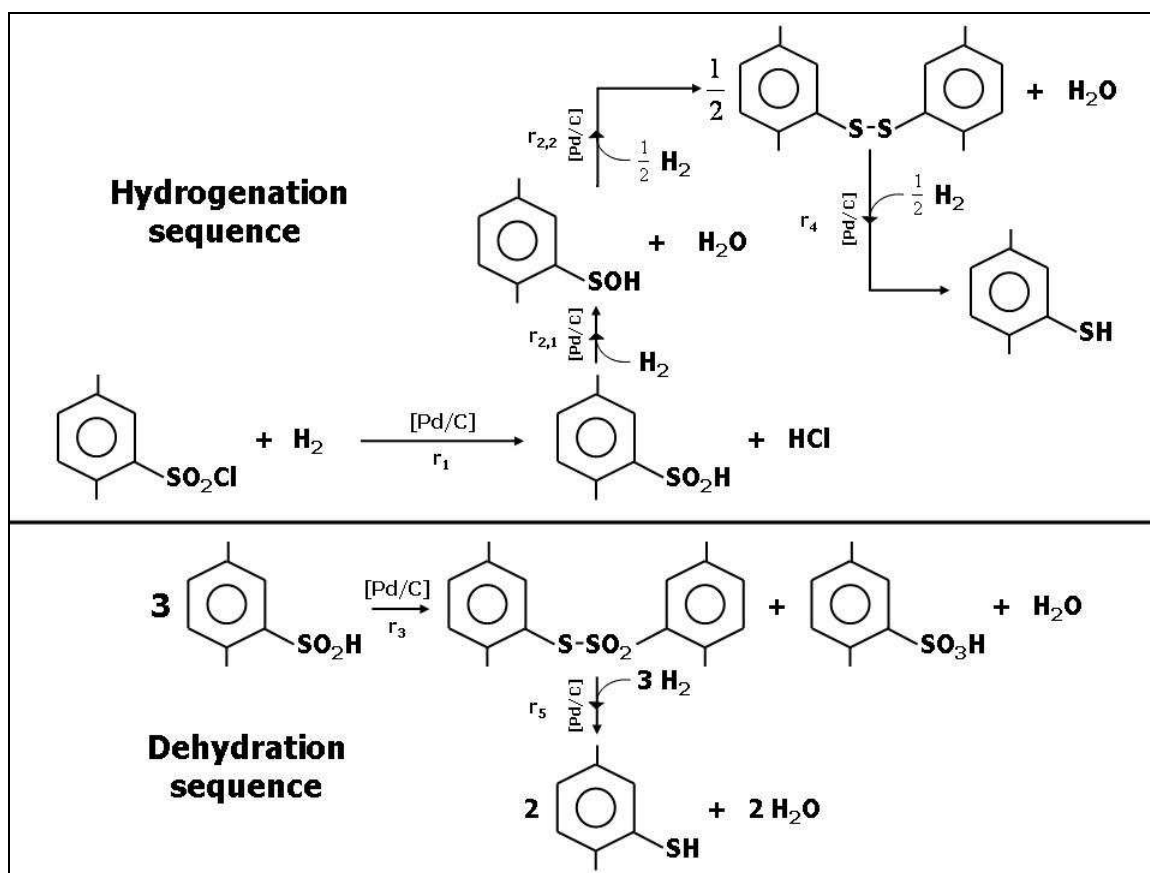


Figure 2.4 Hydrogenation sequence for the aromatic sulfonyl chloride

The aromatic sulfinic acid, which is the first intermediate specie in the hydrogenation sequence, undergoes a dehydrative disproportionation to produce the aromatic thiosulfone, the aromatic sulfonic acid and water. Hydrogenation of the aromatic thiosulfone leads to the formation of the aromatic thiol. The hydrogenation of the aromatic sulfinic acid, which includes the formation of the aromatic sulfenic and the aromatic disulfide with water, was proposed to be the main route for the formation of the aromatic thiol; the dehydration sequence being a side reaction during the catalytic reduction of the aromatic sulfonyl chloride.

Sulfenic acids formed in the hydrogenation sequence are highly reactive and generally unstable [50]. Therefore, it becomes difficult to isolate and detect this compound. Figure 2.5 shows the two tautomer forms of the aromatic sulfenic acid.

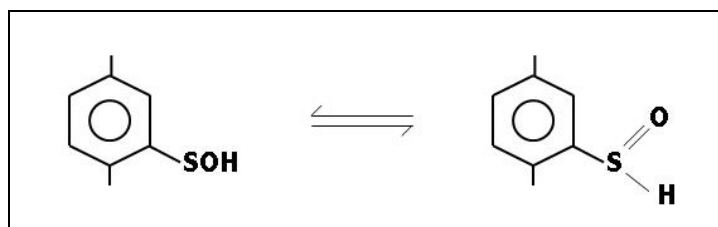
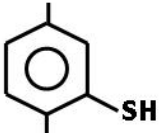
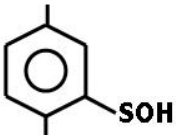
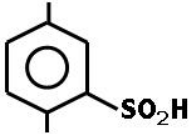
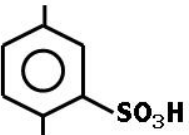
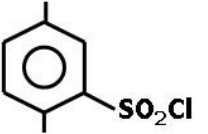
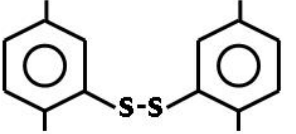
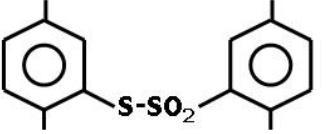


Figure 2.5 Tautomer forms for the aromatic sulfenic acid

It has been shown using microwave spectroscopic analysis that the divalent tautomer form **RSOH** predominates [50].

Table 2.7 Sulfur-based compounds involved in the hydrogenation of 2,5-dimethylbenzene sulfonyl chloride

Chemical name	Chemical structure	Molecular weight (g/mol)	Source
2,5-dimethyl thiophenol		138.2	Product in the hydrogenation and dehydration sequences
2,5-dimethyl benzene sulfenic acid		154.0	Intermediate in the hydrogenation sequence
2,5-dimethyl benzene sulfinic acid		170.0	Intermediate in the hydrogenation sequence
2,5-dimethyl benzene sulfonic acid		186.0	Water soluble by-product in the dehydration sequence
2,5-dimethyl benzene sulfonyl chloride		204.7	Reactant of the hydrogenation sequence
Bis(2,5-dimethyl phenyl)disulfide		274.5	Intermediate in the hydrogenation sequence
Bis(2,5-dimethyl phenyl)thiosulfone		306.0	Water insoluble intermediate in the dehydration sequence

The high reactivity of sulfenic acid is explained by the formation of thiosulfates RSOSR by intermolecular hydrogen bonding as shown in Figure 2.6.

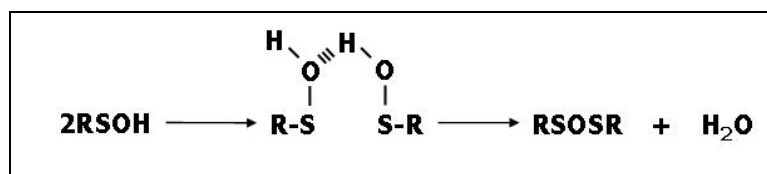


Figure 2.6 Intermolecular hydrogen bonding in the formation of thiosulfinate [50]

Thiosulfates are thermally unstable and formed at temperatures as low as -50 °C. The mechanism of the thermal disproportionation of thiosulfates involves radicals $\text{RS}\cdot$ and $\text{RSO}\cdot$ which recombine to give disulfide RS-SR and thiosulfonate RSO_2SR as shown in Figure 2.7.

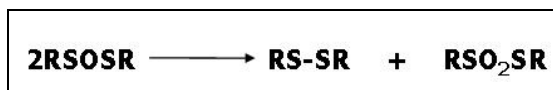


Figure 2.7 Disproportionation of thiosulfinate [50]

Benson listed bond dissociation energies in several sulfur-based compounds [51]. The dissociation energy of the sulfur-sulfur bond and sulfur-oxygen bond in the diphenyl thiosulfinate Ph-SOS-Ph compound have been reported equal to 36 and 83 kcal/mol, respectively. The dissociation energy of the sulfur-oxygen bond in the diphenyl thiosulfonate $\text{Ph-SO}_2\text{S-Ph}$ has been listed equal to 115 kcal/mol. The standard heat of formation ΔH_f^0 of the latter compound is equal to -22 kcal/mol (± 4) at 298 K.

Sulfinic acids RSOOH are stronger acids than carboxylic acids and are thermally unstable [8]. Burkard and coworkers investigated the acidity constants of several aromatic sulfinic acids and found values of pK_a around 1.8-2.0 [52]. Sulfinic acids undergo auto-catalysed dehydrative disproportionation [53]. The reaction is catalysed

not only by the sulfinic acid itself but also by the addition of other strong acids such as hydrochloric acid [8]. Kice studied the kinetics of disproportionation of various sulfinic acids in acetic acid solvent and with known amounts of water and sulfuric acid [53]. A second order reaction for the disappearance of the aromatic sulfinic acids is suggested in the study. The mechanism for the dehydrative disproportionation with the formation followed by a thermal decomposition of an intermediate sulfinyl sulfone has been proposed in Figure 2.8.

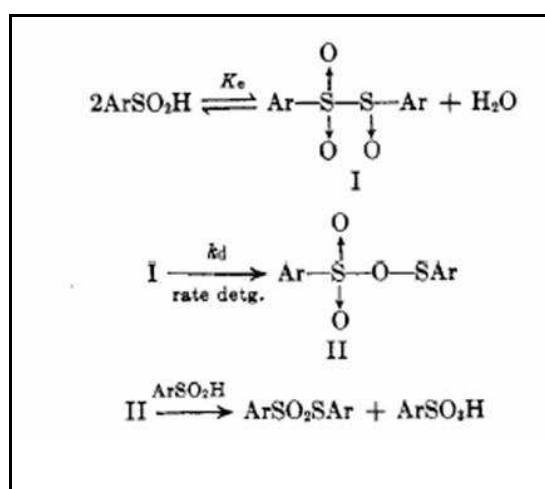


Figure 2.8 Dehydrative disproportionation mechanism of the aromatic sulfinic acid proposed by J.L Kice [53]

Aromatic thiosulfonates ArSO_2SAr produced by dehydrative disproportionation of the corresponding sulfinic acid are thermally stable above 100°C for many hours and exhibit the same resistance to homolysis as aromatic disulfides [8]. Sulfonic acids RSO_3H are organic acids with strength comparable to nitric and hydrochloric acid. The acidity constant is lower than the one found for the sulfinic acids. Reduction of this compound by LiAlH_4 , B_2H_6 and AlH_3 is difficult and removal of the proton only occurs [8].

Many aromatic disulfides ArS-SAr undergo homolytic dissociation of the sulfur-sulfur bond under heat to produce thiyl radical $\text{RS}\cdot$. Senning reported a homolytic dissociation constant greater than $2.0 \times 10^{-8} \text{ sec}^{-1}$ at $100 \text{ }^\circ\text{C}$ for p-toluene disulfide [54]. Kende measured the rate of fission of $(\text{CH}_3\text{S}_2)_2$ in toluene and suggested a first order disappearance with respect to dimethyl tetrasulfide. An activation energy of 33.6 kcal/mol and a pre-exponential factor of $1.8 \times 10^{19} \text{ hr}^{-1}$ were reported [51, 54]. Aromatic disulfides are easily reduced by reducing agents such as LiAlH_4 and NaH . The cleavage of the sulfur-sulfur bond in the disulfide is easier when an aromatic ring is attached to the sulfur atoms. Indeed, the electron density in the sulfur atom attached to the aromatic ring is lower due to the resonance stabilization which weakens the p-bonding interaction of the sulfur-sulfur bond [55]. The dissociation energy of the sulfur-sulfur bond in the phenyl disulfide PhS-SPh compound is about 20 to 26 kcal/mol which is different from the one reported by Benson (55 kcal/mol) [51, 55, 56]. The standard heat of formation ΔH_f^0 of the latter compound is 58.4 kcal/mol at 298 K [51].

The thermochemistry of the hydrogenation of the aromatic sulfonyl chloride was investigated using an Accelerating Rate Calorimeter (ARC) equipped with a magnetic stirrer [57]. The hydrogenation reaction was conducted with a palladium on carbon catalyst without any base. Heats of reaction from the 2,5-dimethylbenzenesulfonyl chloride to the 2,5-dimethylthiophenol and from the 2,5-dimethylbenzenesulfonyl chloride to the intermediate aromatic disulfide were found to be equal to -63 kcal/mol and -45 kcal/mol , respectively. The disappearance of the 2,5-dimethylbenzenesulfonyl chloride was represented by a first order rate equation. The pre-exponential factor and activation energy were determined to be equal to $1.15 \times 10^9 \text{ hr}^{-1}$ and 14.6 kcal/mol .

2.6 Catalyst Deactivation

Three kinds of deactivation of catalyst occur: sintering, catalyst poisoning and fouling [58, 59]. Sintering is associated with a loss of area of the catalyst when the catalyst is operated above the normal range of temperature. Poisoning occurs when a small amount of material or impurity adsorb on the active sites of the catalyst. Poisons are either present initially in a feed stream such as sulfur-based compounds in natural gas or naphtha fractions are formed during the reaction. Most poisoning processes are irreversible which means that the catalyst should be discarded if not regenerated. Elements most frequently encountered as poisons include sulfur, arsenic, halogens, phosphorus and lead. Fouling is associated with a large amount of material present in the feed and covering the active sites of the catalyst. Coking and fouling are two different mechanisms in the sense that the coke is formed by a side reaction.

Bartholomew gives a description of the mechanisms in catalyst deactivation as represented in Table 2.8 [60].

Table 2.8 Mechanisms of catalyst deactivation [60]

Poisoning	Chemical	Strong chemisorption of species on catalytic sites, thereby blocking sites for catalytic reaction
Fouling	Mechanical	Physical deposition of species from fluid phase onto the catalytic surface and in catalyst pores
Thermal degradation	Thermal	Thermally induced loss of catalytic surface area, support area, and active phase-support reactions
Vapor formation	Chemical	Reaction of gas with catalyst phase to produce volatile compound
Vapor-solid and solid-solid reactions	Chemical	Reaction of fluid, support, or promoter with catalytic phase to produce inactive phase
Attrition/crushing	Mechanical	Loss of catalytic material due to abrasion Loss of internal surface area due to mechanical-induced crushing of the catalyst particle

Radovic and coworkers investigate the sulfur tolerance of some supported palladium and copper-based catalysts during methanol synthesis [61]. A mixture of gas containing CO, CO₂ and H₂ is fed to a differential fixed-bed reactor operated at 523 K and 1.5 MPa. A rapid decrease in activity of both catalysts is observed as soon as a small amount (2 ppm) of H₂S is fed with the initial gas mixture. From the activity test on a 5 wt% Pd on charcoal, it is shown that the catalyst retains more than 1.5 mol of sulfur per mol of palladium on the surface of the catalyst.

Novakova and coworkers investigate the hydrogenation/hydrogenolysis of a range of aromatic disulfides over a 10 wt% palladium supported on charcoal catalyst [62]. Reactions were conducted in a range of pressures of 5 to 50 bars in THF at 75 °C. Catalyst deactivation is observed by X-ray diffraction and attributed to the transformation of an active PdS phase into an amorphous Pd₄S inactive phase on the surface of the catalyst. The mechanism of the sulfur poisoning is believed to involve an initial step in which the sulfur atom is highly dispersed on the surface of catalyst and covers at least between 4 and 5 palladium atoms. PdS phase identification shows phases of PdS, PdS₂, Pd₃S, Pd₄S and Pd₁₆S₇ depending on the temperature and the sulfur content. Figure 2.9 shows Taylor's investigation on the temperature-composition phase relationships and thermodynamic properties of the Pd-S system [63].

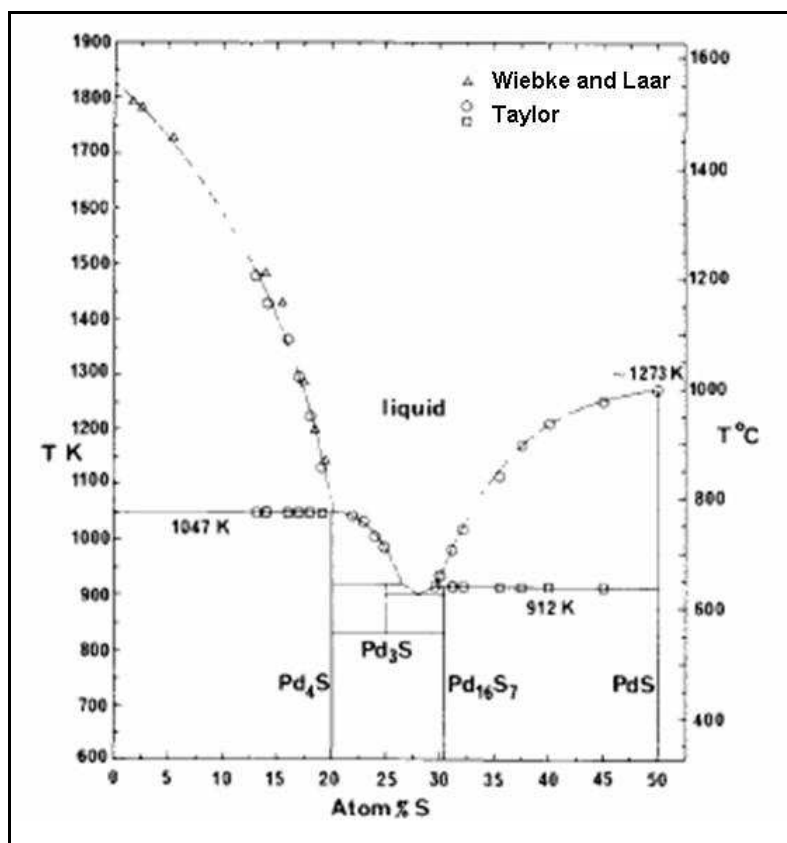


Figure 2.9 Temperature-composition PdS phase diagram [63]

Two factors influence essentially the heat of formation of chemisorbed sulfur on metal surfaces: the dispersion or coverage of the sulfur atom on the catalyst surface and the coordination of the active sites [64]. The structure of the metal surface and the location of chemisorbed sulfur atom on the surface determine the number of active sites available for surface reaction. At high coverage, sulfur chemisorbed can deactivate several neighboring sites for adsorption of the reacting species and deactivate completely the catalyst. At low coverage, chemisorbed sulfur may cover preferentially some active sites and therefore, reaction between reacting species may occur.

The d-orbitals of the metal are involved in the bonding with the sulfur atom. The sulfur 2s and 2p_z orbitals form a molecular σ bond and the remaining 2p orbitals of the sulfur form a Π bond with orbitals d and s of the metal. The binding energy of sulfur to the metals shows little variations between transition metals and noble metals.

Compared to platinum catalyst, the sulfur coverage is higher for palladium catalyst but the palladium-sulfur bond is less stable than the platinum-sulfur bond. The free energies of formation of bulk sulfides on the surface of palladium and platinum catalysts were reported equal to -78 kJ/mol and -88 kJ/mol, respectively [65].

CHAPTER III

DESCRIPTION OF THE EXPERIMENTAL UNIT

3.1 Experimental Unit

A hydrogenation unit was designed and built. Experiments are conducted either in a batch or continuous process mode. The laboratory reactor to conduct the catalytic hydrogenation of the aromatic sulfonyl chloride is a stirred 300 cm³ EZE-SEAL Robinson-Mahoney stationary catalyst basket reactor manufactured by Autoclave Engineers (AE). The body of the reactor is made of Hastelloy C-276 with an inner diameter of 1.82 inch and 0.75 inch thickness. The maximum allowable working pressure is 3300 psig at 454 °C.

Figure 3.1 shows a detail description of the design of the Robinson Mahoney stationary basket reactor. The U-shape overflow tube has been replaced in the top of the reactor in opening H instead of a connection to the bottom opening L, as shown in Figure 3.1. With this modified design, the tip of the overflow tube reaches the top of the reactor to let the mixture of liquid and gas flow out of the reactor. Therefore, the reactor is operated completely filled with gas and liquid.

The reactor has eight ports, two bottom and six top connections. It is equipped with a thermowell and an OSECO rupture disc with a burst pressure of 2482 psig at 22.2 °C. Both thermowell and rupture disk are made of Hastelloy C-276. External accessories include a pressure relief valve, a manual vent valve, a 0-1000 psi pressure gauge, a pressure transducer and a heating jacket.

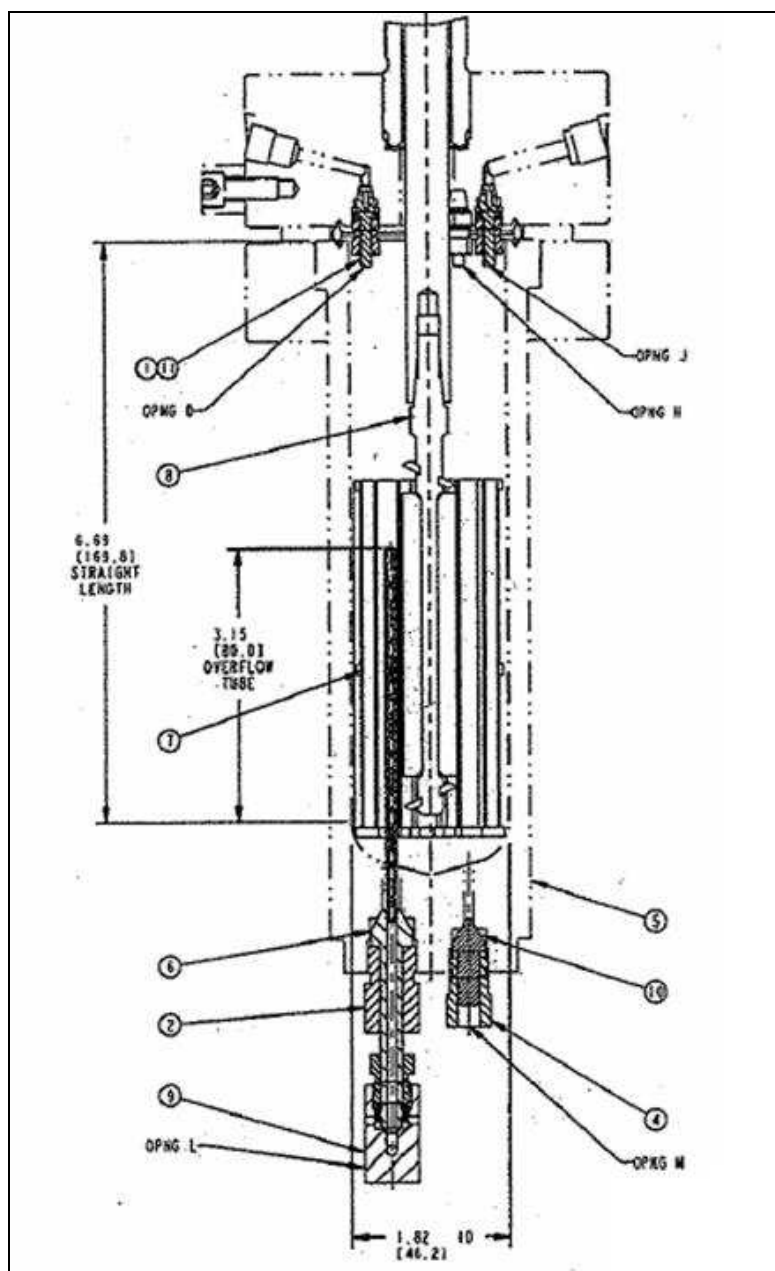


Figure 3.1 Robinson-Mahoney stationary basket reactor design, Property of, and used with the permission of Snap-Tite, Inc. The overflow tube has been placed in opening H in a U-shape design instead of a connection to the bottom opening L

The agitation is performed by rotation of external magnets, which actuate internal magnets attached to the agitator shaft. The agitation assembly is composed of a belt driven MAGNEDRIVE with purebon carbon graphite bearings, a speed sensor, a 90 volt direct current motor, an agitator with three upthrust blades and three downthrust blades (six blades total) and an agitator shaft. The motor is capable of delivering 0.5 hp at 3000 RPM. An aluminum cooling jacket between the drive connection and the magnet zone maintains the temperature below 149 °C.

An Autoclave Engineers tower controller has been installed to control motor speed, process temperature and heating jacket internal temperature. Process pressure measured from the pressure transducer is also displayed. The internal temperature of the heating jacket is adjusted to control accurately the process temperature, which is measured by an OMEGA type-J thermocouple inserted into a thermowell. The tower controller has a communication port for use with the AE towerview software and uses a touch pad for incremental increases in the speed of the motor and temperature of the heating jacket. The power to the heater and to the agitator is shutdown with the front panel ON/OFF switch.

The basket is a fixed annular design with baffles inside and outside to prevent fluid vortexes. The basket screen has an opening of 0.051 inch and the size of the mesh is 14×14 . It has been manufactured using Hastelloy C-276 with a 0.020 inch wire. The agitator shaft is located directly at the center of the basket to force the fluid through the basket, then up and down along the reactor wall after passing the basket and back into the center of the basket. Figure 3.2 shows the flow pattern of the fluid around the basket within the reactor.

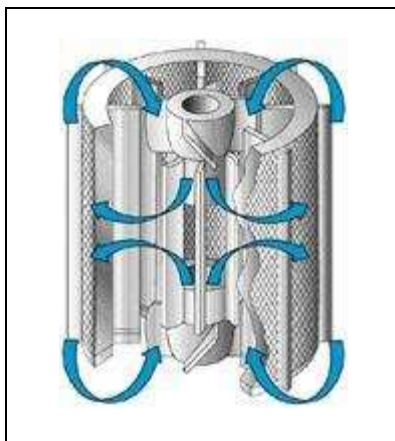


Figure 3.2 Flow pattern of the fluid around the basket within the reactor. Property of, and used with the permission of Snap-Tite, Inc.

The re-circulation of the fluid and the perfect mixing between the liquid and gas phases as well as the continuous radial flow through the basket create a gradient-free concentration in the liquid phase and uniform temperature within the reactor. Mass transfer resistances at the gas-liquid and liquid-solid interfaces are eliminated and intrinsic reaction rates of the reacting species on the surface of the catalyst are obtained.

Figure 3.3 shows a simplified flow diagram of the hydrogenation unit built to investigate the catalytic hydrogenation of the aromatic sulfonyl chloride into the aromatic thiol in continuous mode. A detailed flow diagram, which includes all the equipment used, is given in Figure 3.4. Figure 3.5 shows a simplified diagram of the hydrogenation unit in the semi-batch mode.

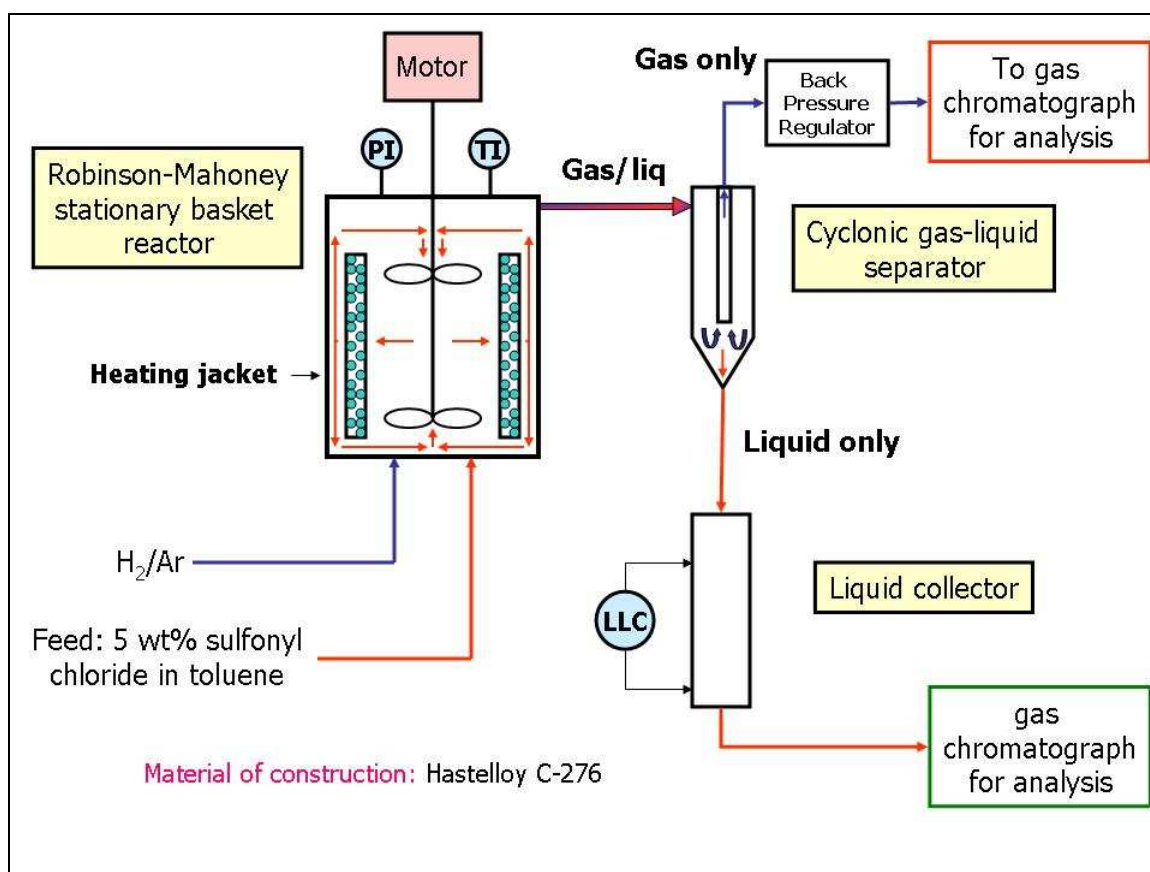


Figure 3.3 Simplified flow diagram of the hydrogenation unit in continuous mode

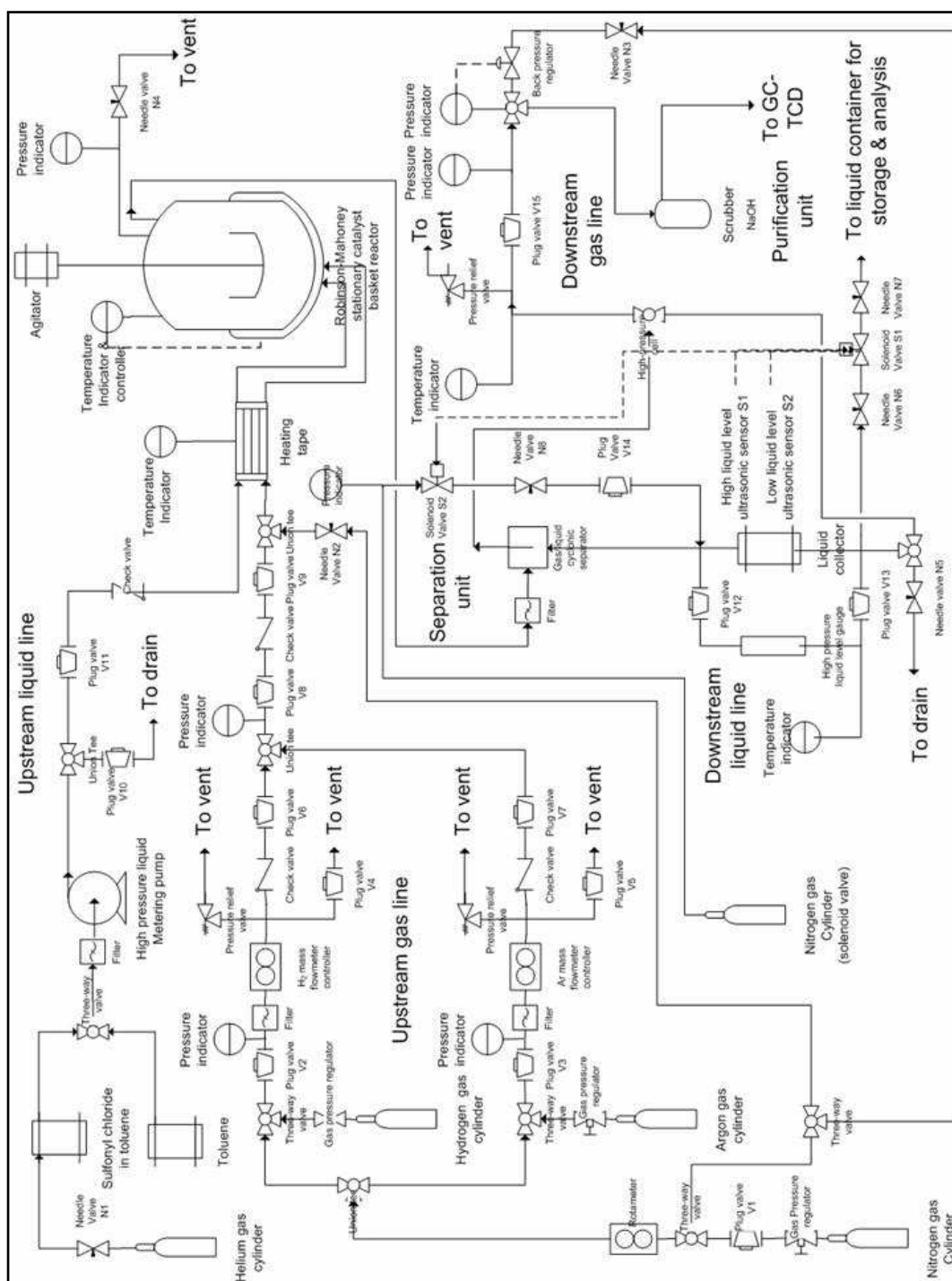


Figure 3.4 Detailed flow diagram of the hydrogenation unit in continuous mode

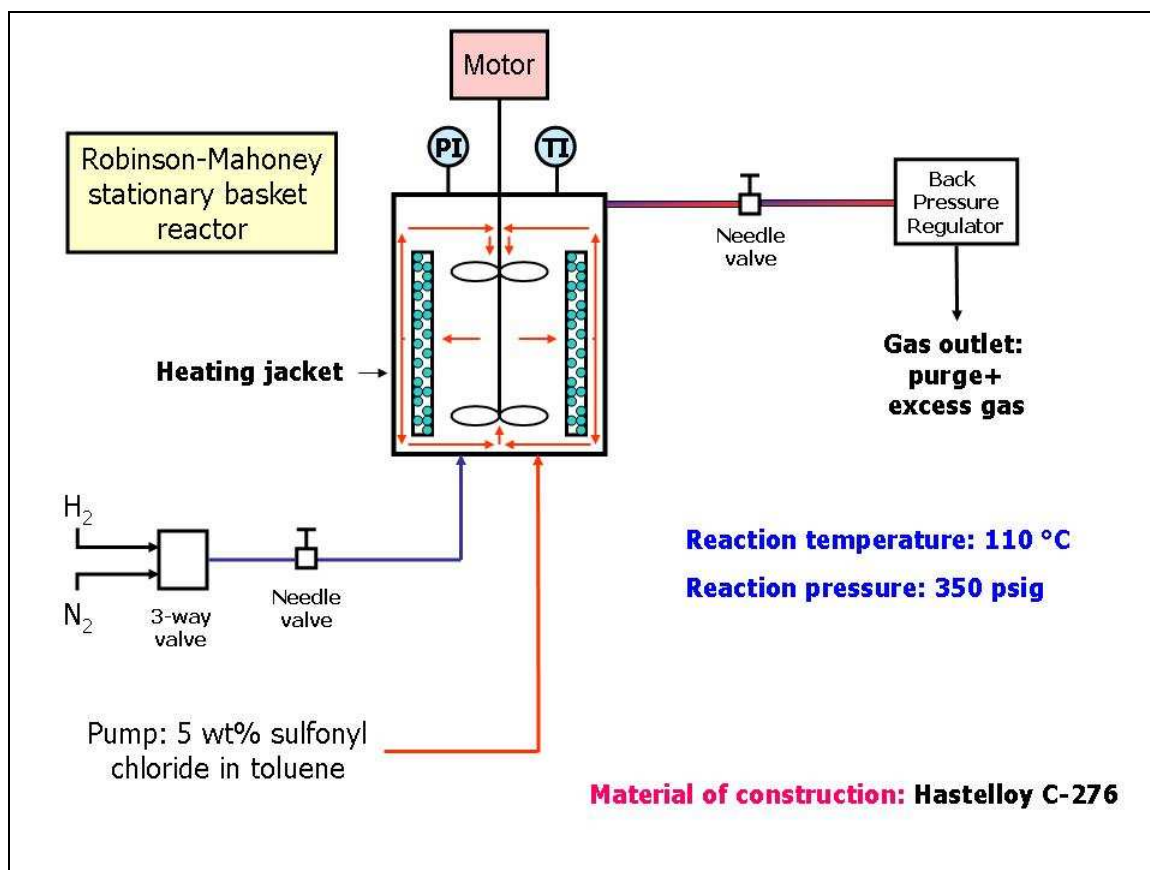


Figure 3.5 Simplified flow diagram of the hydrogenation unit in semi-batch mode

Hydrogen is the gas-phase reactant for the hydrogenation of the aromatic sulfonyl chloride and argon is used as a tie component. Feed gases are supplied in cylinders. Two Brooks Instrument model 5850 I mass flow controllers, equipped with a Brooks Instrument microprocessor 0154 control and read out unit, have been installed in the unit to control the flowrates of hydrogen and argon fed to the reactor. Mass flow controllers were calibrated using a soap bubble flowmeter. The hydrogen and argon mass flow controllers have a full scale flow range of 0 to 300 standard centimeter per minute (SCCM). The manufacturer indicated that the measurement percent error range of the flowrate setpoint for the hydrogen mass flow controller is 0.01 to 0.06 % and that of argon is -0.35 to +0.25 %.

Liquid feeds were prepared in a 1-liter glass bottle. 25 grams of 98 % purity 2,5-dimethylbenzene sulfonyl chloride from TCI America were weighed with a OHAUS AV2102 C balance and 475 grams of 99.5 % purity toluene were added. After strong agitation of the glass bottle, the liquid feed preparation was completed by shaking the bottle manually and weighting again the glass bottle with its content.

The liquid mixture containing a 5 wt% aromatic sulfonyl chloride in toluene is placed in a glass bottle, with a maximum allowable pressure of 10 psig, and fed to the reactor. The inlet volumetric flowrate is controlled by an Autoclave Engineers high-pressure micro-metering liquid pump with a PEEK material pressure head capable of pressures up to 1500 psi and liquid flowrates range from 0.01 to 40.0 cm³/min.

The pump is a positive displacement pump and it is equipped with a self-flush head which provides continuous washing of the piston by a 20% volume methanol in water solution. The manufacturer indicated that the measurement percent error range of the volumetric flowrate setpoint is -0.4 % to 0.1 %. Both liquid and gas inlet lines are preheated by heating tapes before reaching the reactor.

The mobile phase contains atmospheric gases, primarily nitrogen and oxygen. These dissolved gases may lead to bubble formation as well as other impurities in air and should be removed before entering the pump and the reactor. Degassing the mobile phase is accomplished by sparging continuously the mobile phase with helium at 5 psig. The mobile phase is also filtered with a 0.5 micron filter prior to entering the pump. This ensures that no particles will interfere with the operation of the piston seals and check valve in the pump.

A gas/liquid cyclonic separator is located on the outlet of the reactor to separate liquid and gas for proper analysis in the outlet stream. The design of the separator with its specific dimensions is shown in Figure 3.6. The gas and liquid mixture flows first through a 40 micron-mesh filter to remove any catalyst particles that can obstruct the inlet opening of the separator. The material of construction of the separator is Hastelloy C-276.

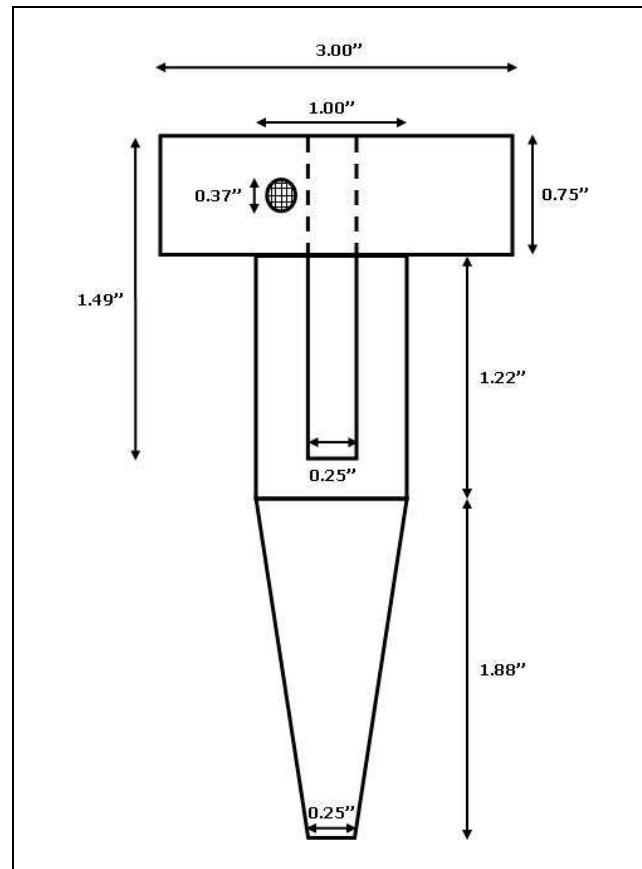


Figure 3.6 Design of the gas-liquid cyclonic separator

Liquid flowing from the cyclonic separator accumulates in a liquid collector made of Hastelloy C-276. The liquid collector is a pipe with a nominal pipe size of 1 ½ inch schedule 40 and a length of 10 1/8 inch. The outside diameter is 1.9 inch and the inside diameter is 1.61 inch. The volume of the collector is approximately 340 cm³. A Jerguson high-pressure liquid level transparent gauge is used to visualize the level of the liquid inside the collector. The pressure gauge is placed parallel and at the same level as the liquid collector. The gauge is 10 ¼ inch long, 3 3/8 inch wide and 5 1/16 inch deep. The material of construction of the chamber is stainless steel 316. The transparent window is made of glass and the gaskets are made of Teflon. The volume of the chamber is 75 cm³.

The liquid collector is drained by opening simultaneously two normally-closed ASCO red-cap solenoid valves depending on the vertical location of the liquid level within the collector. The solenoid valve located in the bottom of the collector, when energized, drains the collector. The solenoid valve located on top of the collector injects nitrogen to counteract the loss of pressure when the bottom solenoid valve opens. Two HITECH technologies SONOCONTROL ultrasonic liquid level sensors are mounted vertically on the outside of the liquid collector to detect the position of the liquid level within the collector. The distance between the two sensors is 3 ¼ inch which controls a volume of liquid of approximately 110 cm³ within the collector.

The interface between the solenoid valves and the ultrasonic sensors includes two PKK-312 type 2 current controlled switches and a differential level switch. One current controlled switch powers the lower ultrasonic sensor whereas the other current controlled switch powers the upper ultrasonic sensor. Two LED lights indicate the change in ultrasonic signal when the liquid reaches the top or bottom sensor. Both current controlled switches are connected to a differential level switch, which energized and/or de-energized the solenoid valves depending on the vertical position of the liquid within the collector.

Gas flowing from the cyclonic separator is directed to a small transparent pressure gauge. A second-stage separation is needed because of the insufficient separation between the gas and the liquid in the cyclonic separator. Separation of liquid and gas is essentially performed by impact of the gas on the wall of the pressure gauge. The bottom connection of the pressure gauge is connected with the liquid collector to allow the remaining liquid to accumulate in the liquid collector. The top connection of the pressure gauge is connected to the back-pressure regulator. The material of construction of the pressure gauge is stainless steel 316.

Hydrochloric acid is a by-product of the hydrogenation of the aromatic sulfonyl chloride. Gas flowing from the back-pressure regulator enters a 500 cm³ glass scrubber, which contains a sodium hydroxide solution with a concentration of 2 mol/l. After passing the purification unit and removal of the hydrochloric acid, the flow of gas is directed to a gas chromatograph (GC) for analysis of its content or vented through the fume hood.

3.2 Experimental Procedure and Gathering of Kinetic Data

3.2.1 Continuous Mode

The annular section of the basket is filled with 12.03 grams of 1 wt % palladium on carbon catalyst from Sigma Aldrich catalog number 205753-100G. A silane treated glass wool is placed on top of the basket in the annular section to avoid any loss of the catalyst during the reaction. After installation of the basket in the reactor, the vessel body is installed in the flange ring and the O-ring seal is placed into the body seal groove. Closure of the reactor is performed with the EZE-seal pressure vessel head and the socket head cap screws previously lubricated with Jet-Lube SS-30 pure copper anti-seize. The inlet gas and liquid lines are connected to the appropriate bottom connections in the reactor.

The liquid collector is thereafter filled with approximately 60 cm³ of toluene for proper circulation of the flows of gas and liquid in the downstream section of the hydrogenation unit.

The unit is blanketed first with nitrogen and a leak test is performed by checking the rate of decrease of the pressure within the unit. If no decrease of pressure is observed within 15 minutes, the mixture of gas containing hydrogen and argon is fed to the reactor overnight with the appropriate hydrogen to argon gas feed ratio.

The reaction conditions and parameters used to investigate the catalytic hydrogenation of the aromatic sulfonyl chloride into the aromatic thiol are presented in Table 3.1.

Table 3.1 Reaction conditions in continuous process for the hydrogenation of 2,5-dimethylbenzene sulfonyl chloride

Process temperature	85, 97 and 110 °C
Process pressure	364.7 psia
Agitation speed	950 RPM
Average liquid residence time (approximation)	0.6*, 1.0, 1.5, 2.0, 3.1 hr
Hydrogen to aromatic sulfonyl chloride ratio	8
Hydrogen to argon gas feed ratio	3
Type of catalyst	1 wt% Pd on charcoal
Mass of catalyst	12.03 g
Bulk Density of catalyst	0.55 g/cm ³
Catalyst size	2.8 to 3.35 mm (6-7 mesh)
Liquid feed composition	5 wt% sulfonyl chloride in toluene
Liquid feed density at room temperature	0.879 g/cm ³

* Only at a process temperature of 110 °C

Five different residence times θ of the liquid within the reactor have been investigated for each of the process temperatures listed in Table 3.1. Fresh catalyst is used for each experiment.

The next day, the experiment is started by turning on the liquid metering pump and feeding pure toluene to the reactor with a flowrate of $25 \text{ cm}^3/\text{min}$ with the mixture of hydrogen and argon flowing through the hydrogenation unit. At the same time, the heating jacket and the agitator are turned on and the reactor is brought to the desired process temperature. The volumetric flowrate of toluene is changed to a specified experimental liquid volumetric flowrate when the liquid level rises in the high-pressure transparent liquid gauge. At this moment, toluene has reached the downstream section of the unit and, therefore, the reactor is full of liquid. Toluene is fed until the reactor stabilizes at the desired experimental conditions. It takes approximately 35 to 40 minutes to bring the reactor to the reaction conditions.

Before feeding the organic liquid mixture, toluene accumulated during the stabilization of the reactor is removed from the liquid collector. The feed is switched to the glass bottle container containing a 5 wt % aromatic sulfonyl chloride in toluene by directing the liquid flow with a three-way valve. Process time is taken equal to zero when the liquid mixture reaches the liquid bottom connection of the reactor. Samples of liquid accumulated in the collector are collected at different interval of process time in a small vial.

Improvements in the operating procedures and gathering of the kinetic data include a change in the sampling method for the experiments conducted at process temperatures of 85 and 97 °C. In these experiments, samples are taken every hour by opening manually the top and bottom needle valves installed with the liquid collector. The solenoid valves are disconnected during these experiments. However, experiments conducted at a process temperature of 110 °C are performed with the automatic

operation of the two solenoid valves. Opening manually the needle valves to obtain liquid samples from the collector increases the frequency of the data collection and thus monitors more accurately the catalyst activity during the hydrogenation of the aromatic sulfonyl chloride.

Reaching steady state operation of the reactor is of particular concern during the time of an experiment. Steady state operation of the reactor is normally approached when the process time equal to three to five times the residence time of the liquid within the reactor, whatever the order of the reaction [66]. Therefore, for all experiments, the hydrogenation reaction was conducted more than three times the residence time of the liquid within the reactor.

The hydrogenation unit is shut down by turning off the liquid metering pump and closing the inlet liquid and gas lines with the appropriate plug valves. The heating jacket and agitator are turned off as well. After depressurization of the unit, both bottom connections of the reactor are opened and the content of the reactor is collected into a flask. Cleaning of the reactor and the basket is performed by using tap water and acetone. Appropriate safety precautions such as face shields, face mask, long sheets etc., are taken to protect the operator during emptying of the reactor.

3.2.2 Semi-batch Mode

The purpose of the hydrogenation batch mode reaction is to investigate the reactivity of several aromatic sulfonyl chlorides: 2,5-dimethylbenzene sulfonyl chloride, benzene sulfonyl chloride, p-chlorobenzene sulfonyl chloride.

The procedure described in the continuous mode to charge the basket with the catalyst and closure of the reactor is the same. The reactor is blanketed with nitrogen at 350 psig by opening the needle valve located in the inlet gas line. The purpose is to

remove air from the reactor and check for any leaks. This needle valve is thereafter kept closed. The reactor is charged with a liquid mixture of 5 wt% aromatic sulfonyl chloride in toluene by turning on the liquid metering pump. It takes about 10 minutes to charge the reactor at a liquid flowrate of $25 \text{ cm}^3/\text{min}$. The needle valve located in the outlet of the reactor is reopened during the operation of the liquid pump to remove the nitrogen previously used to purge the reactor. The pump is turned off when liquid flows from the back-pressure regulator indicating that the reactor is full of liquid.

The gas is switched to the hydrogen line by directing the flow of gas with a three-way valve. The reactor is purged with hydrogen by opening the needle valve located in the gas inlet line. The needle valve located in the outlet line is reopened to let hydrogen flow out of the reactor during the purge. Some liquid flows at the same time from the back-pressure regulator during the hydrogen purge meaning that the reactor will not be operated full of liquid during the batch reaction.

After closing both needle valves (inlet and outlet lines), the heating jacket is turned on as well as the agitator. During the stabilization of the reactor at the experimental conditions, the heating jacket is turned off when the process temperature reaches $85 \text{ }^\circ\text{C}$ to avoid excessive overshooting in the process temperature setpoint of $110 \text{ }^\circ\text{C}$. With this method, the process temperature reaches a maximum at $115 \text{ }^\circ\text{C}$ and decreases to $110 \text{ }^\circ\text{C}$ with the heating jacket turned off. The heating jacket is turned back on at a process temperature of $112 \text{ }^\circ\text{C}$ to control the process temperature at the appropriate setpoint. During the heating process, an increase of pressure has been noticed due mainly to the increase of the vapor pressure of toluene (solvent). The needle valve located in the outlet line is opened when the process pressure is greater than 355 psig. This valve remains closed otherwise.

It takes 30 minutes to stabilize the reactor at a process temperature of 110 °C. Due to the consumption of hydrogen, the pressure swing method is used to maintain the reactor at a pressure of 350 psig \pm 5 psig. The needle valve located in the inlet line is opened anytime the reaction pressure falls below 345 psig. This valve remains closed otherwise. No consumption of hydrogen is observed after 3 hours of operation. The hydrogenation reaction is maintained for an additional 5 hours with a total reaction time of 8 hours.

An increase of the reactor pressure has been observed after 4 hours of reaction time, which corresponds to one hour after discontinuing the hydrogen feed, and until the end of the reaction. Therefore, the needle valve located in the outlet line needs to be opened during the hydrogenation reaction due to the increase of the process pressure. Vapor pressure of toluene and the formation of hydrogen sulfide (H₂S) and HCl are eventually responsible for the increase of the process pressure. After 8 hours of operation, the heating jacket and agitator are turned off. The reactor is depressurized and its content is collected in a flask and analyzed by GC/MS.

3.3 Analytical Procedure

3.3.1 On-line Gas Analysis

A gas chromatograph (GC) GOW-MAC series 550 with a thermal conductivity detector (TCD) is used to analyze on-line the content of the gas flowing from the purification unit. A manual gas sampling valve allows the injection of approximately 400 μ l of gas into a packed column mole sieve 13X 80/100. The gas chromatograph settings are as follows: the carrier gas is nitrogen with a flowrate of 30 cm³/min and head pressure of 50 psig, the oven temperature is 70 °C, the injector temperature is 120 °C, the detector temperature is 120 °C and the detector power setting is 150 mA. To ensure

reproducibility of the gas analysis, five to eight injections are performed in the GC and the composition of the gas phase is averaged.

To calibrate gas standard mixtures, known fractions of pure hydrogen and argon were mixed and fed to the gas chromatograph by means of the mass flow meters. Samples were injected ten times into the GC and areas for each peak were averaged. Six different fraction levels were used. The calibration was completed by plotting the mole ratio of hydrogen to argon versus the area ratio of hydrogen to argon. The response factor for hydrogen is determined from the slope of the curve.

3.3.2 Off-line Liquid Analysis

A gas chromatograph HP G1800C series with an electron ionization detector is used to analyze off-line the effluent organic liquid phase collected in the downstream section. A 1 μl injection with a microsyringe is performed for each analysis of the liquid phase. The content of the syringe is injected into a HP-5 crosslinked 5% phenylmethyl silicone capillary column. The length of the column is 30 m, the diameter of the column is 0.25 mm and the film thickness is 0.25 μm . The gas chromatograph provides sample separation and the detector generates retention time and abundance information. The detector gives also mass spectral (MS) data for each component of the sample. One injection is performed to determine the content of the effluent organic liquid phase.

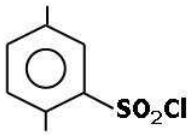
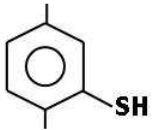
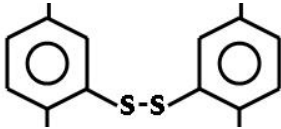
The gas chromatograph settings are as follows: the carrier gas is helium with a flowrate of 0.68 cm^3/min and a head pressure of 50 psig, the injector temperature is 200 $^\circ\text{C}$, the detector temperature is 280 $^\circ\text{C}$ and the split ratio is 50/1.

The temperature program is as follows: the initial temperature of the oven is 50 °C and it is held for 5 minutes after injection of the sample into the capillary column. During this period of time, the detector is turned off to avoid analysis of toluene which can damage the filament in the detector when a large amount of toluene is injected. Thereafter, there is a 10 °C/minute heating rate until the temperature of the oven reaches 280 °C. This temperature is held during 15 minutes. The total time for the analysis of a sample is 43 minutes.

Calibration of the gas chromatograph for the aromatic sulfonyl chloride, aromatic disulfide and aromatic thiol is necessary in order to determine the amount of each compound in an unknown sample. Based on Figure 2.1 in section 2.1, toluene is, obviously, resistant to the hydrogenation in the temperature range used for the experiments, and can be used as a tie-compound for the liquid phase.

To calibrate compound j, five different mole ratio levels of sulfur-based compound j to toluene were prepared with a FISCHER XA-200DS analytical balance and injected into the GC. The calibration was completed by plotting the mole ratio of the sulfur-based compound j to toluene versus the area of sulfur-based compound j. Table 3.2 shows the calibration constants obtained. Calibration constants for the sulfur-based aromatic compounds were determined each time the MS detector was tuned. Liquid samples collected at the process temperatures of 85 and 97 °C were analysed with the same tuning of the MS detector. The MS detector was retuned for the analysis of the liquid samples collected at a process temperature of 110 °C.

Table 3.2 Calibration constants of the aromatic sulfur-based compounds for the gas chromatograph HP G1800 C

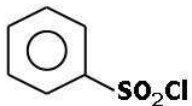
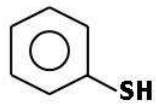
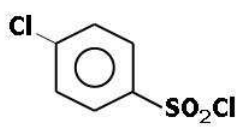
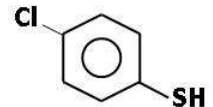
Chemical name	Chemical structure	Molecular weight (g/mol)	Calibration constants: 110 °C experiment	Calibration constants: 85 °C and 97 °C experiments
2,5-dimethylbenzene sulfonyl chloride		204.68	$1.07 \cdot 10^{-9}$	$1.12 \cdot 10^{-9}$
2,5-dimethylbenzene thiol		138.23	$7.28 \cdot 10^{-10}$	$7.84 \cdot 10^{-10}$
Bis(2,5-dimethylphenyl) disulfide		274.45	$1.21 \cdot 10^{-9}$	$1.83 \cdot 10^{-9}$

Since Bis(2,5-dimethyl phenyl)thiosulfone compound is not available commercially, a rough estimate of the calibration constant h was performed from the calibration of S-phenyl benzenethiosulfonate 99 % purity obtained from Aldrich. A calibration constant of $2.43 \cdot 10^{-9}$ has been found for S-phenyl benzenethiosulfonate. A 12 % increase in the calibration constant between the phenyl disulfide and bis(2,5-dimethylphenyl)disulfide reflects the substitution of the four methyl groups in the aromatic ring. Applying the same percentage increase between the unsubstituted and substituted aromatic thiosulfones, a calibration constant of $2.72 \cdot 10^{-9}$ has been estimated for Bis(2,5-dimethyl phenyl)thiosulfone. The method used to estimate the calibration constant h for the bis(2,5-dimethyl phenyl)thiosulfone is as follows:

$$h_{\text{substituted thiosulfone}} = \left(\frac{h_{\text{substituted disulfide}} - h_{\text{unsubstituted disulfide}}}{h_{\text{substituted disulfide}}} \right) \times 100 \times h_{\text{unsubstituted thiosulfone}} \quad (3.1)$$

Table 3.3 shows the calibration constants obtained for other aromatic sulfur-based compounds.

Table 3.3 Calibration constants of several aromatic sulfur-based compounds for the gas chromatograph HP G1800 C

Chemical name	Chemical structure	Molecular weight (g/mol)	Calibration constants
Benzene sulfonyl chloride		176.62	$1.12 \cdot 10^{-9}$
Benzene thiol		110.18	$1.07 \cdot 10^{-9}$
p-chlorobenzene sulfonyl chloride		211.07	$2.67 \cdot 10^{-9}$
p-chlorobenzene thiol		144.62	$1.01 \cdot 10^{-9}$

3.4 Calculation Methods

3.4.1 Liquid Phase

The overall reaction is shown in Figure 3.7.

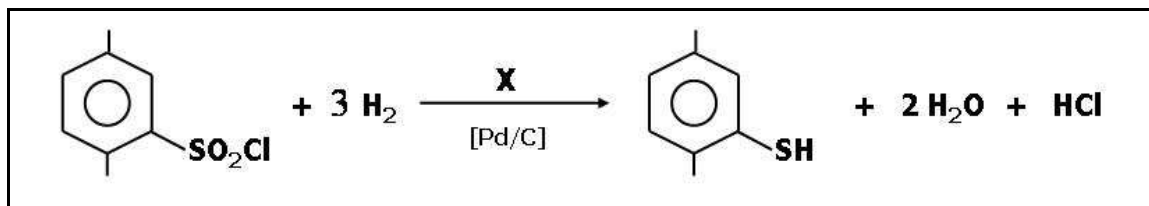


Figure 3.7 Overall hydrogenation reaction of the aromatic sulfonyl chloride

The reactions involved in the hydrogenation sequence of the aromatic sulfonyl chloride are presented in Figure 3.8.

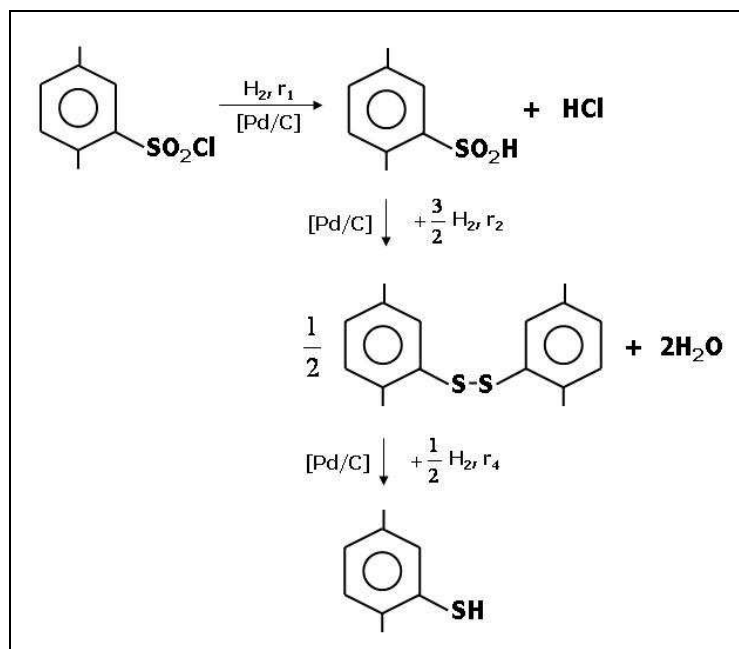


Figure 3.8 Reaction scheme of the catalytic hydrogenation of the aromatic sulfonyl chloride

The reactions involved in the dehydration sequence of the aromatic sulfinic acid are presented in Figure 3.9.

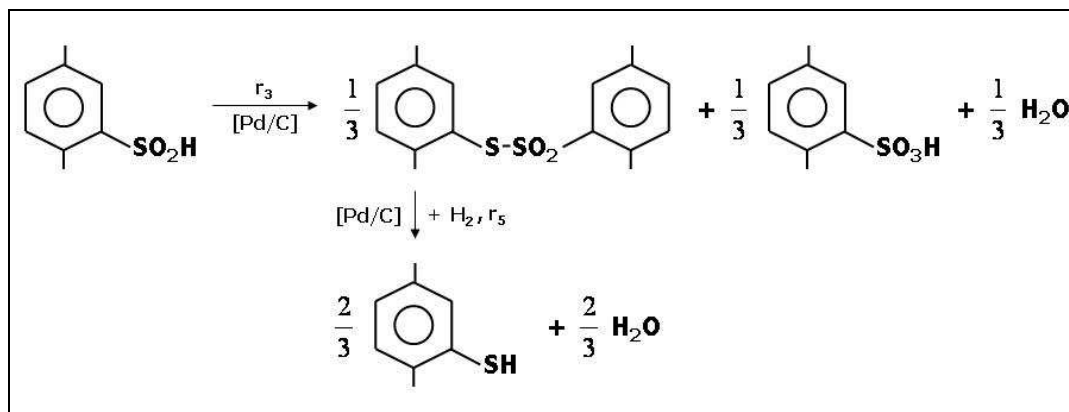


Figure 3.9 Reaction scheme of the dehydration of the aromatic sulfinic acid

The overall conversion of the aromatic sulfonyl chloride X is defined as:

$$X = \frac{F_{SC}^0 - F_{SC}}{F_{SC}^0} \quad (3.2)$$

The molar yield of the aromatic sulfonyl chloride into the aromatic disulfide Y_1 is determined by:

$$Y_1 = \frac{F_{DS}}{\frac{1}{2} F_{DS}^0} \quad (3.3)$$

and the molar yield of the aromatic sulfonyl chloride into the aromatic thiol Y_2 is calculated as following:

$$Y_2 = \frac{F_{THIOL}}{F_{SC}^0} \quad (3.4)$$

The molar yield of the aromatic sulfonyl chloride into the aromatic thiosulfone Y_3 is determined by:

$$Y_3 = \frac{F_{TS}}{\frac{1}{3}F_{SC}^0} \quad (3.5)$$

where F_{SC}^0 is the inlet molar flowrate of the aromatic sulfonyl chloride ($kmol/hr$), $F_{sulfonyl}$, F_{DS} , F_{TS} and F_{THIOL} are the outlet molar flowrates of the aromatic sulfonyl chloride ($kmol/hr$), aromatic disulfide, aromatic thiosulfone and aromatic thiol, respectively.

The molar flowrates of the aromatic sulfonyl chloride, aromatic disulfide, aromatic thiosulfone and aromatic thiol in the outlet of the reactor are determined by using toluene as a tie component and analysis of the liquid phase, by injecting the liquid phase into the GC/MS detector.

The total outlet molar flowrate of the aromatic sulfur-based compounds F_t ($kmol/hr$) is determined by:

$$F_t = F_{SC} + F_{DS} + F_{TS} + F_{THIOL} \quad (3.6)$$

and the concentration of the aromatic sulfur-based compound j ($kmol/m^3$) in the liquid mixture accumulated in the collector is calculated by:

$$C_j = \frac{F_j}{V_{T,liq}} \quad (3.7)$$

with j referring to the aromatic sulfonyl chloride, aromatic disulfide, aromatic thiosulfone and aromatic thiol and $V_{T,liq}$ is the outlet liquid volumetric flowrate (m^3/hr).

The molar density of the effluent liquid mixture, $C_{S,total}$, containing toluene and the aromatic sulfur-based compounds is calculated from:

$$C_{S,total} = \frac{F_{toluene}^0 + \sum_j F_j}{V_{T,liq}} \quad (3.8)$$

with j referring to the aromatic sulfur-based compounds, F_j the outlet molar flowrate of compound j ($kmol/hr$), $F_{toluene}^0$ the inlet molar flowrate of toluene ($kmol/hr$) and $V_{T,liq}$ the volumetric flowrate of the liquid (m^3/hr) leaving the reactor.

The outlet liquid volumetric flowrate $V_{T,liq}$ calculation is based on the change of density of the liquid mixture due to the reaction conditions (essentially the process temperature), the mass flowrate \dot{m}_t (kg/hr) of the liquid mixture, the mole fractions $x_{toluene}$ and x_j as well as the molecular weights $Mw_{toluene}$ and Mw_j ($kg/kmol$) of toluene and each aromatic sulfur-based compound j . The calculation of $V_{T,liq}$ is presented in Equations 3.9 to 3.13.

The densities of pure toluene and the liquid feed mixture, containing a 5 wt% aromatic sulfonyl in toluene, at room temperature (23 °C) and measured with a hydrometer are 866 kg/m^3 and 879 kg/m^3 , respectively. Since the difference of density is small (1.5 %), the unknown liquid mixture density ρ_L containing the aromatic sulfur-based compounds and toluene is assumed to be approximately equal to the density of pure toluene $\rho_{toluene}$ at the reaction conditions. The same assumption is applied to estimate other thermophysical properties of the liquid mixture, such as surface tension and viscosity, within the reactor at the reactions conditions.

$$x_j = \frac{F_j}{F_t + F_{toluene}^0} \quad (3.9)$$

$$x_{toluene} = \frac{F_{toluene}^0}{F_t + F_{toluene}^0} \quad (3.10)$$

$$Mw_{liquid} = (x_{toluene} Mw_{toluene}) + \sum_j x_j Mw_j \quad (3.11)$$

$$\dot{m}_t = (F_t + F_{toluene}^0) Mw_{liquid} \quad (3.12)$$

$$V_{T,liq} \approx \frac{\dot{m}_t}{\rho_{toluene}} \quad (3.13)$$

To back-calculate the concentration of the aromatic sulfur-based compound j in the outlet stream of the reactor from the concentration of the aromatic sulfur-based compound j determined in Equation 3.7 after draining the liquid collector, the following material balance in the liquid collector should be applied as represented in Figure 3.10.

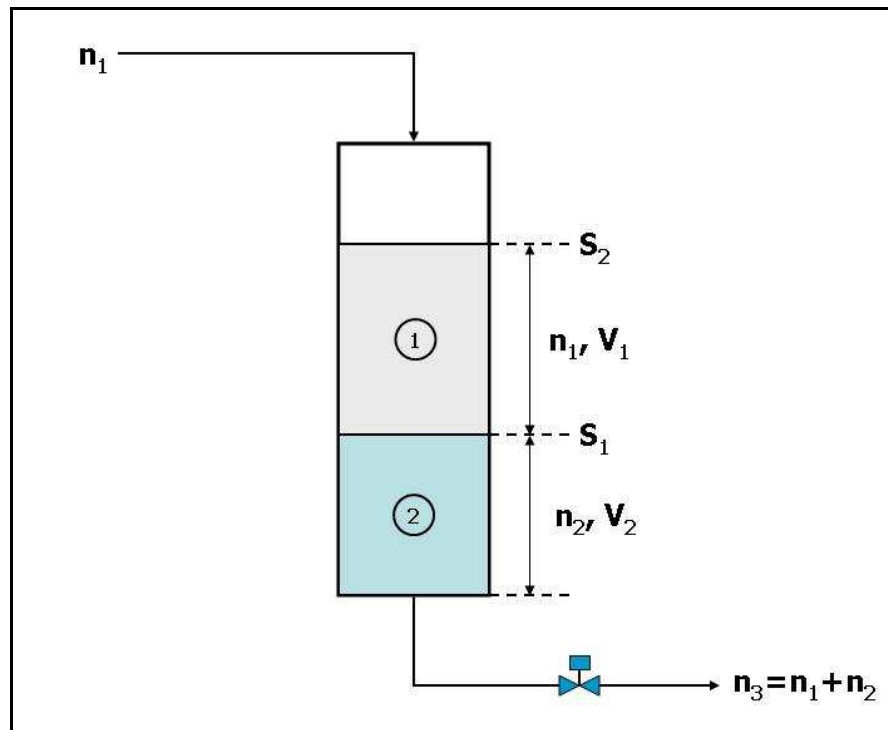


Figure 3.10 Material balance applied to the liquid collector

Assuming complete mixing between the liquid mixture (1) flowing from the reactor and accumulated into the collector and the liquid mixture (2) remaining after draining the collector, the concentration of the aromatic sulfur-based compound j ($kmol/m^3$) C_1 in the outlet stream of the reactor is determined by:

$$C_1 = \frac{C_3(V_1 + V_2) - C_2 V_2}{V_1} \quad (3.14)$$

with C_3 the concentration of an aromatic sulfur-based compound j determined from Equation 3.7, C_2 the concentration of the aromatic sulfur-based compound j remaining after draining the liquid collector ($kmol/m^3$) and V_2 equal to 60 cm^3 . V_1 is determined by:

$$V_1 = V_{T,liq} \times \Delta t \quad (3.15)$$

with Δt the time elapsed (hr) between the accumulation of the liquid mixture into the collector and drainage of the collector for analysis of the liquid mixture into the GC/MS detector. Since n_1 is the number of moles of the reacting species accumulated during the period Δt in the collector, C_1 represents the concentration of the reacting species in the outlet stream of the reactor at the average process time of $(t_n + t_{n+1})/2$.

The residence time of the liquid θ within the reactor (hr) is defined as:

$$\theta = \frac{V_L}{V_{T,liq}} \quad (3.16)$$

with V_L the volume of liquid within the reactor (m^3) and $V_{T,liq}$ the outlet liquid volumetric flowrate (m^3/hr).

The volume of liquid V_L within the reactor is approximately determined from:

$$V_L \approx \left(V_{reactor} - V_{basket} - V_{catalyst} \right) \times (1 - \varepsilon) \quad (3.17)$$

$$V_L \approx V \times (1 - \varepsilon) \quad (3.18)$$

with $V_{reactor}$ the volume of the reactor (m^3), V_{basket} the volume occupied by the basket (m^3), $V_{catalyst}$ the volume occupied by the catalyst (m^3), ε the gas holdup within the reactor (m^3/m^3) and V the true volume of the liquid corrected from the volume occupied by the basket V_{basket} and the volume occupied by the catalyst $V_{catalyst}$ (m^3). The volume of the basket V_{basket} has been estimated to 40 cm^3 by Autoclave Engineer. The volume of the catalyst $V_{catalyst}$ is calculated from the information given in Table 3.1 and it has been estimated to be 21.8 cm^3 .

Table 3.4 shows the density, surface tension and viscosity of the liquid organic mixture within the reactor, approximated from the thermophysical properties given for toluene [13, 14], at each process temperature. The gas holdup ε within the reactor is determined from the Calderbank correlation given in Equation 2.7 of section 2.2. The volume of liquid V_L calculated from Equation 3.17 is listed at all the residence times and process temperatures in Tables 3.5 to 3.7.

Table 3.4 Approximated thermophysical properties of the liquid phase within the reactor at each process temperature

Process temperature (°C)	ρ_L (kg/m^3)	σ_L (kg/s^2)	μ_L ($Pa.s$)
85	$8.07 \cdot 10^2$	$2.07 \cdot 10^{-2}$	$3.12 \cdot 10^{-4}$
97	$7.94 \cdot 10^2$	$1.94 \cdot 10^{-2}$	$2.75 \cdot 10^{-4}$
110	$7.88 \cdot 10^2$	$1.80 \cdot 10^{-2}$	$2.50 \cdot 10^{-4}$

Table 3.5 Power injected in the liquid, total superficial gas velocity, gas and liquid holdup within the reactor at process temperature of 85 °C

θ (hr)	P/V (W/m^3)	V_S (m^3/m_r^2s)	ε (m^3/m^3)	V_L (cm^3)
1.0	$6.91 \cdot 10^5$	$1.12 \cdot 10^{-4}$	0.047	226.80
1.5	$6.91 \cdot 10^5$	$7.6 \cdot 10^{-5}$	0.038	228.93
2.0	$6.91 \cdot 10^5$	$5.61 \cdot 10^{-5}$	0.033	230.28
3.1	$6.91 \cdot 10^5$	$3.65 \cdot 10^{-5}$	0.026	231.88

Table 3.6 Power injected in the liquid, total superficial gas velocity, gas and liquid holdup within the reactor at process temperature of 97 °C

θ (hr)	P/V (W/m^3)	V_S (m^3/m_r^2s)	ε (m^3/m^3)	V_L (cm^3)
1.0	$6.91 \cdot 10^5$	$1.16 \cdot 10^{-4}$	0.050	226.21
1.5	$6.91 \cdot 10^5$	$7.84 \cdot 10^{-5}$	0.041	228.45
2.0	$6.91 \cdot 10^5$	$5.80 \cdot 10^{-5}$	0.035	229.87
3.1	$6.91 \cdot 10^5$	$3.78 \cdot 10^{-5}$	0.028	231.54

Table 3.7 Power injected in the liquid, total superficial gas velocity, gas and liquid holdup within the reactor at process temperature of 110 °C

θ (hr)	P/V (W/m^3)	V_S (m^3/m_r^2s)	ε (m^3/m^3)	V_L (cm^3)
0.6	$6.91 \cdot 10^5$	$2.1 \cdot 10^{-4}$	0.072	220.98
1.0	$6.91 \cdot 10^5$	$1.2 \cdot 10^{-4}$	0.053	225.42
1.5	$6.91 \cdot 10^5$	$8.11 \cdot 10^{-5}$	0.043	227.80
2.0	$6.91 \cdot 10^5$	$6.0 \cdot 10^{-5}$	0.037	229.29
3.1	$6.91 \cdot 10^5$	$3.9 \cdot 10^{-5}$	0.030	231.08

Autoclave Engineer documentation for stirred reactor [67] shows an average static torque T_o of 16 inch-lbs (1.8 N-m) for the type of agitator installed with the Robinson-Mahoney stationary basket reactor. To determine the horsepower hp at a certain agitation speed N (RPM), Equation 3.19 is applied.

$$hp = \frac{T_o \times N}{63025} \quad (3.19)$$

and the power dissipated by the agitator per unit volume of the liquid, P/V , in the Calderbank correlation, is evaluated.

3.4.2 Gas Phase

The conversion of hydrogen X_{H_2} in the gas phase is defined by:

$$X_{H_2} = \frac{F_{H_2}^0 - F_{H_2}}{F_{H_2}^0} \quad (3.20)$$

with $F_{H_2}^0$ equal to the inlet molar flowrate ($kmol/hr$) of hydrogen. The flowrate of hydrogen, F_{H_2} in the outlet of the reactor is determined by using argon as a tie component and analyzing the gas phase by using a gas chromatograph with a thermo-conductivity detector. Argon is used as an internal standard for the gas phase. For calibration purposes, an arbitrary value of 1 can be assigned as the value of the response factor for argon. A response factor of 0.1119 ± 0.002 has been found for hydrogen.

The fraction of hydrogen in the gas phase y_{H_2} is calculated based on the area of hydrogen A_{H_2} and argon A_{Ar} obtained by integration of the peaks in the gas chromatogram as well as the response factor Rf for each compound:

$$y_{H_2} = \frac{(Rf)_{H_2} \times A_{H_2}}{(Rf)_{H_2} \times A_{H_2} + (Rf)_{Ar} \times A_{Ar}} \quad (3.21)$$

The fraction of argon y_{Ar} in the gas phase is determined by:

$$y_{Ar} = 1 - y_{H_2} \quad (3.22)$$

The following equations can be established for the gas mixture:

$$F_{t\,mix} = F_{H_2} + F_{Ar} \quad (3.23)$$

$$F_{H_2} = y_{H_2} \times F_{t\,mix} \quad (3.24)$$

$$F_{Ar} = y_{Ar} \times F_{t\,mix} \quad (3.25)$$

with F_{H_2} , the outlet molar flowrate of hydrogen ($kmol/hr$), F_{Ar} the outlet molar flowrate of argon ($kmol/hr$) and $F_{t\,mix}$ the total outlet molar flowrate of the gas mixture ($kmol/hr$).

Since argon is defined as an internal standard, the inlet molar flowrate of argon is equal to the outlet molar flowrate of argon:

$$F_{Ar} = F_{Ar}^0 \quad (3.26)$$

The total outlet molar flowrate of the gas mixture is calculated as follows:

$$F_{t\,mix} = \frac{F_{Ar}}{y_{Ar}} \quad (3.27)$$

and the outlet molar flowrate of hydrogen is found by:

$$F_{H_2} = y_{H_2} \times F_{t\,mix} \quad (3.28)$$

The total pressure within the reactor is given by:

$$P_{reactor} = P_{H_2} + P_{Ar} + P_{toluene} + \sum_j P_j \quad (3.29)$$

with P_{H_2} the partial pressure of hydrogen (Pa), P_{Ar} the partial pressure of argon (Pa), $P_{toluene}$ the partial pressure of toluene (Pa) and j referring to the aromatic sulfur-based compounds.

The total pressure measured within the reactor is assumed to be represented essentially by the partial pressures of hydrogen P_{H_2} and argon P_{Ar} :

$$P_{reactor} \cong P_{H_2} + P_{Ar} \quad (3.30)$$

Thermodynamic equilibrium between the gas and liquid phases is assumed for the calculation of the hydrogen concentration in the liquid phase. The gas-liquid and liquid-solid mass transfer resistances presented in Figure 2.3 of section 2.2 for hydrogen

and the reacting species are negligible due to the high turbulence in the liquid created by the agitator within the reactor. From Figure 2.2 in section 2.1, the mole fraction of hydrogen dissolved in toluene $x_{H_2,liq}$ at a given temperature is calculated by:

$$x_{H_2,liq} = K \times P_{H_2} \quad (3.31)$$

with K the solubility constant (Pa^{-1}), and P_{H_2} the partial pressure of hydrogen within the reactor (Pa).

The solubility constant of hydrogen dissolved in toluene at the process temperatures of 85, 97 and 110 °C and a process pressure within the reactor of 364.7 psia is listed in Table 3.8.

Table 3.8 Solubility constant K of hydrogen dissolved in toluene at process temperatures of 85, 97, 110 °C

Temperature (°C)	K (Pa ⁻¹)
85	4.53 10 ⁻⁰⁹
97	4.87 10 ⁻⁰⁹
110	5.02 10 ⁻⁰⁹

The concentration of hydrogen in the liquid phase $C_{H_2,liq}$ is:

$$C_{H_2,liq} = x_{H_2,liq} C_{S,total} \quad (3.32)$$

with $x_{H_2,liq}$ the fraction of hydrogen dissolved in toluene and $C_{S,total}$ the molar density of the effluent organic mixture calculated from Equation 3.8 ($kmol/m^3$).

Including Equation 3.31 in Equation 3.32, the concentration of hydrogen $C_{H_2,liq}$ ($kmol/m^3$) in the effluent organic phase becomes:

$$C_{H_2,liq} = K \times P_{H_2} C_{S,total} \quad (3.33)$$

The partial pressure of hydrogen P_{H_2} is calculated assuming ideal gas:

$$P_{H_2} = C_{H_2,gas} RT \quad (3.34)$$

with R the gas constant ($m^3 Pa/kmol \cdot K$) and T the process temperature (K). The concentration of hydrogen in the gas phase $C_{H_2,gas}$ is calculated from:

$$C_{H_2,gas} = \frac{F_{H_2,gas}}{V_{T,gas}} \quad (3.35)$$

with $F_{H_2,gas}$ the outlet molar flowrate of hydrogen ($kmol/hr$) and $V_{T,gas}$ the volumetric flowrate of the gas leaving the reactor (m^3/hr).

Assuming that the gas phase is only composed of hydrogen and argon and the vapor pressures of toluene and the aromatic sulfur-based compounds are negligible, the outlet volumetric flowrate of the gas leaving the reactor $V_{T, gas}$ is calculated as following:

$$V_{T, gas} = \frac{\left(F_{H_2, gas} + F_{Ar, gas} \right) RT}{P_{reactor}} \quad (3.36)$$

with $F_{H_2, gas}$ and $F_{Ar, gas}$ the outlet molar flowrate of hydrogen and argon ($kmol/hr$), respectively, R the gas constant ($m^3 Pa/kmol \cdot K$), T the reaction temperature (K) and P the process pressure (Pa).

Finally, the concentration of hydrogen in the liquid phase $C_{H_2, liq}$ is calculated as following:

$$C_{H_2, liq} = K \times \frac{F_{H_2, gas}}{V_{T, gas}} R \times T \times C_{S, total} \quad (3.37)$$

CHAPTER IV

EXPERIMENTAL RESULTS

4.1 Hydrogenation of Toluene

Most of the catalytic hydrogenations of the aromatic sulfonyl chlorides were conducted in solvent such as toluene, benzene or tetrahydrofuran (THF) [6, 9, 10, 15, 57]. One important aspect to take into account to be defined as a good solvent is that it should be resistant to the hydrogenation reaction. Figure 4.1 shows the thermodynamic equilibrium between toluene and methyl cyclohexane in the presence of hydrogen:

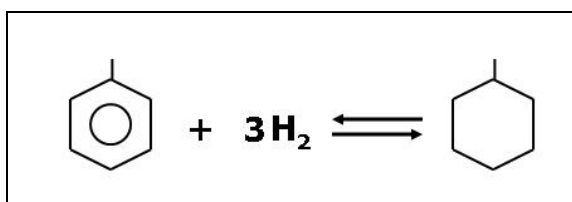


Figure 4.1 Thermodynamic equilibrium between toluene and methylcyclohexane in the presence of hydrogen

Makar'ev et al [12] investigated the hydrogenation of toluene using a palladium on zeolite support at process pressure of 40 atm. In the range of temperatures from 100 °C to 200 °C, as shown in Figure 2.1 of section 2.1, they determined that the formation of methylcyclohexane dominates and no cyclohexane is formed. The formation of cyclohexane from the demethylation of methylcyclohexane is initiated only at temperatures above 200 °C. Furthermore, the hydrogenation of toluene into methylcyclohexane can be assumed negligible at temperatures equal to and less than 110 °C.

Calibration of the gas chromatograph for the aromatic sulfonyl chloride, aromatic disulfide, aromatic thiosulfone and aromatic thiol is necessary in order to determine the amount of each compound in an unknown sample. Based on Figure 2.1 of section 2.1, toluene is, obviously, resistant to the hydrogenation in the temperature range used for the experiments, and can be used as a tie-compound for the liquid phase.

The purpose of this section is to verify that toluene is resistant to the hydrogenation reaction and can be effectively used as a tie-compound for the liquid phase. The experiment was carried out at the highest process temperature, 110 °C, in continuous process. Since the equilibrium constant between toluene and methylcyclohexane is dependent upon the temperature, hydrogenation of toluene should not occur at temperatures of 85 and 97 °C; if no hydrogenation of toluene is observed at 110 °C.

Toluene and hydrogen were fed only to the reactor. The gas and liquid phases were analysed periodically to verify that consumption of hydrogen and formation of methylcyclohexane do not occur during the experiment. Table 4.1 shows the reaction conditions applied during the hydrogenation of toluene.

Table 4.1 Reaction conditions for the hydrogenation of toluene

Process temperature	110 °C
Process pressure	364.7 psia
Agitation speed	950 RPM
Averaged liquid residence time (approximation)	0.62 hr
Toluene to hydrogen feed ratio	0.12
Hydrogen to argon gas feed ratio	3.47
Type of catalyst	1 wt% Pd on charcoal
Mass of catalyst	12.03 g
Density of catalyst	0.55 g/cm ³
Catalyst size	2.8 to 3.35 mm (6-7 mesh)
Liquid feed composition	Pure toluene
Liquid feed density at room temperature	0.866 g/cm ³

Figure 4.2 shows the outlet molar flow rate of toluene:

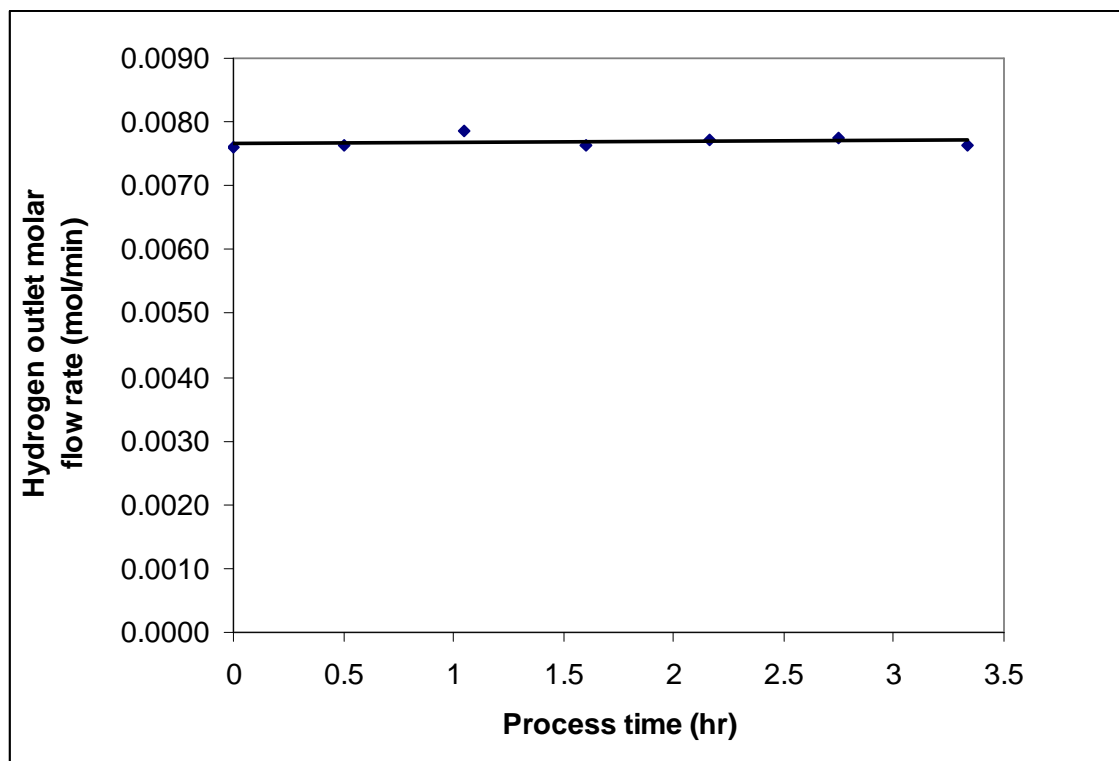


Figure 4.2 Hydrogen outlet molar flow rate during the hydrogenation of toluene.

$T = 110\text{ }^{\circ}\text{C}$, $P = 364.7\text{ psia}$ and liquid residence time of 0.62 hr

The outlet flowrate of hydrogen remains constant during the experiment and therefore no consumption of hydrogen occurs. Furthermore, methylcyclohexane formation is not observed by analysis of the liquid phase, which was also observed in the experimental work of Makar'ev et al [12]. The hydrogenation treatment of toluene at a process temperature of $110\text{ }^{\circ}\text{C}$ and at a 2 hr-residence time of the liquid within the reactor was also conducted and no formation of methylcyclohexane was observed. Therefore, toluene is not hydrogenated at a temperature of $110\text{ }^{\circ}\text{C}$ and, it can be used as a tie-compound for the liquid phase during the hydrogenation of aromatic sulfonyl chloride.

4.2 Catalytic Hydrogenation of 2,5-Dimethylbenzene Sulfonyl Chloride into Thiophenol in Continuous Process Mode

The experimental procedure is the same as the one described in section 3.2.1. The catalytic hydrogenation of the aromatic sulfonyl chloride was conducted using a 1 wt% palladium on charcoal at three different temperatures: 85, 97 and 110 °C and five different residence times θ : 0.6 (only at 110 °C), 1.0, 1.5, 2.0 and 3.1 hr. The process pressure is 364.7 psia and the following molar ratios were used:

$F_{H_2}^0 / F_{sulfonyl}^0 = 8.0 \text{ mol/mol}$, $F_{H_2}^0 / F_{Ar}^0 = 3.0 \text{ mol/mol}$ during the catalytic

hydrogenation.

The overall conversions of the aromatic sulfonyl chloride (SC), X, and hydrogen (H_2), XH_2 , as well as the molar yield of the aromatic sulfonyl chloride into the aromatic disulfide (DS), Y_1 , the molar yield of the aromatic sulfonyl chloride into the aromatic thiol (THIOL), Y_2 and the molar yield of the aromatic sulfonyl chloride into the aromatic thiosulfone (TS), Y_3 , with respect to process time at all the residence times and process temperatures investigated, are shown in Figures 4.3. to 4.17.

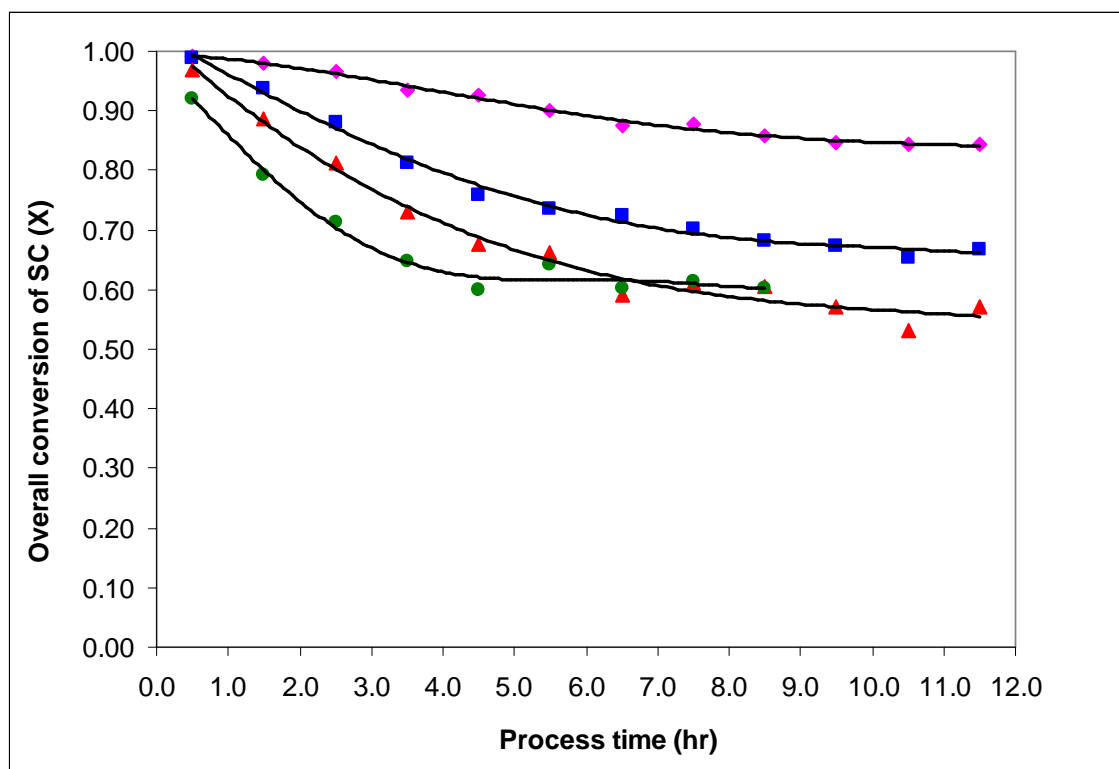


Figure 4.3 Overall conversion of the aromatic sulfonyl chloride (SC) X with respect to process time at residence times θ : 1.0 (●), 1.5 (▲), 2.0 (■) and 3.1 hr (◆), process temperature: 85 °C, process pressure: 364.7 psia, $F_{H_2}^0 / F_{sulfonyl}^0 = 8.0 \text{ mol/mol}$,

$$F_{H_2}^0 / F_{Ar}^0 = 3.0 \text{ mol/mol}$$

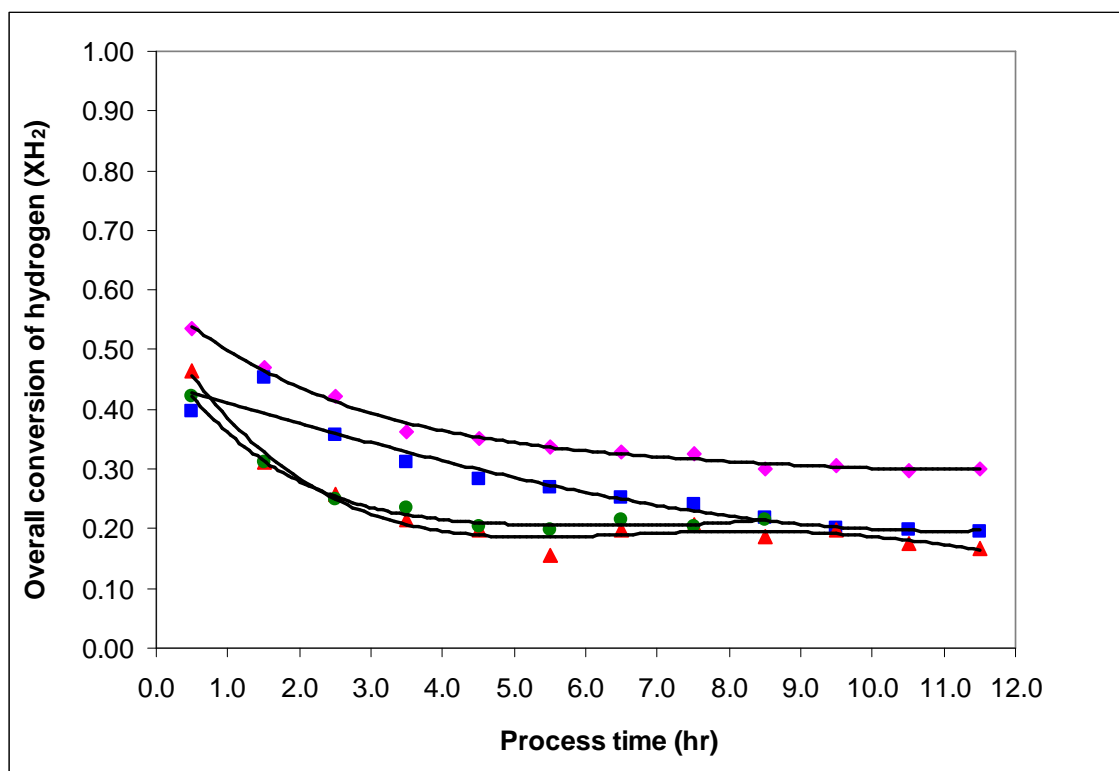


Figure 4.4 Overall conversion of hydrogen XH₂ with respect to process time at residence times θ : 1.0 (●), 1.5 (▲), 2.0 (■) and 3.1 hr (◆), process temperature: 85 °C, process pressure: 364.7 psia, $F_{H_2}^0 / F_{sulfonyl}^0 = 8.0 \text{ mol/mol}$, $F_{H_2}^0 / F_{Ar}^0 = 3.0 \text{ mol/mol}$

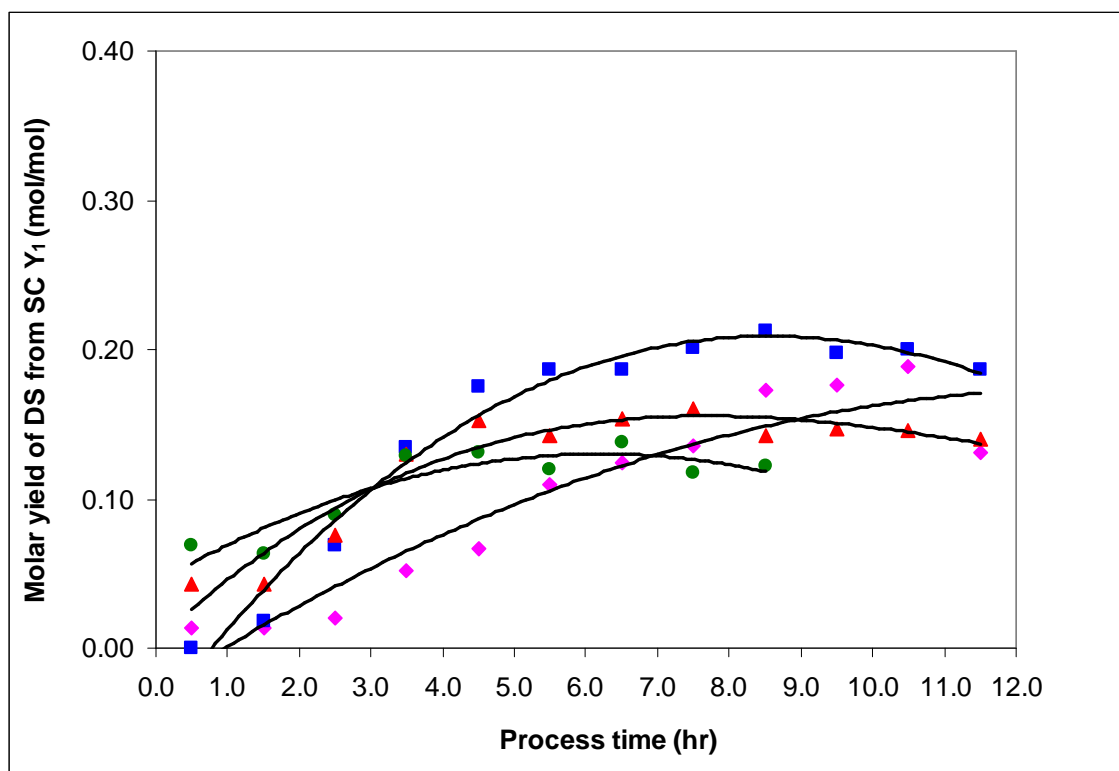


Figure 4.5 Molar yield of the aromatic disulfide (DS) Y_1 from the aromatic sulfonyl chloride (SC) with respect to process time at residence times θ : 1.0 (●), 1.5 (▲), 2.0 (■) and 3.1 hr (◆), process temperature: 85 °C, process pressure: 364.7 psia,

$$F_{H_2}^0 / F_{sulfonyl}^0 = 8.0 \text{ mol/mol}, F_{H_2}^0 / F_{Ar}^0 = 3.0 \text{ mol/mol}$$

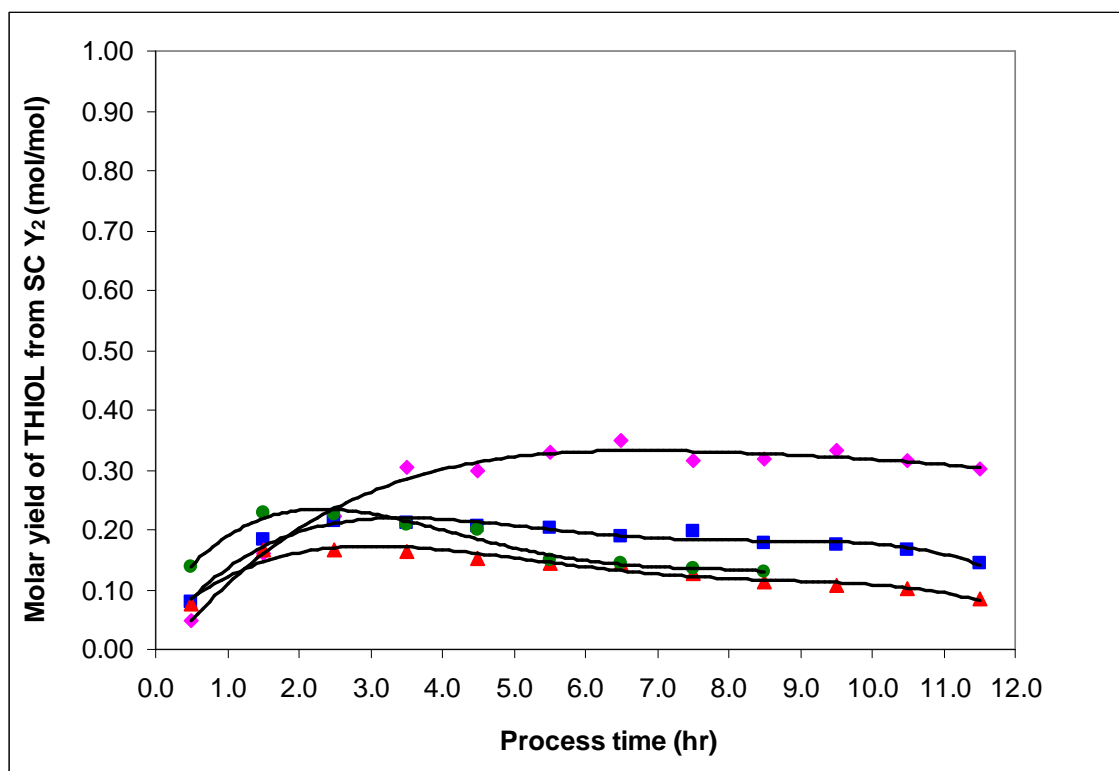


Figure 4.6 Molar yield of the aromatic thiol (THIOL) Y_2 from the aromatic sulfonyl chloride (SC) with respect to process time at residence times θ : 1.0 (●), 1.5 (▲), 2.0 (■) and 3.1 hr (◆), process temperature: 85 °C, process pressure: 364.7 psia,

$$F_{H_2}^0 / F_{sulfonyl}^0 = 8.0 \text{ mol / mol}, F_{H_2}^0 / F_{Ar}^0 = 3.0 \text{ mol / mol}$$

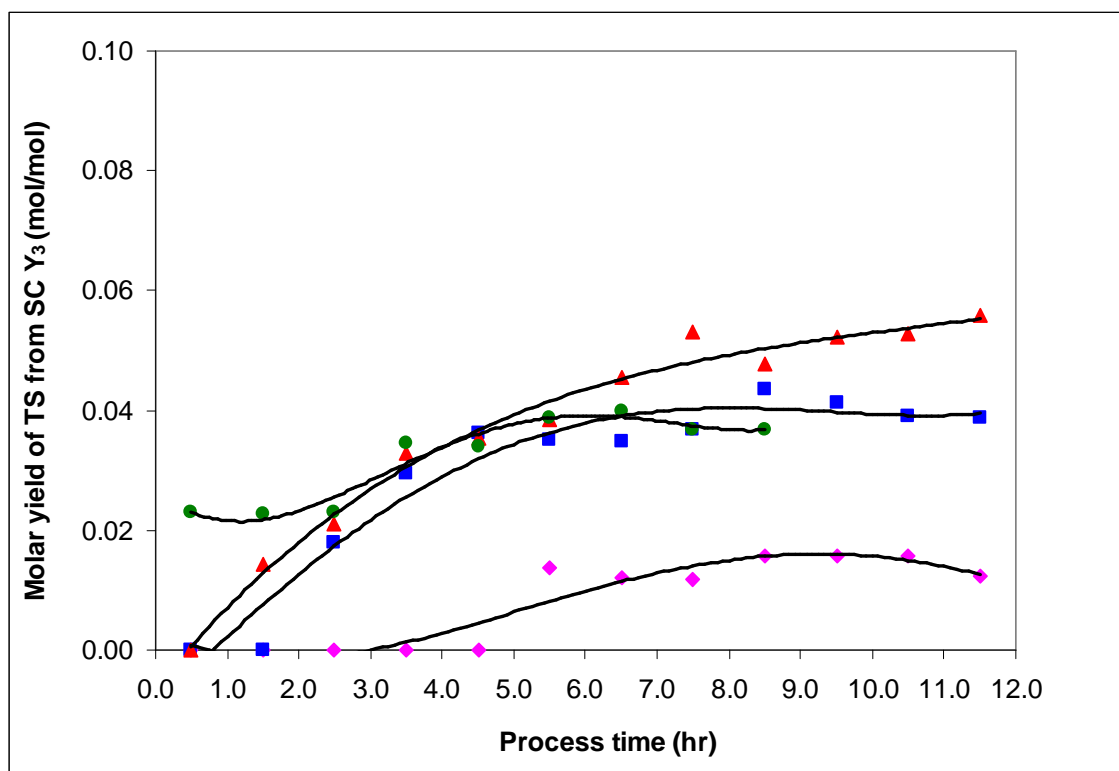


Figure 4.7 Molar yield of the aromatic thiosulfone (TS) Y_3 from the aromatic sulfonyl chloride (SC) with respect to process time at residence times θ : 1.0 (●), 1.5 (▲), 2.0 (■) and 3.1 hr (◆), process temperature: 85 °C, process pressure: 364.7 psia,

$$F_{H_2}^0 / F_{sulfonyl}^0 = 8.0 \text{ mol/mol}, F_{H_2}^0 / F_{Ar}^0 = 3.0 \text{ mol/mol}$$

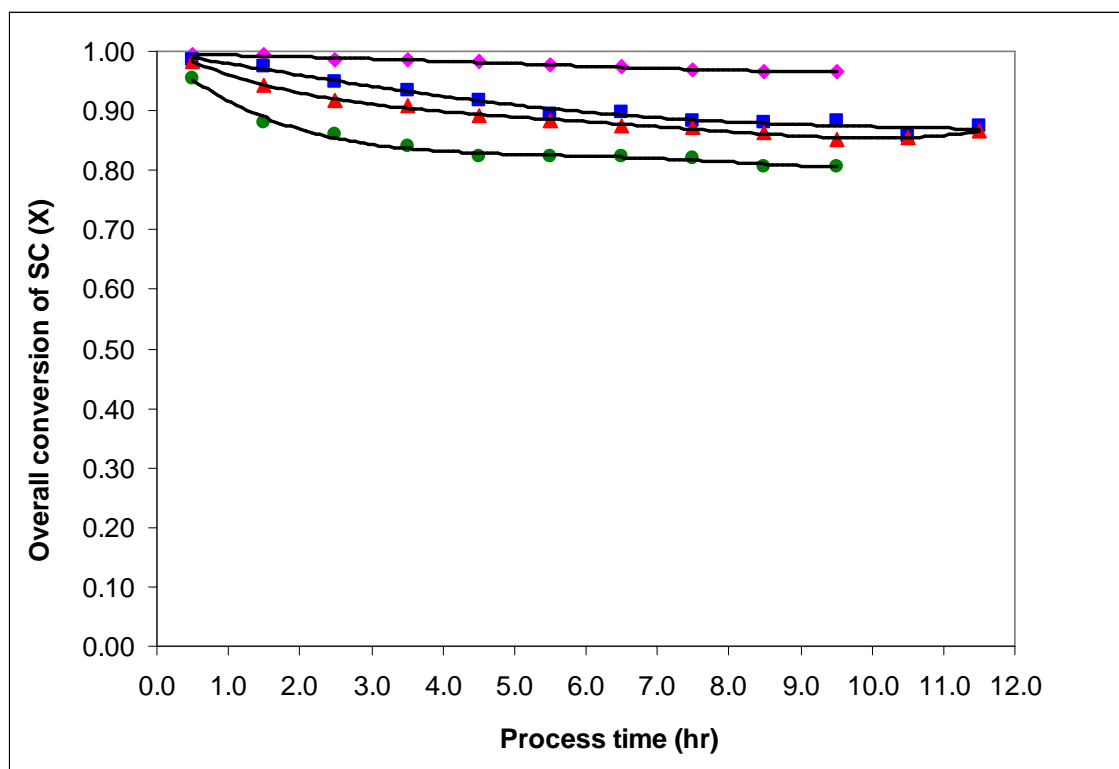


Figure 4.8 Overall conversion of the aromatic sulfonyl chloride (SC) X with respect to process time at residence times θ : 1.0 (●), 1.5 (▲), 2.0 (■) and 3.1 hr (◆), process temperature: 97 °C, process pressure: 364.7 psia, $F_{H_2}^0 / F_{sulfonyl}^0 = 8.0 \text{ mol/mol}$,

$$F_{H_2}^0 / F_{Ar}^0 = 3.0 \text{ mol/mol}$$

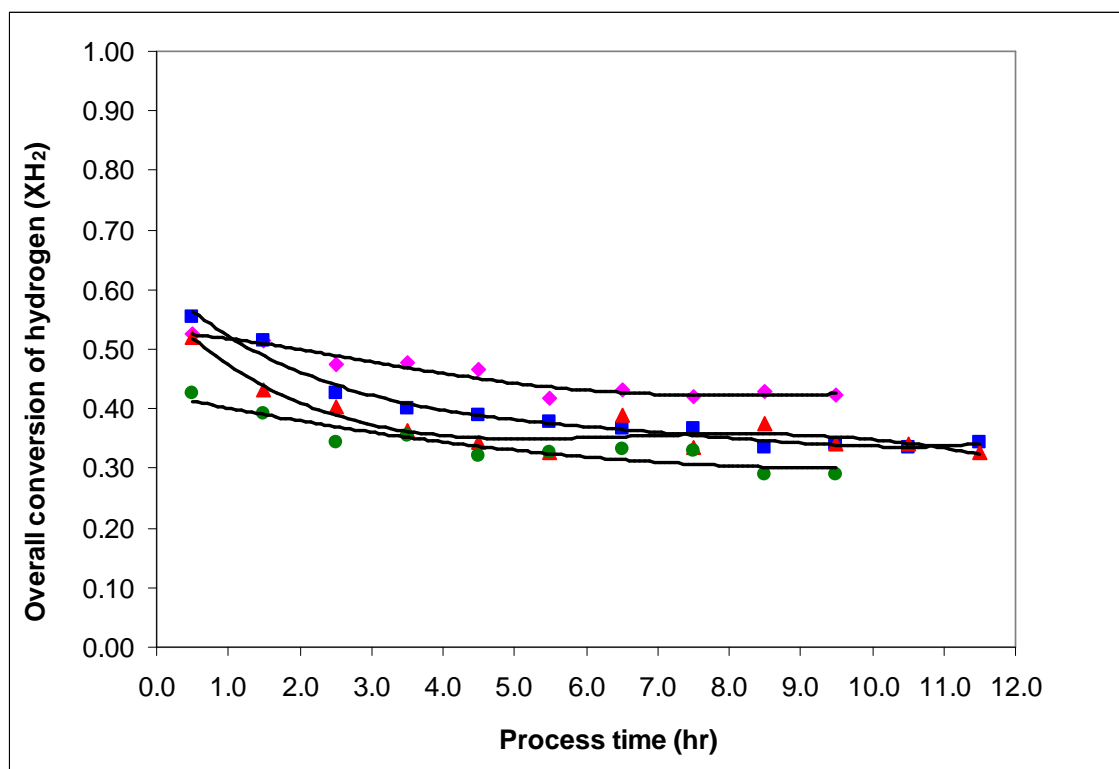


Figure 4.9 Overall conversion of hydrogen XH₂ with respect to process time at residence times θ : 1.0 (●), 1.5 (▲), 2.0 (■) and 3.1 hr (◆), process temperature: 97 °C, process pressure: 364.7 psia, $F_{H_2}^0 / F_{sulfonyl}^0 = 8.0 \text{ mol/mol}$, $F_{H_2}^0 / F_{Ar}^0 = 3.0 \text{ mol/mol}$

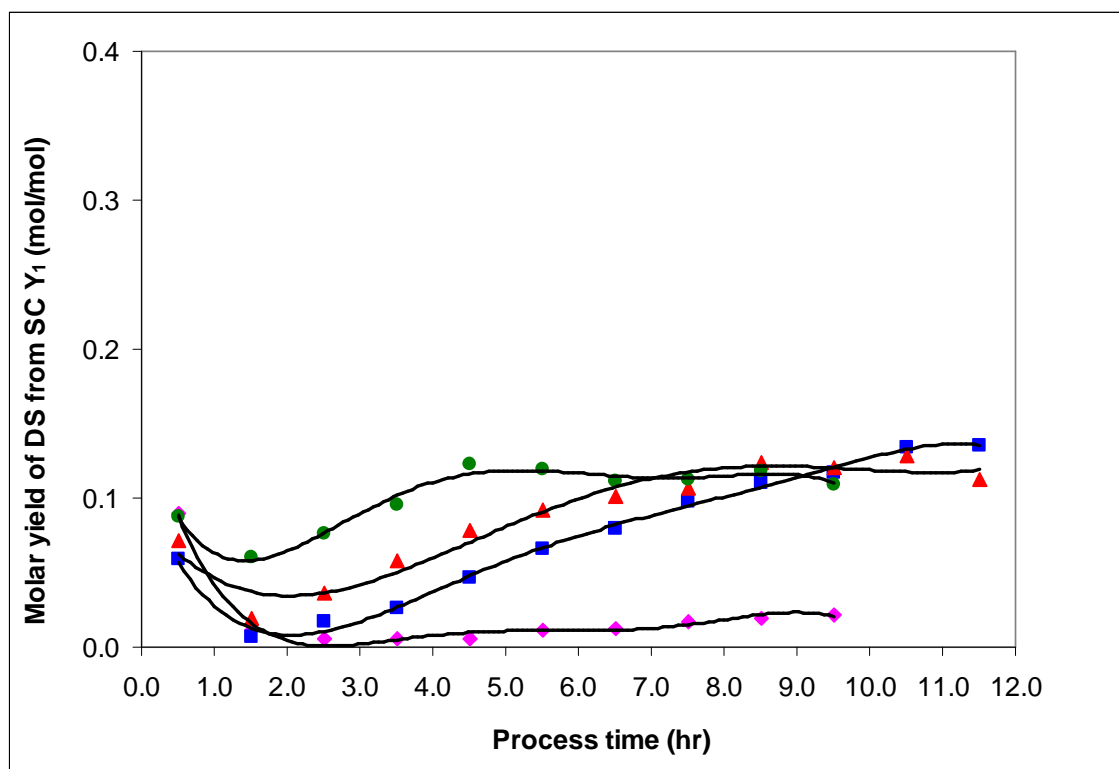


Figure 4.10 Molar yield of the aromatic disulfide (DS) Y_1 from the aromatic sulfonyl chloride (SC) with respect to process time at residence times θ : 1.0 (●), 1.5 (▲), 2.0 (■) and 3.1 hr (◆), process temperature: 97 °C, process pressure: 364.7 psia,

$$F_{H_2}^0 / F_{sulfonyl}^0 = 8.0 \text{ mol/mol}, F_{H_2}^0 / F_{Ar}^0 = 3.0 \text{ mol/mol}$$

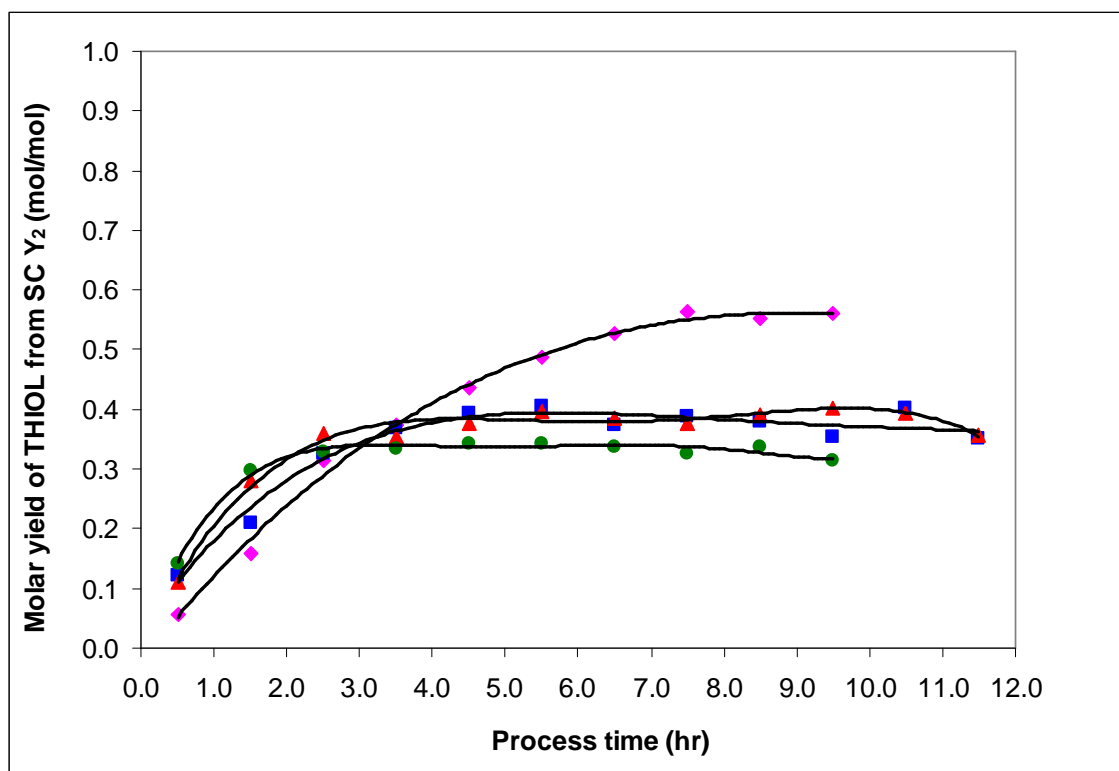


Figure 4.11 Molar yield of the aromatic thiol (THIOL) Y_2 from the aromatic sulfonyl chloride (SC) with respect to process time at residence times θ : 1.0 (●), 1.5 (▲), 2.0 (■) and 3.1 hr (◆), process temperature: 97 °C, process pressure: 364.7 psia,

$$F_{H_2}^0 / F_{sulfonyl}^0 = 8.0 \text{ mol / mol}, F_{H_2}^0 / F_{Ar}^0 = 3.0 \text{ mol / mol}$$

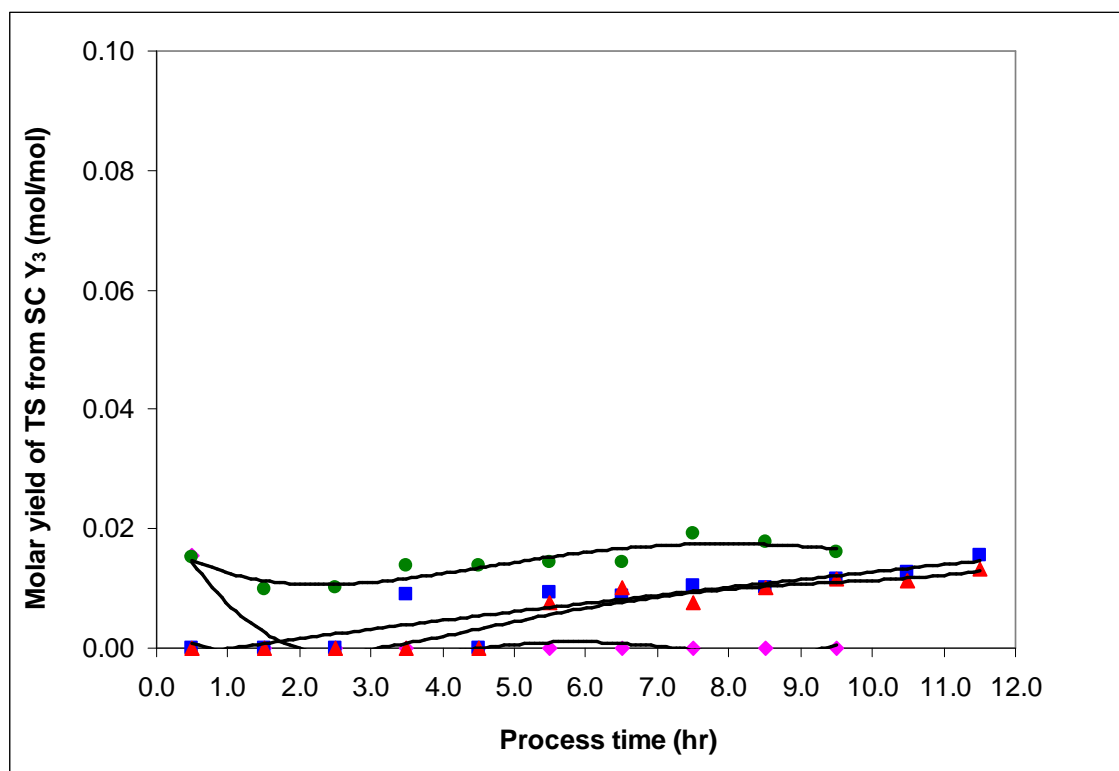


Figure 4.12 Molar yield of the aromatic thiosulfone (TS) Y_3 from the aromatic sulfonyl chloride (SC) with respect to process time at residence times θ : 1.0 (●), 1.5 (▲), 2.0 (■) and 3.1 hr (◆), process temperature: 97 °C, process pressure: 364.7 psia,

$$F_{H_2}^0 / F_{sulfonyl}^0 = 8.0 \text{ mol/mol}, F_{H_2}^0 / F_{Ar}^0 = 3.0 \text{ mol/mol}$$

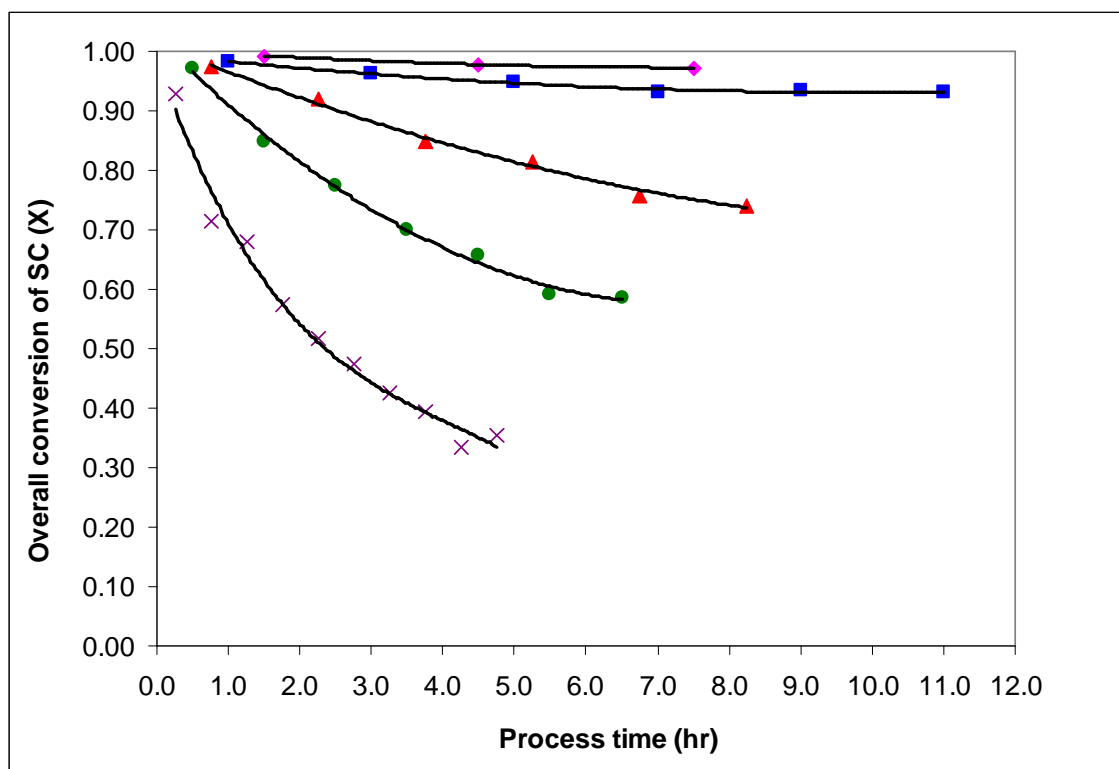


Figure 4.13 Overall conversion of the aromatic sulfonyl chloride (SC) X with respect to process time at residence times θ : 0.6 (x), 1.0 (•), 1.5 (▲), 2.0 (■) and 3.1 hr (◆), process temperature: 110 °C, process pressure: 364.7 psia,

$$F_{H_2}^0 / F_{sulfonyl}^0 = 8.0 \text{ mol/mol}, F_{H_2}^0 / F_{Ar}^0 = 3.0 \text{ mol/mol}$$

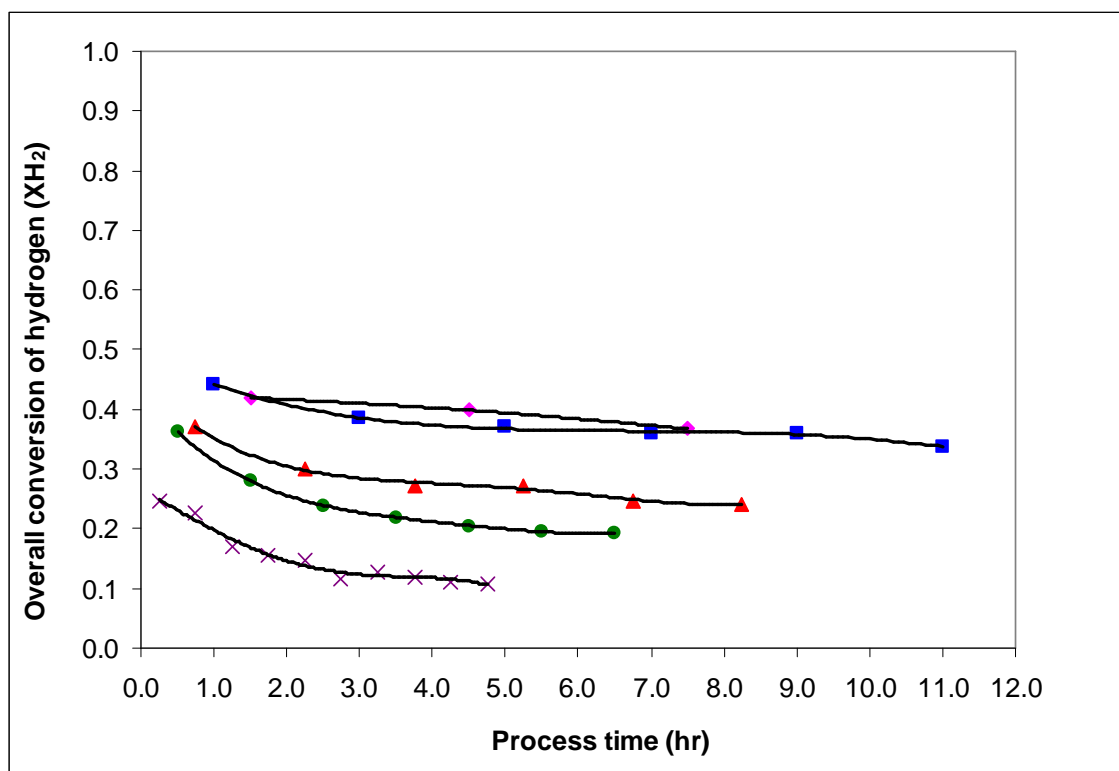


Figure 4.14 Overall conversion of hydrogen X_{H_2} with respect to process time at residence times θ : 0.6 (\times), 1.0 (\bullet), 1.5 (\blacktriangle), 2.0 (\blacksquare) and 3.1 hr (\blacklozenge), process temperature: 110 °C, process pressure: 364.7 psia, $F_{H_2}^0 / F_{sulfonyl}^0 = 8.0 \text{ mol/mol}$,

$$F_{H_2}^0 / F_{Ar}^0 = 3.0 \text{ mol/mol}$$

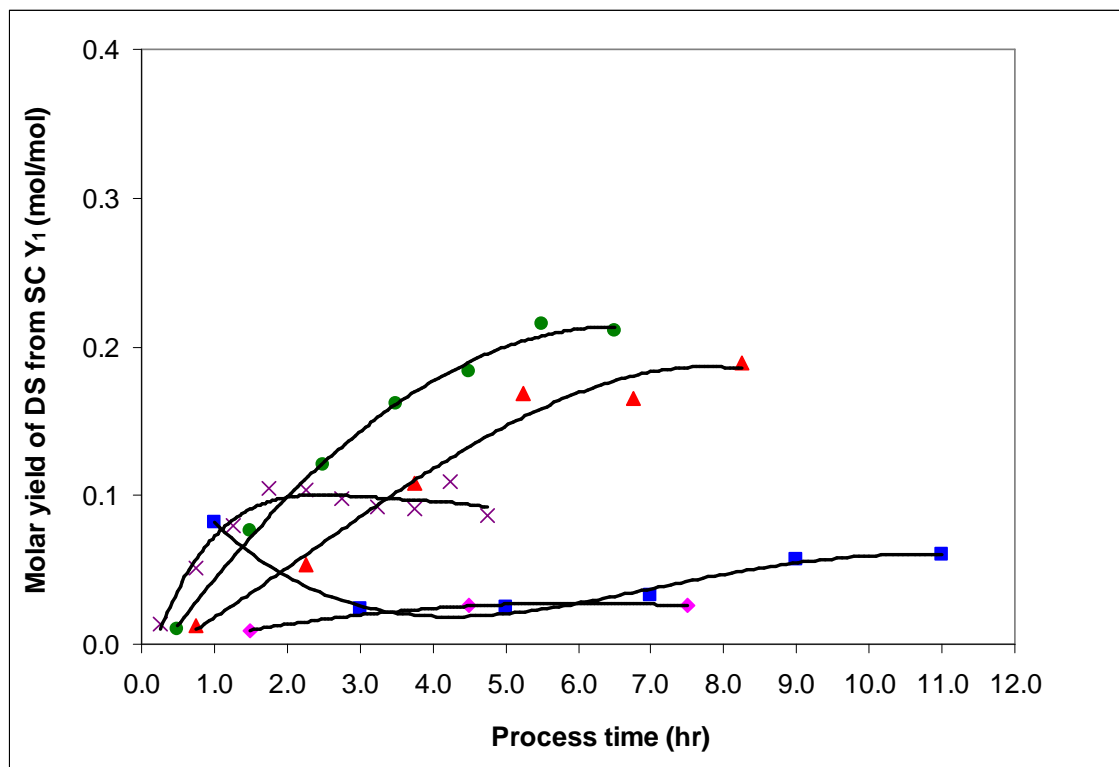


Figure 4.15 Molar yield of the aromatic disulfide (DS) Y_1 from the aromatic sulfonyl chloride (SC) with respect to process time at residence times θ : 0.6 (x), 1.0 (•), 1.5 (▲), 2.0 (■) and 3.1 hr (◆), process temperature: 110 °C, process pressure: 364.7 psia,

$$F_{H_2}^0 / F_{sulfonyl}^0 = 8.0 \text{ mol/mol}, F_{H_2}^0 / F_{Ar}^0 = 3.0 \text{ mol/mol}$$

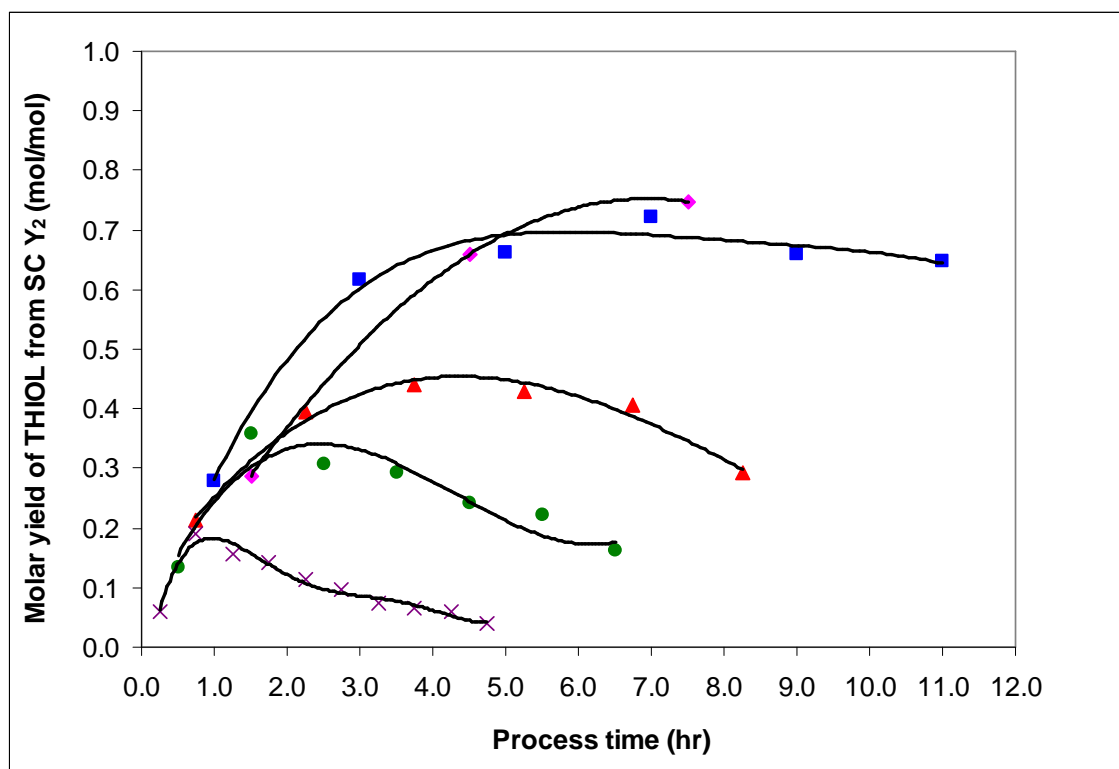


Figure 4.16 Molar yield of the aromatic thiol (THIOL) Y_2 from the aromatic sulfonyl chloride (SC) with respect to process time at residence times θ : 0.6 (x), 1.0 (•), 1.5 (▲), 2.0 (■) and 3.1 hr (◆), process temperature: 110 °C, process pressure: 364.7 psia,

$$F_{H_2}^0 / F_{sulfonyl}^0 = 8.0 \text{ mol/mol}, F_{H_2}^0 / F_{Ar}^0 = 3.0 \text{ mol/mol}$$

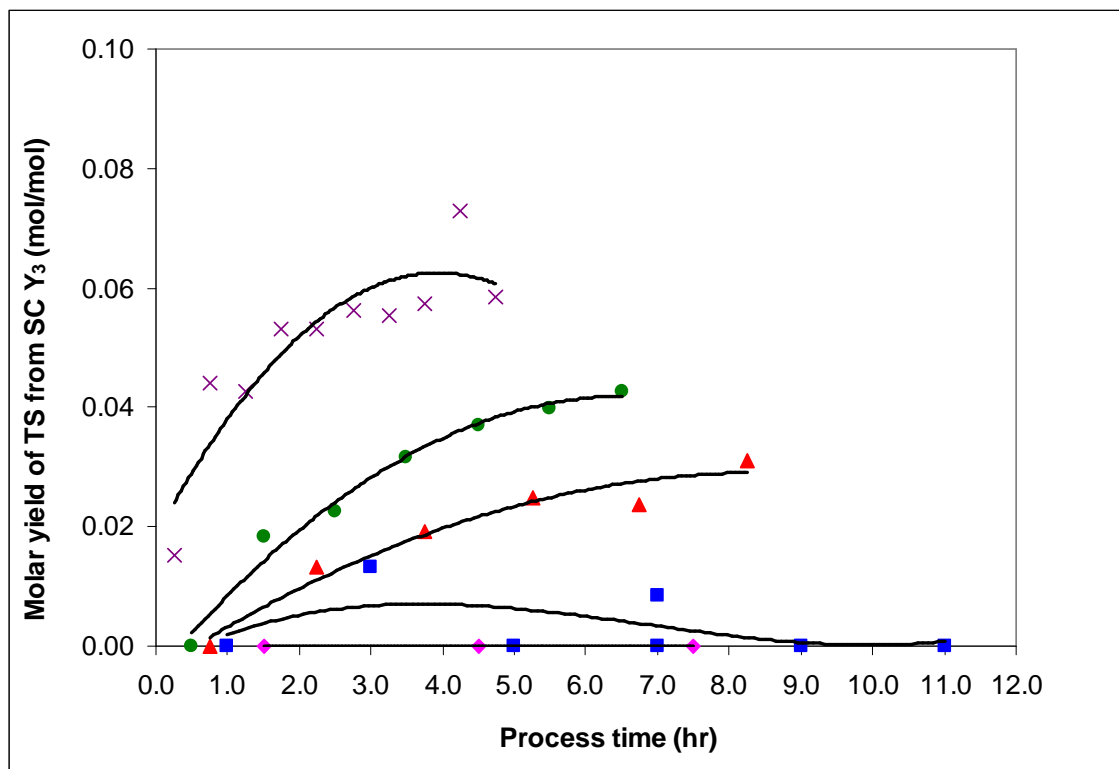


Figure 4.17 Molar yield of the aromatic thiosulfone (TS) Y_3 from the aromatic sulfonyl chloride (SC) with respect to process time at residence times θ : 0.6 (\times), 1.0 (\bullet), 1.5 (\blacktriangle), 2.0 (\blacksquare) and 3.1 hr (\blacklozenge), process temperature: 110 °C, process pressure: 364.7 psia,

$$F_{H_2}^0 / F_{sulfonyl}^0 = 8.0 \text{ mol/mol}, \quad F_{H_2}^0 / F_{Ar}^0 = 3.0 \text{ mol/mol}$$

Only one organic liquid phase was observed after draining the liquid mixture from the collector, which suggests that the water produced during the hydrogenation of the aromatic sulfonyl chloride is soluble in the organic liquid mixture containing toluene and the aromatic sulfur-based compounds. Figure 4.18 shows the solubility of water in toluene at different temperatures [68].

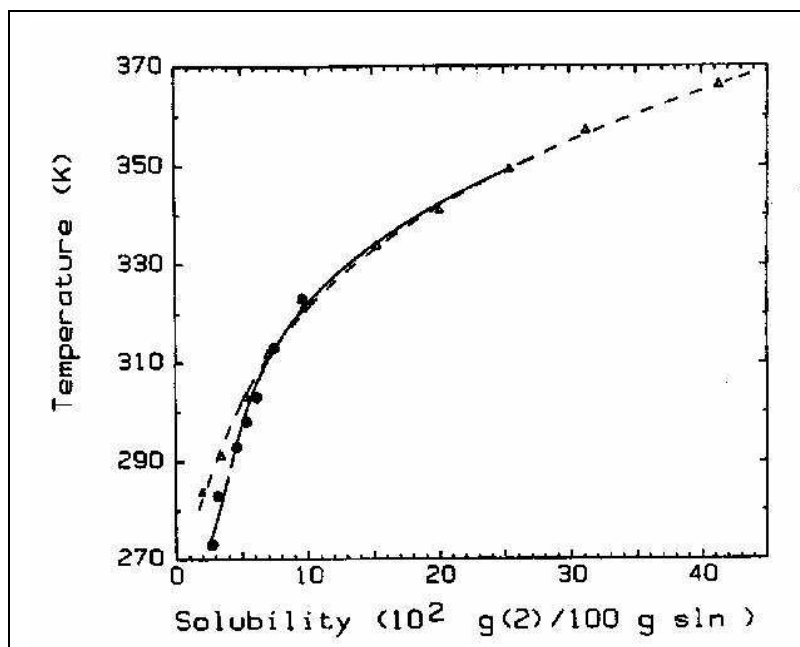


Figure 4.18 Saturated solubility of water in pure toluene at different temperatures [68]

As determined in Figure 4.18, the solubility of water in pure toluene at 85 °C is about 0.33 g of water in 100 g of solution, which represents approximately a fraction of 0.016 of saturated water dissolve in toluene. Higher solubility of water in toluene should be expected at 97 and 110 °C considering the general trend of the solubility curve in Figure 4.18. Based on the stoichiometry of the reaction and the overall hydrogenation of the aromatic sulfonyl chloride at a process temperature of 85 °C, the average fraction of water produced in the liquid organic mixture during the experiments is about 0.0083, which is below the saturated solubility of water in toluene. It is therefore in accordance

with the experiment and the fact that only one liquid phase is observed in the outlet stream of the reactor.

For each of the reaction temperatures investigated, higher overall conversions of the aromatic sulfonyl chloride X and hydrogen XH_2 are obtained by increasing the residence time of the liquid within the reactor. The same trend is observed with the molar yield from the aromatic sulfonyl chloride to the aromatic thiol Y_2 . Higher molar yields of the aromatic disulfide Y_1 from the aromatic sulfonyl chloride and the aromatic thiosulfone Y_3 from the aromatic sulfonyl chloride are obtained by decreasing the residence time of the liquid within the reactor.

Both intermediates aromatic disulfide and aromatic thiosulfone are detected by GC/MS analysis of the effluent organic mixture. According to Figure 2.4 of section 2.5, the presence of the aromatic thiosulfone shows that the dehydrative disproportionation of the aromatic sulfinic acid occurs simultaneously with the hydrogenation sequence. White particles in suspension in the effluent organic phase are also visually observed and can be associated to either the aromatic sulfinic acid or aromatic sulfonic acid. No quantitation has been made due to the complexity of the separation of the white particles from the effluent organic liquid mixture.

For all the residence times and process temperatures investigated, the molar yield of the aromatic disulfide Y_1 is higher than the molar yield of the aromatic thiosulfone Y_3 . One can conclude that the dehydration sequence of the aromatic sulfinic acid is effectively a minor side reaction during the hydrogenation of the aromatic sulfonyl chloride.

Steady state operation of the reactor is normally approached when the process time equal to three to five times the residence time of the liquid within the reactor, whatever the order of the reaction [67]. Short liquid residence time experiments (0.6 and

1 hour at 110 °C) are conducted until the process time reaches seven to ten times the residence time of the liquid within the reactor. At all process temperatures investigated, molar yields Y_1 and Y_3 continuously increase with respect to process time. A decline of the molar yields of the aromatic thiol Y_2 from the aromatic sulfonyl chloride is observed when the process time reaches two to three times the residence time of the liquid within the reactor. One can conclude that steady-state operation of the reactor has never been reached during the event of all the experiments conducted at short residence times. The same trends for the overall conversions of the aromatic sulfonyl chloride and hydrogen and for the molar yields Y_1 , Y_2 and Y_3 are observed by increasing the residence time of the liquid within the reactor and the same conclusions are made. Other factors have to be taken into account in order to explain the reactor not reaching steady-state operation during the event of an experiment.

The conversion and molar yield profiles with respect to process time suggest a deactivation of the 1 wt % palladium on charcoal catalyst. As a result of this catalyst deactivation, a continuous decrease of the overall conversions of the aromatic sulfonyl chloride and hydrogen, a continuous increase of the molar yields Y_1 and Y_3 and a decline of the molar yields Y_2 are observed.

After switching from the pure toluene feed to the liquid mixture containing the 5 wt % aromatic sulfonyl chloride in toluene, the molar yield of the aromatic thiol Y_2 from the aromatic sulfonyl chloride increases to a maximum and thereafter continuously decreases with respect to process time. The maximum observed in the molar yield Y_2 occurs when the process time reaches approximately two to three times the residence time of the liquid within the reactor.

The decline of the molar yield Y_2 is highly correlated with the amount of the aromatic sulfonyl chloride fed to the reactor and the process temperature. At short residence time, meaning high feed molar flowrate, the decline of the molar yield of the

aromatic thiol Y_2 from the aromatic sulfonyl chloride is more pronounced meaning that the intensity of the catalyst deactivation is higher. The decline of the molar yield Y_2 is also more pronounced at elevated temperature. The catalyst deactivation and the intensity of the deactivation is due to the nature of the feed, the aromatic sulfonyl chloride, and the amount of the aromatic sulfonyl chloride fed to the reactor at a given process time.

One can conclude that the catalyst deactivation consists of the formation of a poison (P) from an adsorbed aromatic sulfonyl chloride and palladium free active sites on the surface of the catalyst as shown in Figure 4.19.

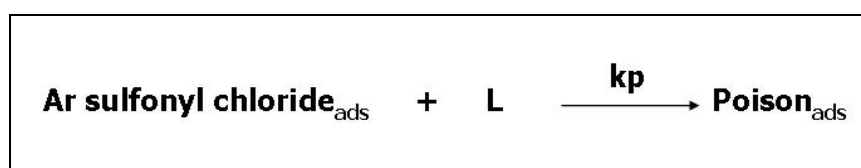


Figure 4.19 Formation of the poison from an adsorbed aromatic sulfonyl chloride and a free metal active site L on the surface of the catalyst

After reaching its maximum and since more of the aromatic sulfonyl chloride is fed to the reactor thereafter, the continuous decline of the molar yield Y_2 with respect to process time suggests that the poison (P) formed is adsorbed irreversibly on the surface of the catalyst.

Figures 4.20 and 4.21 show the X-Ray Diffraction (XRD) analysis of the fresh catalyst and spent catalyst for the experiment conducted at 110 °C and 1-hour residence time. XRD analysis of the catalyst was conducted using a Scintag XDS-2000 apparatus.

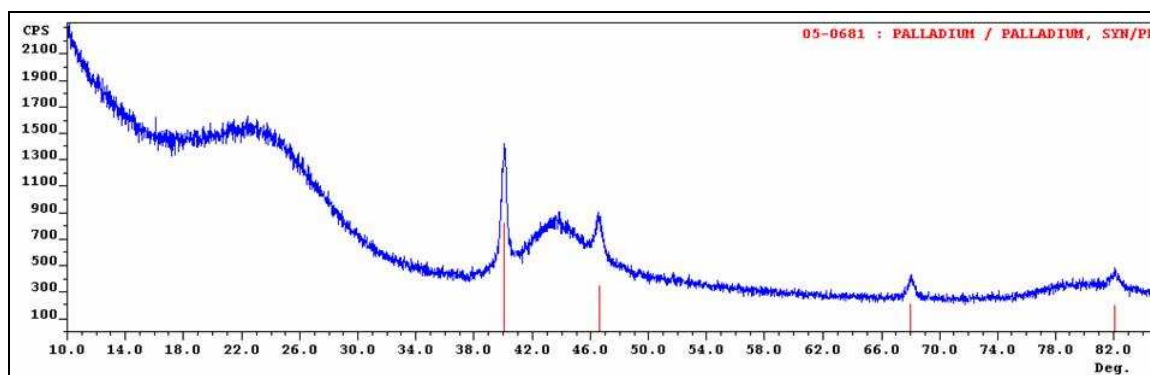


Figure 4.20. XRD analysis of the fresh 1 wt % palladium on charcoal catalyst

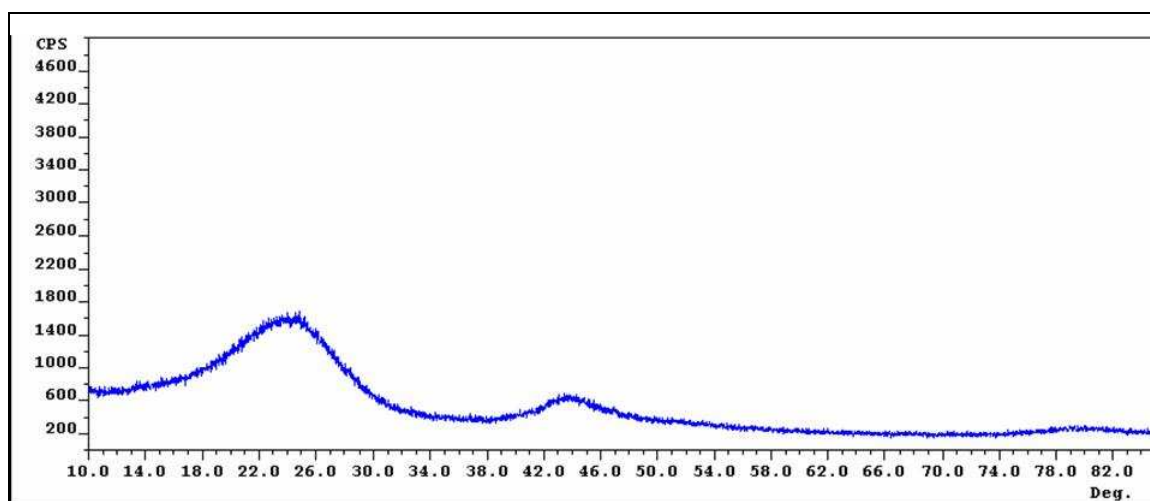


Figure 4.21 XRD analysis of the spent catalyst for the experiment conducted at 110 °C and 1-hour residence time experiment

The peaks corresponding to palladium in the fresh catalyst XRD spectrum disappears in the spent catalyst XRD spectrum. The comparison between the two spectra leads to the conclusion that the poison is responsible for the formation of an amorphous layer on the catalyst surface which blocks the active sites and therefore deactivates the catalyst. Some authors [63] found that the amorphous layer formed on the surface of palladium on charcoal catalyst with sulfur-based compounds consists of a surface configuration of the sulfur atom covering four palladium active sites (Pd_4S).

4.3 Catalytic Hydrogenation of Several Aromatic Sulfonyl Chlorides in Semi-batch Mode Reaction

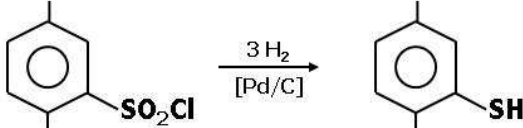
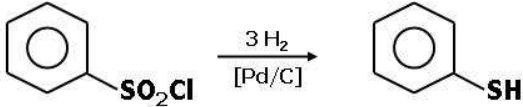
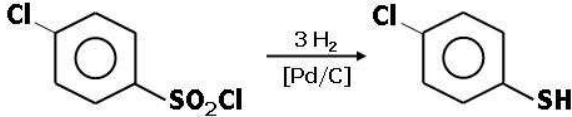
Hydrogenation of the 2,5-dimethylbenzene sulfonyl chloride, benzene sulfonyl chloride and p-chlorobenzene sulfonyl chloride was conducted in semi-batch mode reactor configuration using a 1 wt % palladium on charcoal catalyst. The reaction conditions applied during the catalytic hydrogenation of the aromatic sulfonyl chlorides are listed in Table 4.2.

Table 4.2 Reaction conditions in semi-batch mode catalytic hydrogenation of several aromatic sulfonyl chlorides

Process temperature	110 °C
Process pressure	364.7 psia
Agitation speed	950 RPM
Reaction time	8 hours
Type of catalyst	1 wt% Pd on charcoal
Mass of catalyst	12.03 g
Density of catalyst	0.55 g/cm ³
Catalyst size	2.8 to 3.35 mm (6-7 mesh)
Liquid feed composition	5 wt% of aromatic sulfonyl chloride in toluene

Table 4.3 shows the overall conversions of the 2,5-dimethylbenzene sulfonyl chloride, benzene sulfonyl chloride and p-chlorobenzene sulfonyl chloride and yields of the aromatic sulfonyl chlorides into the corresponding aromatic thiols obtained in semi-batch mode reaction.

Table 4.3 Overall conversions of several aromatic sulfonyl chlorides X and yields Y_2 of several aromatic sulfonyl chlorides into their corresponding aromatic thiols. Semi-batch mode experiments. Reaction conditions: 110 °C, 364.7 psia

Starting material	Desired products	X	Y_2	Reaction Time (hr)
		99.5	77.5	8
		99.8	91.5	8
		100	95.7	8

After 8 hours of reaction time, the intermediates aromatic disulfide and aromatic thiosulfone were not detected by GC/MS for the three reactions investigated. The highest conversion X and yield Y_2 are obtained with the p-chlorobenzene sulfonyl chloride. An average yield Y_2 of 81.0 % for the 2,5-dimethylbenzene sulfonyl chloride to the corresponding aromatic thiol, using a 5 wt % palladium on charcoal, was found in the experimental work of Jacobson [9], which is higher than the yield Y_2 shown in Table 4.3 for the same compound.

Vapor pressure of toluene and the formation of hydrogen sulfide (H_2S) and HCl are eventually responsible for the increase of the process pressure after 4 hour of reaction time when no consumption of hydrogen is observed. Venting periodically the outlet of the reactor until the end of the reaction is needed to maintain the process pressure constant at 364.7 psia.

CHAPTER V

KINETIC MODELING AND PARAMETER ESTIMATION

5.1 Introduction

Transport processes may influence the overall rate of reaction so that the conditions over the reaction sites do not correspond to those in the bulk fluid around the catalyst particle. The reaction rate then depends on the heat and mass transfer between the fluid and the solid or the diffusion of the fluid components inside the porous catalyst. Figure 5.1 shows the steps involved when a molecule A moves from the bulk fluid stream to the catalyst, reacts, and the product R moves back to the bulk fluid stream.

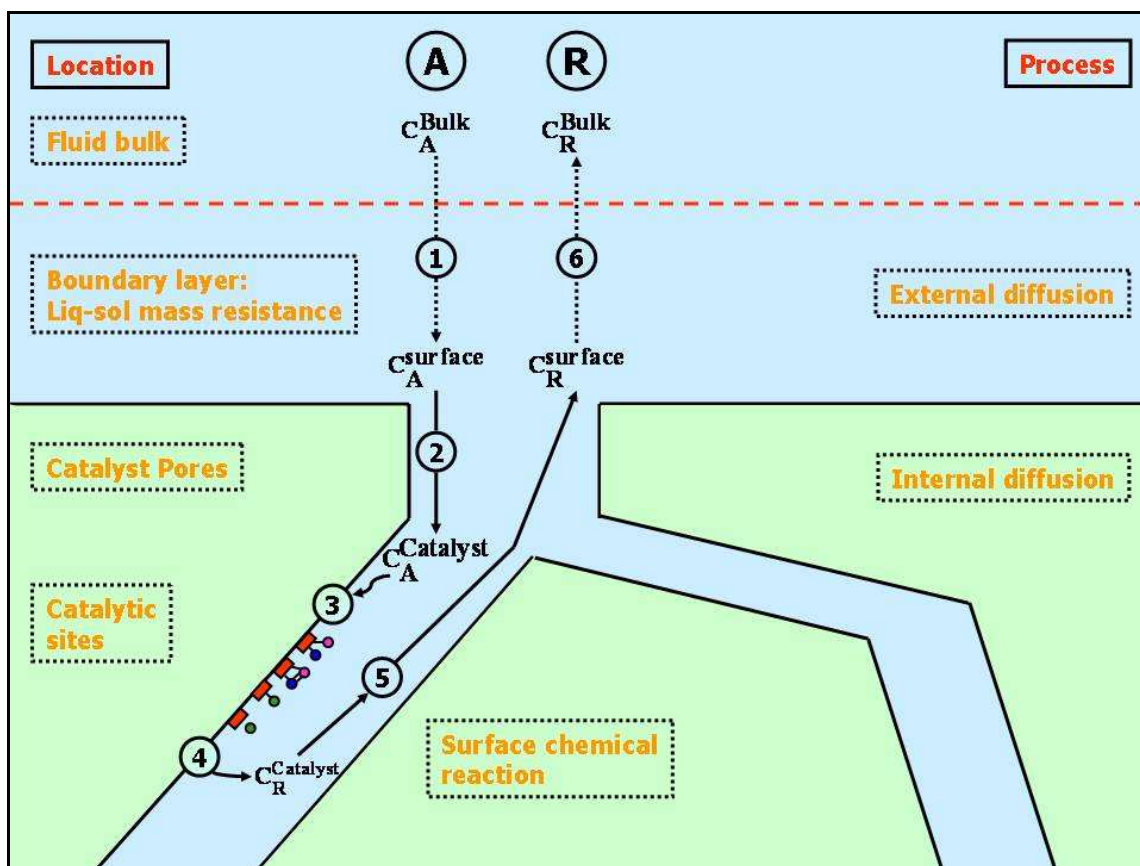


Figure 5.1. Steps involved in reactions on a solid catalyst

The steps involved are:

- 1) Transport of reactants A, B, ... from the main stream to the catalyst pellet surface
- 2) Transport of reactants in the catalyst pores
- 3) Adsorption of reactants on the catalytic site and surface chemical reaction between adsorbed atoms or molecules
- 4) Desorption of products R, S, ...
- 5) Transport of the products in the catalyst pores back to the particle surface
- 6) Transport of products from the particle surface back to the main fluid stream

Steps 1, 3, 4, 5 and 6 are strictly consecutive processes and can be studied separately and then combined into an overall rate, somewhat analogous to a series of resistances in heat transfer through a wall. However, steps 2 and 5 (transport of reactants and products in the catalysts pores) can not be entirely separated: active centers are spread all over the pore walls so that the distance the molecules have to travel, and therefore the resistance they encounter, is not the same for all of them.

5.2 Catalyst Deactivation

The deactivation of a catalyst by poison formation P is expressed by the ratio of fluxes:

$$\frac{N_i(t \text{ or } C_p)}{N_i^0(t \text{ or } C_p = 0)} \quad (5.1)$$

The ratio of fluxes is equal to the ratio of the chemical reaction rates $\frac{r_i}{r_i^0}$ only when there are no diffusional limitations and it is represented by a deactivation function Φ_i , evolving from 1 to 0 with increased deactivation, as follows:

$$\Phi_i = \frac{r_i}{r_i^0} \quad (5.2)$$

where r_i is the rate of reaction in the presence of catalyst deactivation and r_i^0 is the rate of reaction in the absence of catalyst deactivation.

In the way of expressing catalyst deactivation, in-situ measurement of the concentration of the deactivation agent adsorbed on the surface of the catalyst and the fraction of sites remaining active are necessary. In the absence of information regarding the way active sites are deactivated or covered, the deactivation function Φ_i is often expressed in terms of a measurable quantity of deactivating agent by an empirical function. Functions such as exponential or hyperbolic functions have been commonly used to account for the deactivation of catalysts and the decline of the rate of reaction. For the case when the concentration of the deactivating agent is not determined

experimentally during an experiment, the deactivation function can be expressed in term of process time. Froment [69] listed the most common deactivation functions used to express catalyst deactivation with respect to time as shown in Table 5.1.

Table 5.1 Empirical deactivation functions [69]

$\Phi = 1 - \alpha t$	$-\frac{d\Phi}{dt} = \alpha$
$\Phi = \exp(-\alpha t)$	$-\frac{d\Phi}{dt} = \alpha\Phi$
$\Phi = \frac{1}{1 + \alpha t}$	$-\frac{d\Phi}{dt} = \alpha\Phi^2$
$\Phi = \alpha t^{-0.5}$	$-\frac{d\Phi}{dt} = \frac{\Phi^3}{2\alpha}$
$\Phi = (1 + \alpha t)^{-N}$	$-\frac{d\Phi}{dt} = \alpha N\Phi^{1+(1/N)}$

The constant α in the empirical deactivation function with respect to time is a function only of the operating conditions which prevail during the formation and deposition of the deactivating agent. A uniform deactivation of the sites of the catalyst is represented with the decay of the kinetic rates at any given process time. In reality, because of concentration profiles of the deactivating agent and reacting species, nonuniform deactivation occurs within the catalyst pores, which is not accounted for by expressing the deactivation function in term of process time. Therefore, using the deactivation function with respect to process time shows several restrictions and limitations in trying to understand the deactivation mechanism during the event of an experiment.

5.3 Formulation of the Kinetic Model for the Catalytic Hydrogenation of an Aromatic Sulfonyl Chloride

In the hydrogenation of the aromatic sulfonyl chloride, as shown in Figure 2.4 of section 2.5, the first intermediate of reaction is the aromatic sulfinic acid with the formation of hydrochloric acid. Hydrogenation of the aromatic sulfinic acid leads to the formation of the aromatic disulfide and water. Sulfinic acid undergoes a dehydrative disproportionation reaction which leads to the formation of the aromatic thiosulfone, aromatic sulfonic acid and water. The aromatic disulfide and thiosulfone are hydrogenated and lead to the formation of the aromatic thiol. The chemistry involved in the hydrogenation of aromatic sulfonyl chlorides has been presented elsewhere [3, 15]. Figure 5.2 shows the complete reaction scheme for the hydrogenation of the aromatic sulfonyl chloride.

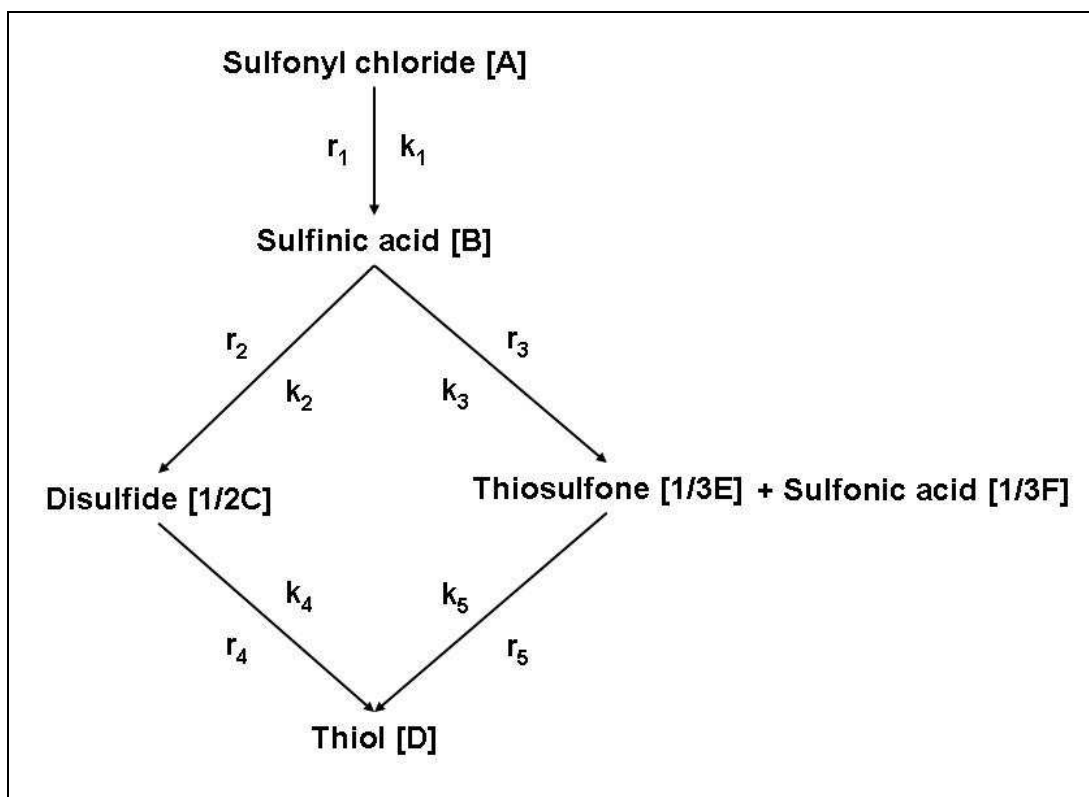


Figure 5.2 Reaction scheme proposed for the hydrogenation of 2,5-dimethylbenzene sulfonyl chloride

Quantum mechanics calculation [70] shows that the free energy of reaction for each of the chemical steps involved in the reaction scheme of Figure 5.2 is negative, which indicates that the equilibrium of reaction is displaced towards the products of reaction. Therefore, the rate determining step for each of the hydrogenation and dehydration reactions is defined as the irreversible surface reaction between adsorbed species on the surface of the catalyst. Computational calculations [70] show that the adsorption of the aromatic sulfonyl chloride on the active sites involves the breakage of the sulfur-chlorine bond with each of the sulfur and chlorine atoms occupying two separate active sites. Therefore, each step of the hydrogenation and dehydration sequences of the aromatic sulfonyl chloride into the aromatic thiol is assumed to involve

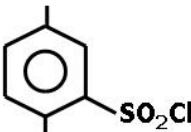
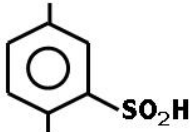
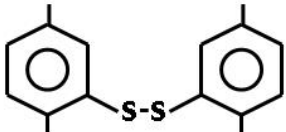
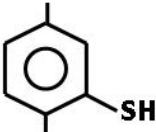
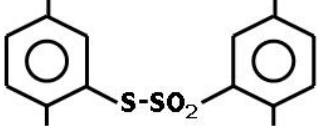
the same number of active sites as the adsorption of the aromatic sulfonyl chloride, i.e., 2 active sites.

Figures 4.13 to 4.17 in section 4.2 show a residual activity of the catalyst for the experiments conducted at long residence times (2.0 and 3.1 hr) with the conversions and molar yields of the reacting species with respect to process time reaching an asymptotically value. A complete deactivation of the catalyst is simulated with the use of an exponential deactivation function, which is in contradiction with the experimental data obtained. A hyperbolic deactivation function should be more suited to fit the experimental data. Since the deactivating agent was not measured in-situ during an experiment, the hyperbolic deactivation function is expressed in terms of process time, i.e., $\Phi = \frac{1}{1 + \alpha t}$ and implemented in the Hougen-Watson rate equations. The alpha parameter of the hyperbolic deactivation function is estimated simultaneously with the adsorption coefficients and kinetic parameters.

Hydrogen adsorbs either molecularly or atomically on the surface of metal catalysts [5]. For the derivation of the rate equations, hydrogen is assumed to adsorb molecularly on the surface of the palladium on carbon catalyst to react with adsorbed aromatic sulfur-based reacting species j . The reacting species involved in the formation of the final product, the aromatic thiol, are considered to be adsorbed on the surface of the catalyst and participate in the rate equations. Experimental data for the aromatic sulfonic acid, water and hydrochloric acid were not collected to the complexity of the quantitation and sampling. Therefore, these compounds were not included in the minimization of the objective function.

Table 5.2 lists the reacting species j involved in the kinetic modeling with their corresponding nomenclature.

Table 5.2 Nomenclature used in the kinetic model of the catalytic hydrogenation of the aromatic sulfonyl chloride

Name	Formula	Abbreviation in the kinetic model
2,5-dimethyl benzene sulfonyl chloride		A
Hydrogen	H₂	H₂
2,5-dimethyl benzene sulfinic acid		B
Bis (2,5-dimethyl phenyl) disulfide		C
2,5-dimethyl thiophenol		D
Bis (2,5-dimethyl phenyl) thiosulfone		E

Assuming that the adsorption of the reacting species on the catalyst surface reaches equilibrium, Figure 5.3 shows the adsorption of the aromatic sulfonyl chloride and hydrogen.

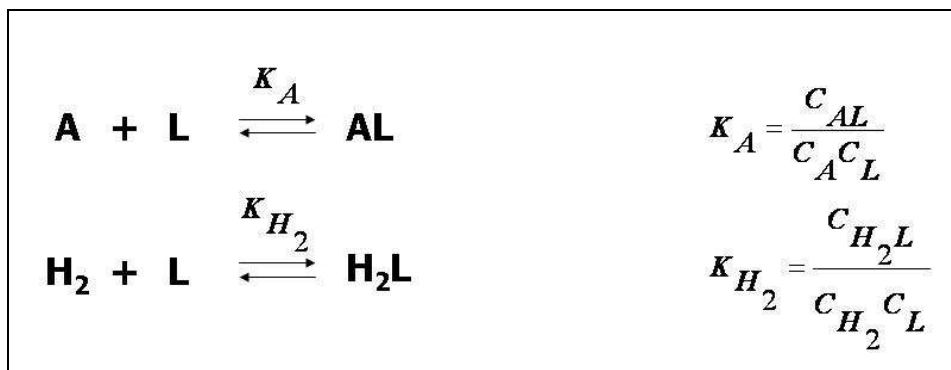


Figure 5.3 Adsorption of the aromatic sulfonyl chloride and molecular hydrogen on a metal active site L with the corresponding adsorption equilibrium constants

The catalytic surface reactions involved are shown in Figure 5.4.

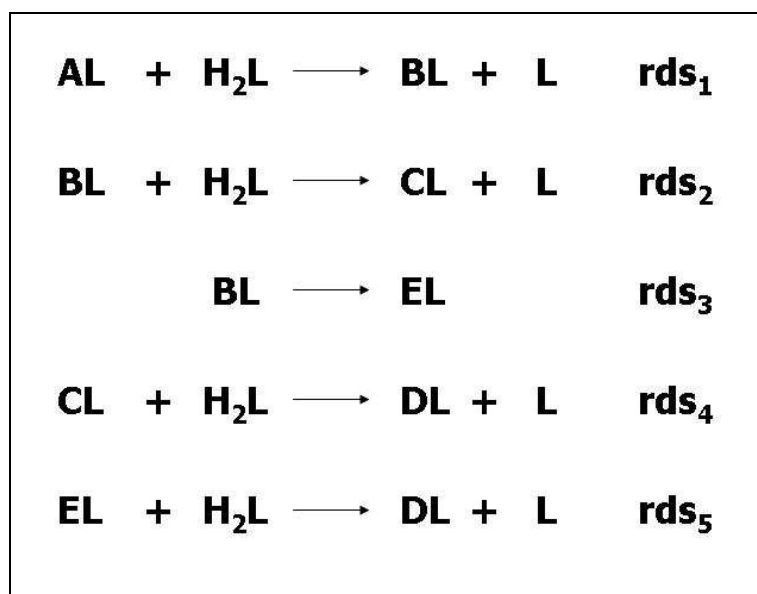


Figure 5.4 Catalytic rate-determining surface reactions between adsorbed reacting species and molecular adsorbed hydrogen

where rds_i stands for the rate-determining step of reaction i .

Figure 5.5 shows the desorption steps involved.

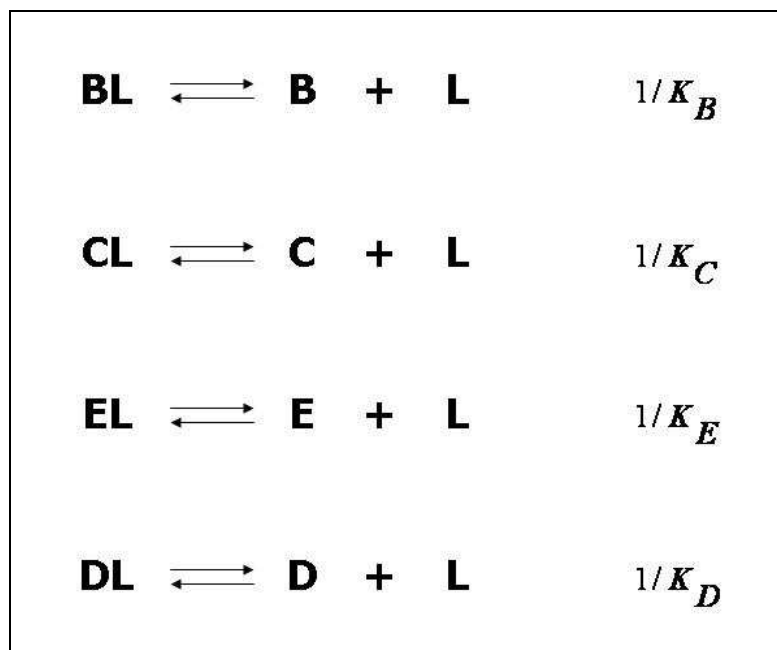


Figure 5.5 Desorption of the reacting species from the metal active site L

The concentrations of the adsorbed aromatic sulfonyl chloride and adsorbed molecular hydrogen are expressed as follows:

$$C_{AL} = K_A C_A C_L \quad (5.3)$$

$$C_{H_2L} = K_{H_2} C_{H_2} C_L \quad (5.4)$$

where C_L is the concentration of a vacant active site and C_{jL} is the concentration of a chemisorbed species j .

The concentrations of the other reacting species are obtained from:

$$C_{BL} = K_B C_B C_L \quad (5.5)$$

$$C_{CL} = K_C C_C C_L \quad (5.6)$$

$$C_{DL} = K_D C_D C_L \quad (5.7)$$

$$C_{EL} = K_E C_E C_L \quad (5.8)$$

Since the concentration of the total active sites C_t is assumed to be constant, the site balance is written as follows:

$$C_t = C_L + C_{AL} + C_{H_2L} + C_{BL} + C_{CL} + C_{DL} + C_{EL} \quad (5.9)$$

$$C_t = C_L + K_A C_A C_L + K_{H_2} C_{H_2} C_L + K_B C_B C_L + K_C C_C C_L + K_D C_D C_L + K_E C_E C_L \quad (5.10)$$

The following Hougen-Watson rate equations were developed for the reacting species:

- *Rate of consumption of the aromatic sulfonyl chloride:*

$$r_1 = \frac{k_1^0 K_A K_{H_2} C_A C_{H_2}}{\left(1 + K_{H_2} C_{H_2} + \sum_j K_j C_j\right)^2} \times \frac{1}{1 + \alpha_1 t} \quad (5.11)$$

- *Overall rate of consumption of the aromatic sulfinic acid:*

$$r_{sulfinic} = r_2 + r_3 \quad (5.12)$$

with r_2 the rate of consumption of the aromatic sulfinic acid via the hydrogenation of the aromatic sulfinic acid:

$$r_2 = \frac{k_2^0 K_B K_{H_2} C_B C_{H_2}}{\left(1 + K_{H_2} C_{H_2} + \sum_j K_j C_j\right)^2} \times \frac{1}{1 + \alpha_2 t} \quad (5.13)$$

with r_3 the rate of consumption of the aromatic sulfinic acid via the dehydration of the aromatic sulfinic acid:

$$r_3 = \frac{k_3^0 K_B C_B}{\left(1 + K_{H_2} C_{H_2} + \sum_j K_j C_j\right)} \times \frac{1}{1 + \alpha_3 t} \quad (5.14)$$

- Overall rate of formation of the aromatic thiol:

$$r_{THIOL} = r_4 + r_5 \quad (5.15)$$

with r_4 the rate of formation of the aromatic thiol via the hydrogenation of the aromatic disulfide:

$$r_4 = \frac{k_4^0 K_C K_{H_2} C_C C_{H_2}}{\left(1 + K_{H_2} C_{H_2} + \sum_j K_j C_j\right)^2} \times \frac{1}{1 + \alpha_4 t} \quad (5.16)$$

and r_5 the rate of formation of the aromatic thiol via the hydrogenation of the aromatic thiosulfone:

$$r_5 = \frac{k_5^0 K_E C_E}{\left(1 + K_{H_2} C_{H_2} + \sum_j K_j C_j\right)^2} \times \frac{1}{1 + \alpha_5 t} \quad (5.17)$$

A zero-order in the concentration of hydrogen is assumed for the catalytic step from the aromatic thiosulfone to the aromatic thiol.

- Net rate of formation of the aromatic sulfinic acid:

$$r_{sulfinic} = r_1 - r_2 - r_3 \quad (5.18)$$

- *Net rate of formation of the aromatic disulfide:*

$$r_{DS} = \left(\frac{1}{2}r_2 - \frac{1}{2}r_4 \right) \quad (5.19)$$

- *Net rate of formation of the aromatic thiosulfone:*

$$r_{TS} = \left(\frac{1}{3}r_3 - \frac{1}{2}r_5 \right) \quad (5.20)$$

- *Net rate of consumption of hydrogen:*

$$r_{H_2} = \left(\frac{5}{2}r_1 + \frac{1}{2}r_4 + \frac{3}{2}r_5 \right) \quad (5.21)$$

The fact that the hydrogen concentration does not evolve with respect to process time is explained from the depletion of hydrogen by the chemical reactions being instantaneously compensated by the hydrogen mass transfer from the gas phase to the liquid phase. Due to convergence problems during the minimization of the objective function and a zero-order assumption in the concentration of hydrogen in the catalytic step from the aromatic thiosulfone to the aromatic thiol, the net rate of consumption of hydrogen is expressed by the chemical rates r_1 and r_4 .

The net rates of formation of the aromatic sulfonic acid, water and hydrochloric acid are written as follows:

$$r_{sulfonic} = \frac{1}{3}r_3 \quad (5.22)$$

$$r_{H_2O} = \left(2r_2 + \frac{1}{3}r_3 + r_5 \right) \quad (5.23)$$

$$r_{HCl} = r_1 \quad (5.24)$$

The aromatic sulfonic acid, water and hydrochloric acid are by-products of reaction during the hydrogenation of the aromatic sulfonyl chloride.

5.4 Continuity Equations and Initial Conditions for the Reacting Species

During the startup of an experiment pure toluene is used to fill the reactor with a mixture of hydrogen and argon flowing through the reactor. Stabilization of the reactor at the reaction conditions occurs by feeding toluene and the gas feed mixture containing hydrogen and argon with a specified flow rate. When the reaction conditions have been reached, the pure toluene feed is switched to the organic liquid mixture containing 5 wt% of the aromatic sulfonyl chloride in toluene. At process time equal to 0, when the liquid feed mixture enters the reactor, a change in the concentration of the aromatic sulfonyl chloride in the feed occurs due to the catalytic hydrogenation reaction taking place in the volume of liquid within the reactor. At time equal to $0 + \Delta t$, the flow rate at which the aromatic sulfonyl chloride enters the reactor is $F_{sulfonyl}^0$, which is different from $F_{sulfonyl}$, the flow rate of the aromatic sulfonyl chloride in the outlet stream of the reactor. The material balance applied to the aromatic sulfonyl chloride over the time period Δt is given by:

$$\int_t^{t+\Delta t} \left[F_{sulfonyl}^0 - F_{sulfonyl} - w r_{sulfonyl} \right] dt = n_{sulfonyl} \Big|_{t+\Delta t} - n_{sulfonyl} \Big|_t \quad (5.25)$$

with w the mass of catalyst (kg). By using the mean-value theorems of integral and differential calculus [71], Equation 5.25 reduces to the following differential equation, Equation 5.26.

$$F_{sulfonyl}^0 - F_{sulfonyl} - w r_{sulfonyl} = \frac{dn_{sulfonyl}}{dt} \quad (5.26)$$

The unsteady state continuity equations derived for the reacting species in a perfectly mixed flow reactor with constant fluid density are as follows:

$$\frac{dC_{sulfonyl}}{dt} = -\frac{C_{sulfonyl}}{\theta} + \frac{F_{sulfonyl}^0}{V_L} - \left(\frac{w}{V_L} \times r_{sulfonyl} \right) \quad (5.27)$$

$$\frac{dC_{H_2}}{dt} = -\frac{C_{H_2}}{\theta} + \frac{F_{H_2}^0}{V_L} - \left(\frac{w}{V_L} \times r_{H_2} \right) \quad (5.28)$$

$$\frac{dC_{sulfinic}}{dt} = -\frac{C_{sulfinic}}{\theta} + \left(\frac{w}{V_L} \times r_{sulfinic} \right) \quad (5.29)$$

$$\frac{dC_{disulfide}}{dt} = -\frac{C_{disulfide}}{\theta} + \left(\frac{w}{V_L} \times r_{disulfide} \right) \quad (5.30)$$

$$\frac{dC_{thiol}}{dt} = -\frac{C_{thiol}}{\theta} + \left(\frac{w}{V_L} \times r_{thiol} \right) \quad (5.31)$$

$$\frac{dC_{thiosulfone}}{dt} = -\frac{C_{thiosulfone}}{\theta} + \left(\frac{w}{V_L} \times r_{thiosulfone} \right) \quad (5.32)$$

with C_j the concentration of the aromatic sulfur-based reacting species j ($kmol/m^3$), θ the average residence time of the liquid within the reactor (hr), V_L the volume of the liquid within the reactor (m^3), w the mass of catalyst (kg_{cat}) and r_i the Hougen-Watson reaction rates defined in Equations 5.11 to 5.17 ($kmol/kg\ hr$). In the parameter estimation program, a Runge Kunta method is used to perform the numerical integration of the set of differential equations.

When the organic mixture enters the reactor at zero process time, and by virtue of complete and immediate mixing within the reactor, some aromatic sulfonyl chloride appears in the effluent with a certain concentration different from the initial concentration of the aromatic sulfonyl chloride in the feed. The concentration of the aromatic sulfonyl chloride in the effluent of the reactor depends upon the amount of toluene in the reactor used in the startup procedure, which has to be displaced, the initial molar feed rate of the aromatic sulfonyl chloride and the conversions into intermediates and products. Even though the latter have not been measured experimentally, a zero concentration can be approximated for the reacting species at zero process time, i.e. $C_j^0 = 0$.

5.5 Parameter Estimation Technique and Statistical Analysis

Estimates of the adsorption coefficients, the kinetic constants and the alpha parameter of the hyperbolic deactivation function are obtained by minimization of the sum of the square of the residual S between the concentrations determined experimentally and the concentrations calculated from the model for each reacting species, j , for a number of process times at all the residence times investigated. The sum of the square of the residual S is calculated at each process temperature investigated.

$$S = \sum_{k=1}^{\theta_{\text{exp}}} \sum_{l=1}^j \sum_{m=1}^{t_{\text{span}}} \left(\left(y_{kl} \right)_m - \left(\hat{y}_{kl} \right)_m \right)^2 \quad (5.33)$$

where θ_{exp} represents the total number of residence times investigated, j the total number of aromatic sulfur-based components, t_{span} the process time until the end of an experiment, $\left(\hat{y}_{kl} \right)_m$ is the calculated value from the kinetic model of the l th response obtained for each aromatic sulfur-based compound j at the m th process time and k th residence time investigated, and $\left(y_{kl} \right)_m$ is the l th response obtained experimentally for each aromatic sulfur-based compound j at the m th process time and k th residence time investigated.

The concentration of the aromatic sulfinic acid was not determined experimentally and therefore, the sum of the square of the residuals for this compound was not included in the minimization of the objective function. Sixteen parameters including the adsorption coefficients of each aromatic sulfur-based reacting species j , kinetic constants and the alpha parameters of the hyperbolic deactivation function for each of the catalytic reactions i were estimated simultaneously. The objective function S was minimized per process temperatures at 85, 97 and 110 °C considering all the responses obtained for the reacting species j at all residence times investigated.

The parameters of the kinetic model were first estimated at a process temperature of 85 °C. The value of the estimated parameters obtained after minimization of the objective function at a process temperature of 85 °C were used as initial values for the set of parameters at a process temperature of 97 °C. The estimated parameters obtained after minimization of the objective function at a process temperature of 97 °C were finally used as the initial values for the set of parameters at a process temperature of 110 °C.

The kinetic parameters are estimated by the means of a quasi-Newton nonlinear multi-variable algorithm and a sequential quadratic program [72]. A final minimization of the objective function was performed using a Levenberg-Marquardt algorithm. The Hougen-Watson equation rates derived in Equations 5.11 to 5.17 are non-linear with respect to the parameters. It is converted into a linear form by Taylor series around the initial guess x_0 given for the parameters:

$$f(x_0 + \Delta x) = f(x_0) + \nabla f(x_0)^T \Delta x + \frac{1}{2} \Delta x^T B_0 \Delta x \quad (5.34)$$

with $\nabla f(x_0)$ the gradient of the function f at $x = x_0$ and B_0 the initial Hessian matrix usually equal to the identity matrix I. The Taylor series of the gradient is given by:

$$\nabla f(x_0 + \Delta x) = \nabla f(x_0) + B_0 \Delta x \quad (5.35)$$

which is equivalent to the secant equation. Solving for $\nabla f(x_0 + \Delta x) = 0$ provides the Newton step:

$$\Delta x_0 = -B_0^{-1} \nabla f(x_0) \quad (5.36)$$

At each iteration k , the search direction Δx_k is updated applying the Newton's step calculated using the current estimate of the Hessian matrix B_k and it is used to find the next point x_{k+1} as follows:

$$\Delta x_k = -\delta_k B_k^{-1} \nabla f(x_k) \quad (5.37)$$

$$x_{k+1} = x_k + \Delta x_k \quad (5.38)$$

with δ_k the optimal step length parameter in the direction found in the first step. In the quasi-Newton method, the Hessian matrix of the second derivative of the objective function to minimize does not need to be computed at any stage. The Hessian matrix is updated by analyzing successive gradient vector instead. The approximation of the inverse of the Hessian matrix is determined from the Broyden-Fletcher-Goldfarb-Shanno (BFGS) method [73] as follows:

$$B_{k+1} = B_k + \frac{q_k q_k^T}{q_k^T s_k} - \frac{(B_k s_k)^T B_k s_k}{s_k^T B_k s_k} \quad (5.39)$$

$$s_k = x_{k+1} - x_k \quad (5.40)$$

$$q_k = \nabla f(x_{k+1}) - \nabla f(x_k) \quad (5.41)$$

A quadratic approximation of the Lagrangian function L can be used and it is defined as:

$$L(x, \lambda) = f(x) + \sum_{p=1}^p \lambda_p g_p(x) \quad (5.42)$$

with λ_p the Lagrange multipliers for each of the parameters of the kinetic model necessary to balance differences in magnitude of the terms in the objective function and gradients. For this case, the approximation of Hessian of the Lagrangian function is calculated from Equation 5.39.

The statistical analysis is based upon the t-test and F-test. The hypothesis that the parameters estimated b_j would be zero is rejected when [74]

$$t_c = \frac{|b_j - 0|}{s(b_j)} > t\left(n - p; 1 - \frac{\beta}{2}\right) \quad (5.43)$$

with $s(b_j)$ the standard deviation of the estimated parameters b_j and $t\left(n - p; 1 - \frac{\beta}{2}\right)$ is the tabulated $\frac{\beta}{2}$ percentage point of the t-distribution with $(n - p)$ degrees of freedom. The value of β is equal to 0.05 for a 95 % confidence interval. The parameters estimates, b_j , are significantly different from 0 and effectively contribute to the kinetic model if the calculated t-values, t_c , are greater than the tabulated t-value.

An estimate of the error variance $\sigma^2(b_j)$ for each estimated parameter b_j is calculated from the jacobian matrix, J , evaluated at the converged values of b_j and the element on the j th row and j th column of the inverse of the covariance matrix $J^T J$ as follows:

$$\sigma^2(b_j) = s^2 (J^T J)^{-1}_{jj} \quad (5.44)$$

with J the jacobian matrix at the converged values of the parameters, J^T the jacobian matrix transposed and s^2 the estimate of the experimental error variance.

The estimated experimental error variance s^2 is given by [74]:

$$s^2 = \frac{\sum_{i=1}^n \left(y_i - \hat{y}_i \right)^2}{n - p} \quad (5.45)$$

with y_i the experimental point, \hat{y}_i the calculated value of y_i , n the number of responses and p the number of parameters. Only the elements in the diagonal of the jacobian matrix (j th row and j th column), representing the gradient of the objective function with respect to each parameter, is considered in the calculation of the error variance $\sigma^2(b_j)$. The other elements, representing the cross-gradient in the i th row and

jth of the jacobian matrix, are not considered. The standard deviation for each estimated parameter is determined from the error variance $\sigma^2(b_j)$ as follows:

$$s(b_j) = \sqrt{\sigma^2(b_j)} \quad (5.46)$$

The significance of the fit between the model and the experimental data is tested by performing the F-test. The model is not rejected when [74]

$$F_C > 10F(p, n-p, 1-\beta) \quad (5.47)$$

with F_C the ratio of the regression sum of the squares and the residual sum of the squares and $F(p, n-p, 1-\beta)$ the tabulated β percentage point of the F-distribution with p parameters and $(n-p)$ degrees of freedom. The F-value F_C is defined as follows [74]:

$$F_C = \frac{\frac{\sum_{i=1}^n \left(\hat{y}_i \right)^2}{p}}{\frac{\sum_{i=1}^n \left(y_i - \hat{y}_i \right)^2}{n-p}} \quad (5.48)$$

with n the total number of responses, p the number of parameters, y_i the experimental point, \hat{y}_i the calculated value of y_i .

5.6 Results and Discussion

5.6.1 Parameter Estimation per Process Temperature

Table 5.3 shows the number of responses used in the non-linear regression and the tabulated t-value, considering β equal to 0.05, at the process temperatures of 85 and 97 °C.

Tables 5.4, 5.5 and 5.6 show the parameter estimates calculated from the simultaneous non-linear regression of all the responses obtained for all the aromatic sulfur-based compounds j at all process times and residence times investigated, standard deviations, calculated t_c -values and lower- and upper-values of the 95 % confidence interval at the process temperatures of 85, 97 and 110 °C.

Table 5.3 Number of responses in the non-linear regression and tabulated t-value and F-value at the process temperatures of 85, 97 and 110 °C

Process temperature (°C)	Number of responses	Tabulated t-value	Tabulated F-value
85	165	1.97	1.71
97	170	1.97	1.70
110	115	1.98	1.73

Table 5.4 Estimates of adsorption coefficients, kinetic constants and alpha parameter of the hyperbolic deactivation function with corresponding standard deviations, tc-value and 95 % confidence intervals for the Hougen-Watson kinetic model at process temperature of 85 °C

Parameters	Unit	Estimate	Standard deviation	t_c -value	95 % confidence interval	
					Lower Value	Upper value
K_A	m ³ /kmol	1.15	42.54	$2.71 \cdot 10^{-2}$	-82.65	84.96
K_{H_2}	m ³ /kmol	1.18	85.08	$1.39 \cdot 10^{-2}$	-166.43	168.79
K_B	m ³ /kmol	0.77	28.36	$2.71 \cdot 10^{-2}$	-55.10	56.64
K_C	m ³ /kmol	0.096	17.02	$5.67 \cdot 10^{-3}$	-33.43	33.63
K_D	m ³ /kmol	0.027	28.36	$9.66 \cdot 10^{-4}$	-55.84	55.90
K_E	m ³ /kmol	1.43	85.08	$1.69 \cdot 10^{-2}$	-166.17	169.04
k_1^0	m ³ /kg _{cat} hr	1.22	42.54	$2.88 \cdot 10^{-2}$	-82.58	85.03
k_2^0	m ³ /kg _{cat} hr	0.73	42.54	$1.71 \cdot 10^{-2}$	-83.07	84.53
k_3^0	m ³ /kg _{cat} hr	0.14	6.08	$2.43 \cdot 10^{-2}$	-11.83	12.13
k_4^0	m ³ /kg _{cat} hr	0.083	12.15	$6.84 \cdot 10^{-3}$	-23.85	24.02
k_5^0	m ³ /kg _{cat} hr	1.42	85.08	$1.68 \cdot 10^{-2}$	-166.18	169.03

Table 5.4 Continued

Parameters	Unit	Estimate	Standard deviation	t_c -value	95 % confidence interval	
					Lower Value	Upper value
α_1	1/hr	0.28	7.73	$3.73 \cdot 10^{-2}$	-14.94	15.52
α_2	1/hr	1.66	85.08	$1.95 \cdot 10^{-2}$	-165.95	169.27
α_3	1/hr	1.27	10.63	$1.20 \cdot 10^{-1}$	-19.66	22.22
α_4	1/hr	0.010	28.36	$3.67 \cdot 10^{-4}$	-55.86	55.88
α_5	1/hr	0.60	28.36	$2.12 \cdot 10^{-2}$	-55.27	56.47

Calculated F-value F_C : 322.6

Table 5.5 Estimates of adsorption coefficients, kinetic constants and alpha parameter of the hyperbolic deactivation function with corresponding standard deviations, tc-value and 95 % confidence intervals for the Hougen-Watson kinetic model at process temperature of 97 °C

Parameters	Unit	Estimate	Standard deviation	t _c -value	95 % confidence interval	
					Lower Value	Upper value
K_A	m ³ /kmol	1.27	3.96	$3.21 \cdot 10^{-1}$	-6.53	9.07
K_{H_2}	m ³ /kmol	1.16	3.84	$3.04 \cdot 10^{-1}$	-6.40	8.73
K_B	m ³ /kmol	0.57	10.57	$5.39 \cdot 10^{-2}$	-20.25	21.39
K_C	m ³ /kmol	0.053	202.49	$2.63 \cdot 10^{-4}$	-398.85	398.96
K_D	m ³ /kmol	0.052	73.28	$7.09 \cdot 10^{-4}$	-144.31	144.41
K_E	m ³ /kmol	1.42	139.90	$1.02 \cdot 10^{-2}$	-274.18	277.03
k_1^0	m ³ /kg _{cat} hr	1.33	3.81	$3.50 \cdot 10^{-1}$	-6.17	8.84
k_2^0	m ³ /kg _{cat} hr	0.51	21.55	$2.39 \cdot 10^{-2}$	-41.94	42.97
k_3^0	m ³ /kg _{cat} hr	0.29	6.14	$4.79 \cdot 10^{-2}$	-11.80	12.39
k_4^0	m ³ /kg _{cat} hr	0.017	130.42	$1.31 \cdot 10^{-4}$	-256.91	256.94
k_5^0	m ³ /kg _{cat} hr	1.41	124.11	$1.14 \cdot 10^{-2}$	-243.08	245.91

Table 5.5 Continued

Parameters	Unit	Estimate	Standard deviation	t_c -value	95 % confidence interval	
					Lower Value	Upper value
α_1	1/hr	0.001	145.18	$1.02 \cdot 10^{-5}$	-286.0	286.01
α_2	1/hr	0.47	57.0	$8.31 \cdot 10^{-3}$	-111.82	112.76
α_3	1/hr	0.62	17.77	$3.51 \cdot 10^{-2}$	-34.38	35.63
α_4	1/hr	0.038	2564.84	$1.47 \cdot 10^{-5}$	-5052.70	5052.77
α_5	1/hr	0.16	31.15	$5.22 \cdot 10^{-3}$	-61.20	61.53

Calculated F-value F_C : 390.1

Table 5.6 Estimates of adsorption coefficients, kinetic constants and alpha parameter of the hyperbolic deactivation function with corresponding standard deviations, tc-value and 95 % confidence intervals for the Hougen-Watson kinetic model at process temperature of 110 °C

Parameters	Unit	Estimate	Standard deviation	t_c -value	95 % confidence interval	
					Lower Value	Upper value
K_A	m ³ /kmol	1.22	9.98	$1.22 \cdot 10^{-1}$	-18.54	20.98
K_{H_2}	m ³ /kmol	1.11	15.97	$7.0 \cdot 10^{-2}$	-30.50	32.74
K_B	m ³ /kmol	0.58	6.63	$8.77 \cdot 10^{-2}$	-12.55	13.71
K_C	m ³ /kmol	0.053	1451.57	$3.70 \cdot 10^{-5}$	-2874.05	2874.16
K_D	m ³ /kmol	0.057	224.89	$2.54 \cdot 10^{-4}$	-445.23	445.34
K_E	m ³ /kmol	1.42	1140.52	$1.24 \cdot 10^{-3}$	-2256.81	2259.65
k_1^0	m ³ /kg _{cat} hr	1.27	6.60	$1.93 \cdot 10^{-1}$	-11.79	14.34
k_2^0	m ³ /kg _{cat} hr	0.53	4.99	$1.08 \cdot 10^{-1}$	-9.34	10.42
k_3^0	m ³ /kg _{cat} hr	0.24	12.98	$1.90 \cdot 10^{-2}$	-25.45	25.95
k_4^0	m ³ /kg _{cat} hr	0.017	614.13	$2.77 \cdot 10^{-5}$	-1215.96	1215.99
k_5^0	m ³ /kg _{cat} hr	1.41	591.38	$2.38 \cdot 10^{-3}$	-1169.52	1172.34

Table 5.6 Continued

Parameters	Unit	Estimate	Standard deviation	t_c -value	95 % confidence interval	
					Lower Value	Upper value
α_1	1/hr	0.26	2.53	$1.04 \cdot 10^{-1}$	-4.75	5.27
α_2	1/hr	0.45	8.20	$5.52 \cdot 10^{-2}$	-15.78	16.69
α_3	1/hr	0.63	25.84	$2.46 \cdot 10^{-2}$	-50.53	51.80
α_4	1/hr	0.038	15967.25	$2.38 \cdot 10^{-6}$	$-3.16 \cdot 10^4$	$3.16 \cdot 10^4$
α_5	1/hr	0.16	74.96	$2.18 \cdot 10^{-3}$	-148.26	148.58

Calculated F-value F_C : 78.5

The estimated parameters do not satisfy the t-value statistical analysis. The calculated t-values listed in Tables 5.4, 5.5 and 5.6 for each of the parameters are greater than the tabulated t-value listed in Table 5.3 for the process temperatures of 85, 97 and 110 °C. Therefore, the estimated parameters do not contribute significantly to the kinetic model and the null hypothesis that the parameter estimates b_j would be zero is not rejected, i.e. $b_j = 0$.

The F-value calculated from Equation 5.48, considering all the experimental data collected at each process temperature with the corresponding simulated data, is greater than $10F$ of the tabulated F-value, meaning that the regression is meaningful. The kinetic model used to fit the experimental data and, which involves the Hougen-Watson equation rates for the reacting species adsorbed on two active sites and with the deactivation of the catalyst represented with a hyperbolic empirical function with respect to process time, is not rejected.

The equilibrium adsorption coefficients and kinetic constants obtained from parameter estimation do not display much variation with respect to the process temperature. The equilibrium adsorption coefficients can be assumed independent of the process temperature. A certain deficiency in the kinetic model appears with the kinetic constants with small variations of the k_i^0 with respect to the process temperature. Due to the large standard deviations and 95 % confidence intervals, further improvements in the values of the kinetic parameters need to be conducted.

5.6.2 Comparison Between Experimental and Calculated Values

Figures 5.6 to 5.26 show the comparison of experimental and simulated concentrations profiles with respect to process time for the reacting species listed in Table 5.2 at a residence time θ : 1.0 hr, process temperatures: 85, 97 and 110 °C, process pressure: 364.7 psia, $F_{H_2}^0 / F_{sulfonyl}^0 = 8.0 \text{ mol/mol}$, $F_{H_2}^0 / F_{Ar}^0 = 3.0 \text{ mol/mol}$ and with the parameter estimates listed in Tables 5.4, 5.5 and 5.6 using the continuity equations defined in Equations 5.27 to 5.32.

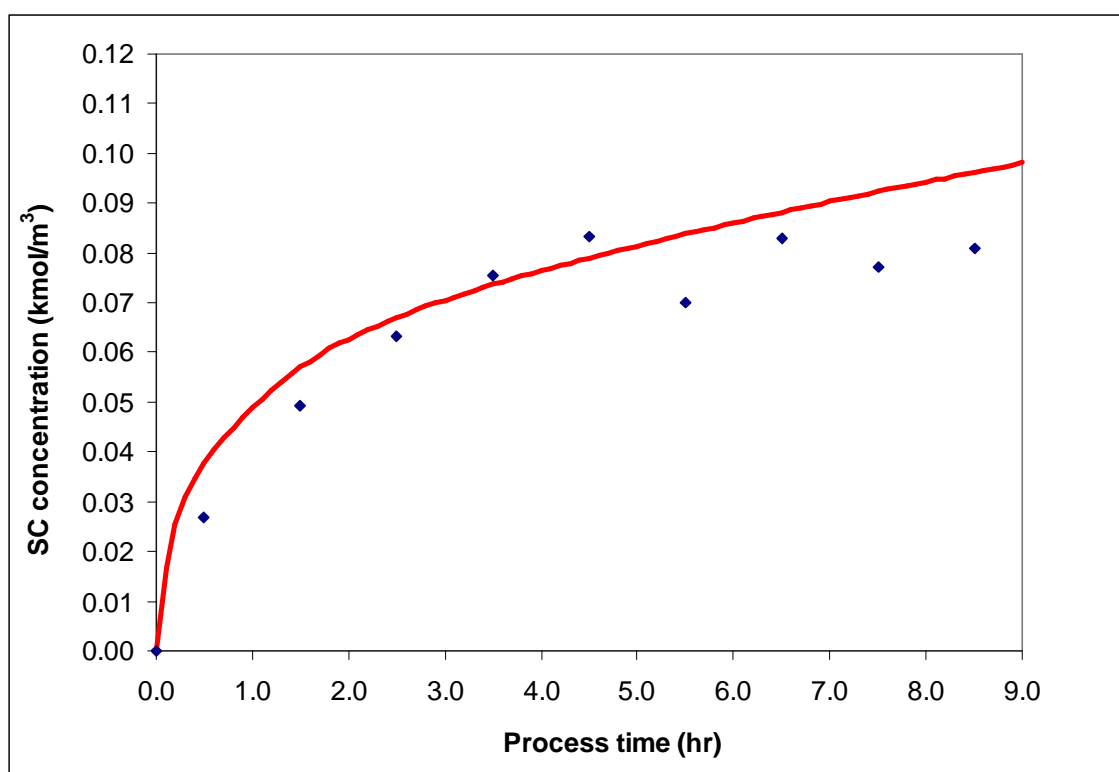


Figure 5.6 Comparison of simulated (—) and experimental (◆) concentration profiles of the aromatic sulfonyl chloride (SC) with respect to process time at residence time θ : 1.0 hr, process temperature: 85 °C, process pressure: 364.7 psia, $F_{H_2}^0 / F_{sulfonyl}^0 = 8.0 \text{ mol/mol}$, $F_{H_2}^0 / F_{Ar}^0 = 3.0 \text{ mol/mol}$

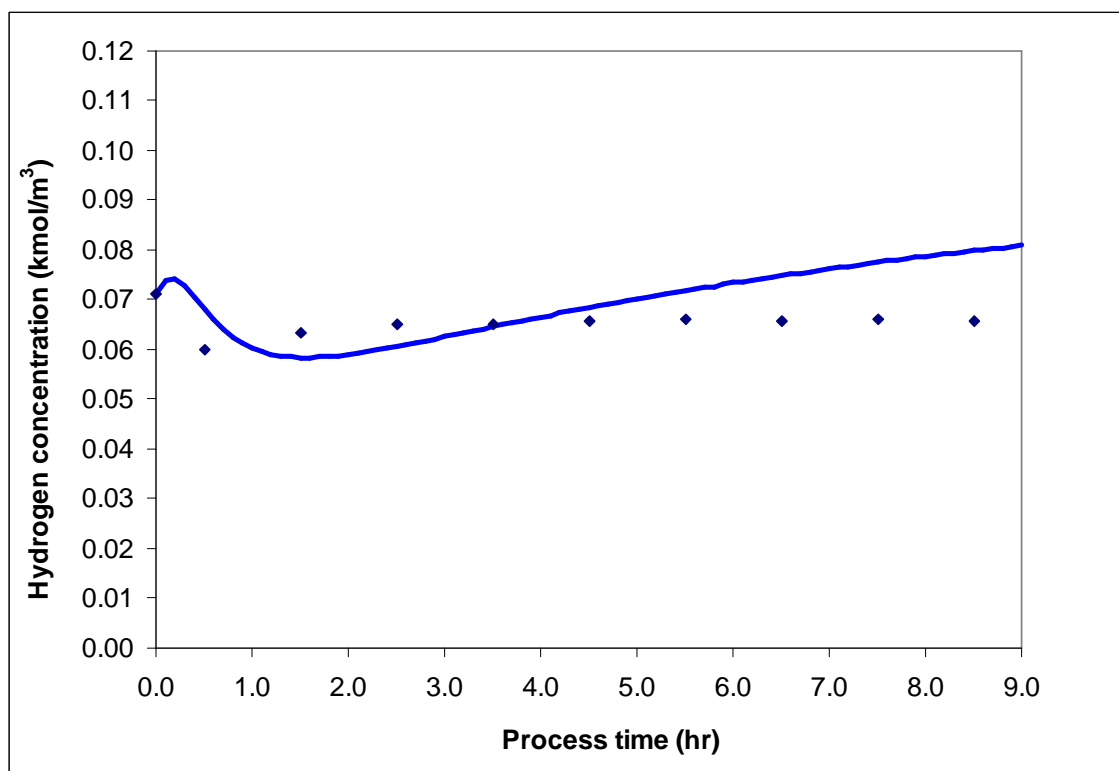


Figure 5.7 Comparison of simulated (—) and experimental (◆) concentration profiles of hydrogen with respect to process time at residence time θ : 1.0 hr, process temperature:

85 °C, process pressure: 364.7 psia, $F_{H_2}^0 / F_{sulfonyl}^0 = 8.0 \text{ mol/mol}$,

$F_{H_2}^0 / F_{Ar}^0 = 3.0 \text{ mol/mol}$

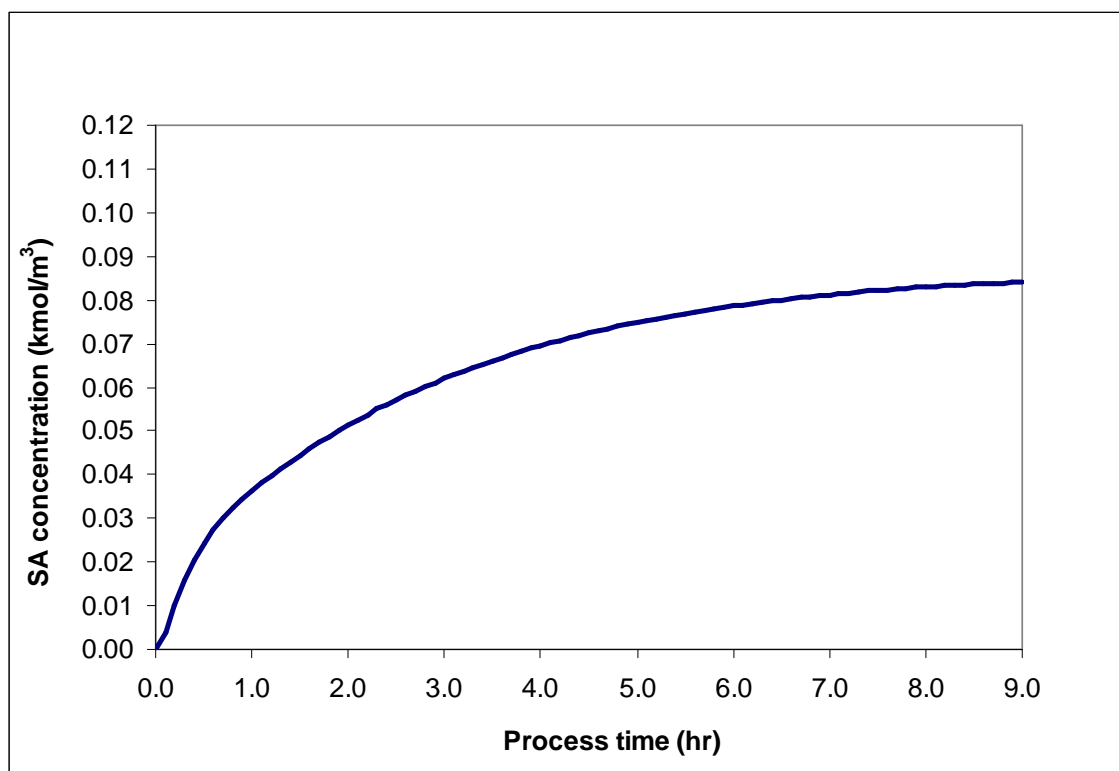


Figure 5.8 Simulated concentration profile of the aromatic sulfonic acid (—) (SA) with respect to process time at residence time θ : 1.0 hr, process temperature: 85 °C, process pressure: 364.7 psia, $F_{H_2}^0 / F_{sulfonyl}^0 = 8.0 \text{ mol/mol}$, $F_{H_2}^0 / F_{Ar}^0 = 3.0 \text{ mol/mol}$

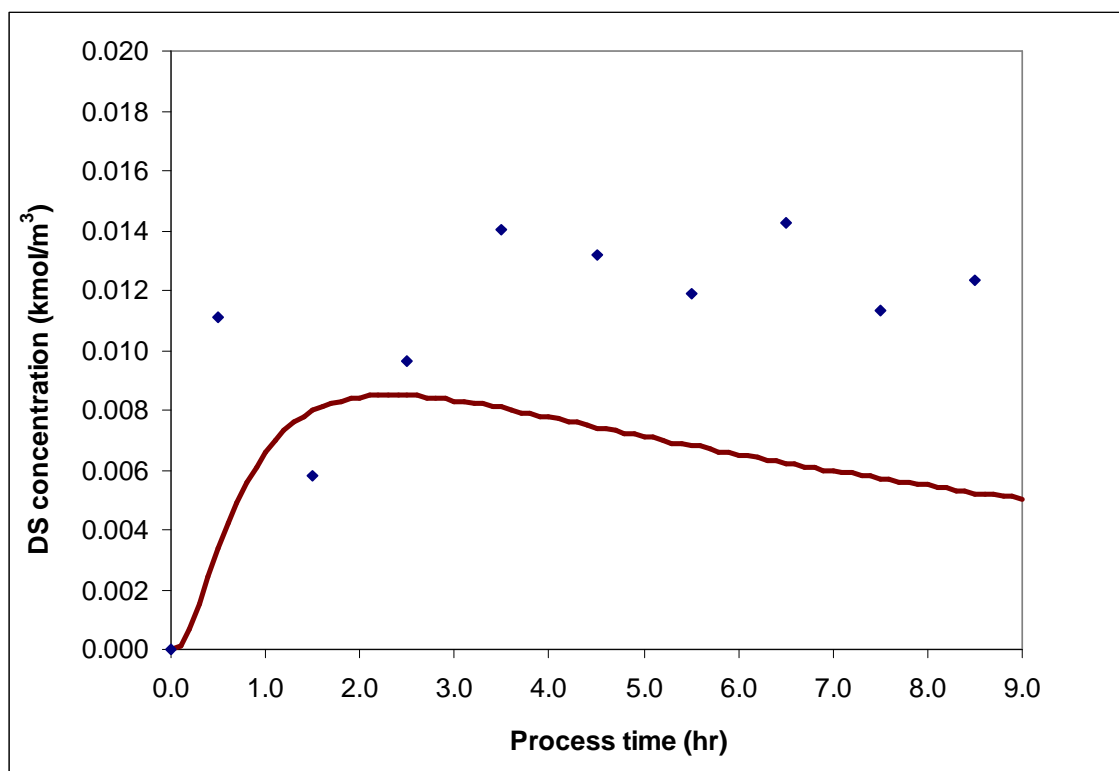


Figure 5.9 Comparison of simulated (—) and experimental (◆) concentration profiles of the aromatic disulfide (DS) with respect to process time at residence time θ : 1.0 hr, process temperature: 85 °C, process pressure: 364.7 psia,

$$F_{H_2}^0 / F_{sulfonyl}^0 = 8.0 \text{ mol/mol}, F_{H_2}^0 / F_{Ar}^0 = 3.0 \text{ mol/mol}$$

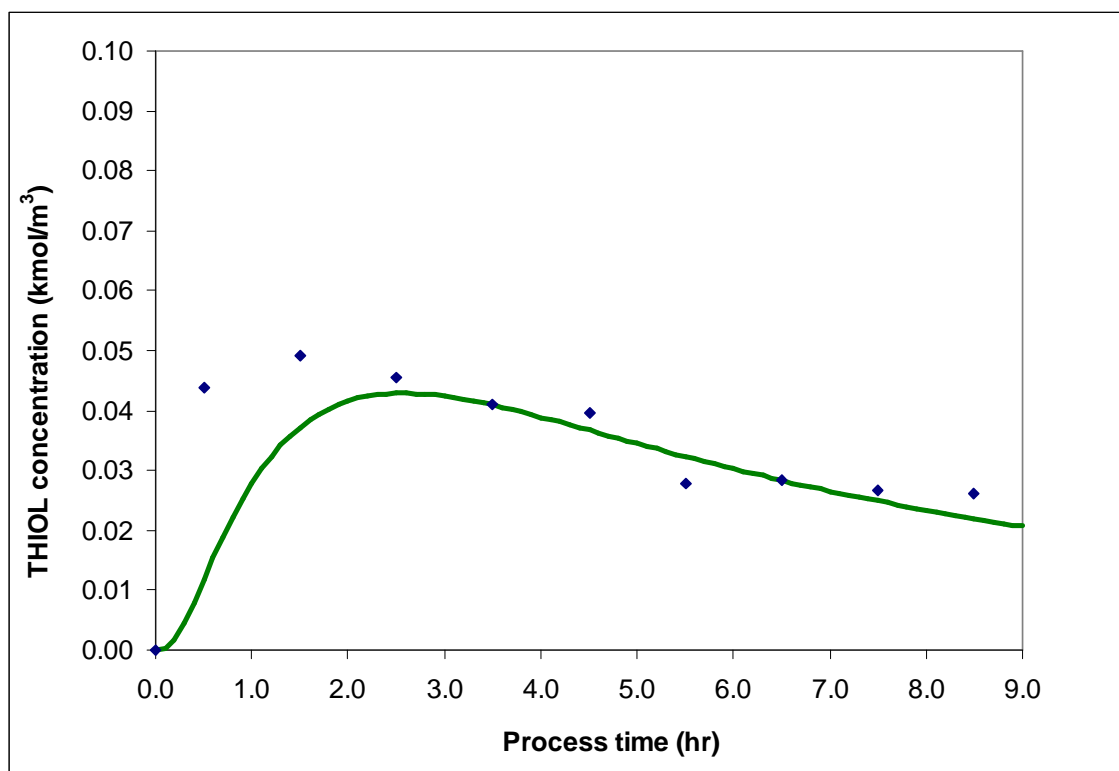


Figure 5.10 Comparison of simulated (—) and experimental (◆) concentration profiles of the aromatic thiol (THIOL) with respect to process time at residence time θ : 1.0 hr, process temperature: 85 °C, process pressure: 364.7 psia,

$$F_{H_2}^0 / F_{sulfonyl}^0 = 8.0 \text{ mol/mol}, F_{H_2}^0 / F_{Ar}^0 = 3.0 \text{ mol/mol}$$

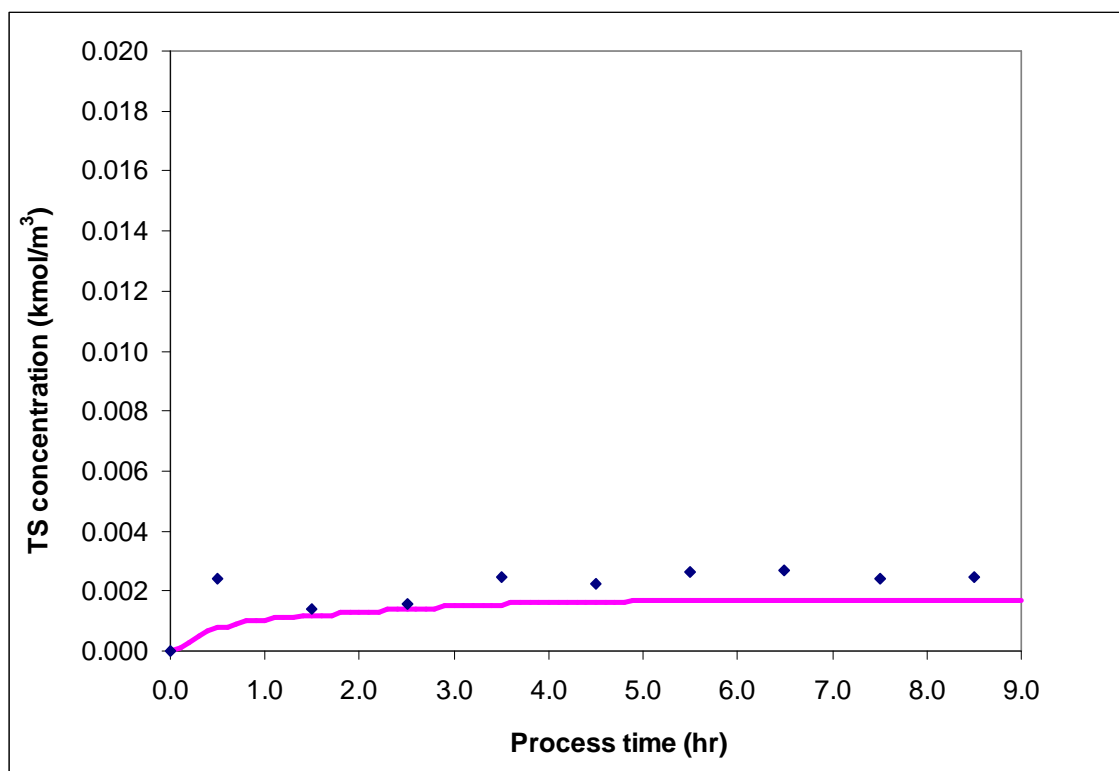


Figure 5.11 Comparison of simulated (—) and experimental (◆) concentration profiles of the aromatic thiosulfone (TS) with respect to process time at residence time θ : 1.0 hr, process temperature: 85 °C, process pressure: 364.7 psia,

$$F_{H_2}^0 / F_{sulfonyl}^0 = 8.0 \text{ mol/mol}, F_{H_2}^0 / F_{Ar}^0 = 3.0 \text{ mol/mol}$$

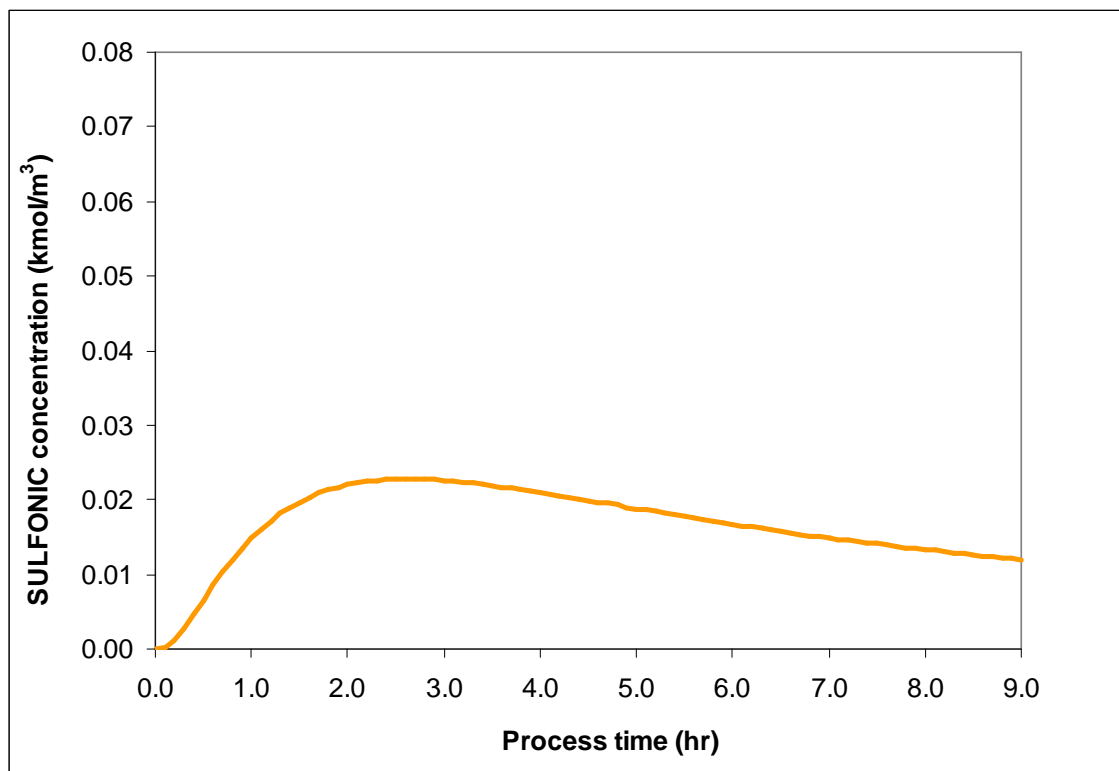


Figure 5.12 Simulated concentration profile of the aromatic sulfonic acid (—) (SULFONIC) with respect to process time at residence time θ : 1.0 hr, process temperature: 85 °C, process pressure: 364.7 psia, $F_{H_2}^0 / F_{sulfonyl}^0 = 8.0 \text{ mol/mol}$,

$$F_{H_2}^0 / F_{Ar}^0 = 3.0 \text{ mol/mol}$$

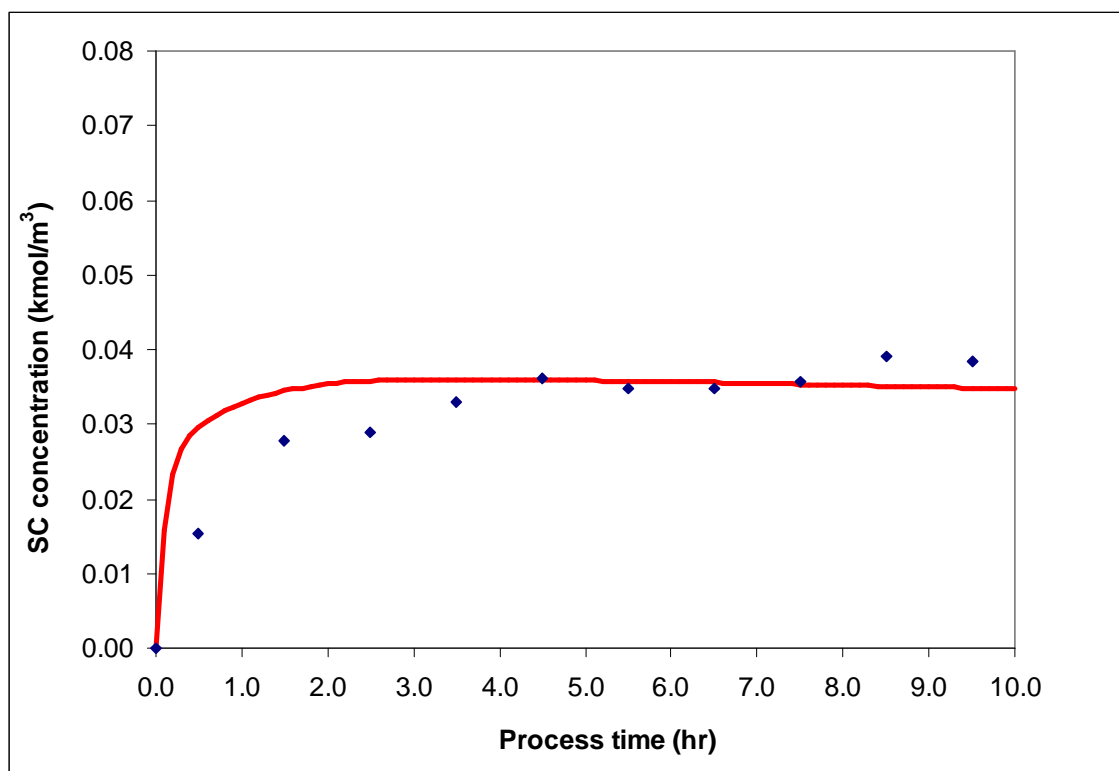


Figure 5.13 Comparison of simulated (—) and experimental (◆) concentration profiles of the aromatic sulfonyl chloride (SC) with respect to process time at residence time θ : 1.0 hr, process temperature: 97 °C, process pressure: 364.7 psia,

$$F_{H_2}^0 / F_{sulfonyl}^0 = 8.0 \text{ mol/mol}, F_{H_2}^0 / F_{Ar}^0 = 3.0 \text{ mol/mol}$$

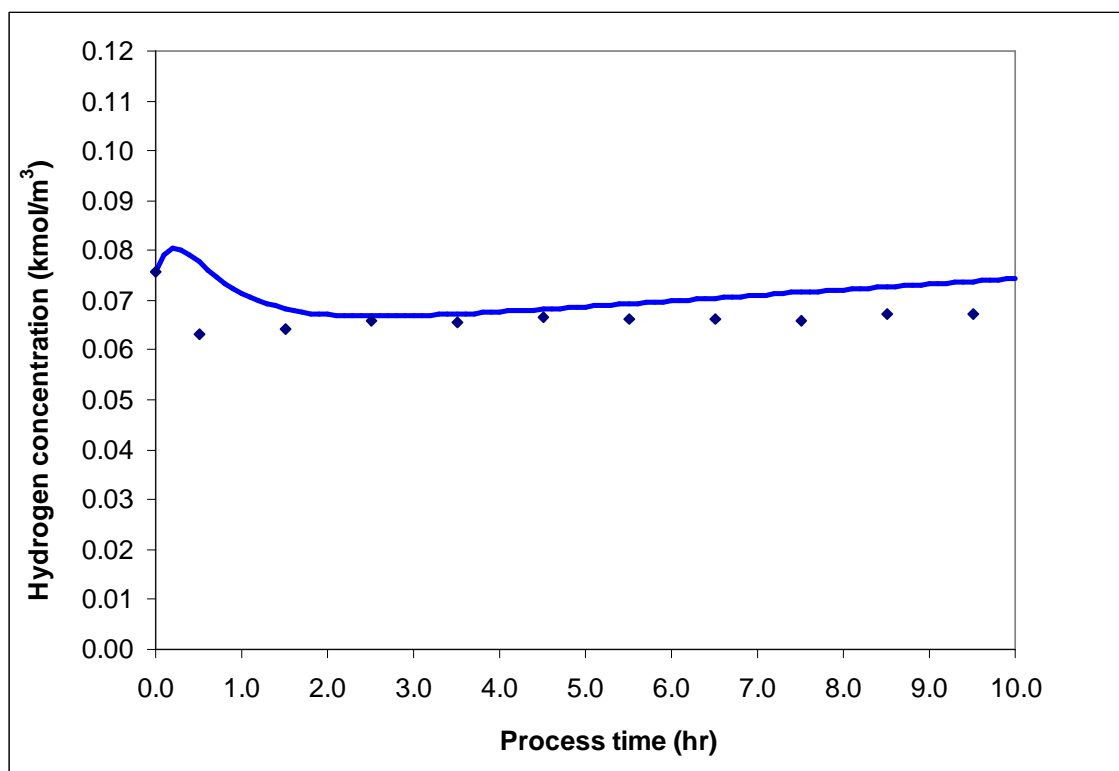


Figure 5.14 Comparison of simulated (—) and experimental (◆) concentration profiles of hydrogen with respect to process time at residence time θ : 1.0 hr, process temperature:

97 °C, process pressure: 364.7 psia, $F_{H_2}^0 / F_{sulfonyl}^0 = 8.0 \text{ mol/mol}$,

$F_{H_2}^0 / F_{Ar}^0 = 3.0 \text{ mol/mol}$

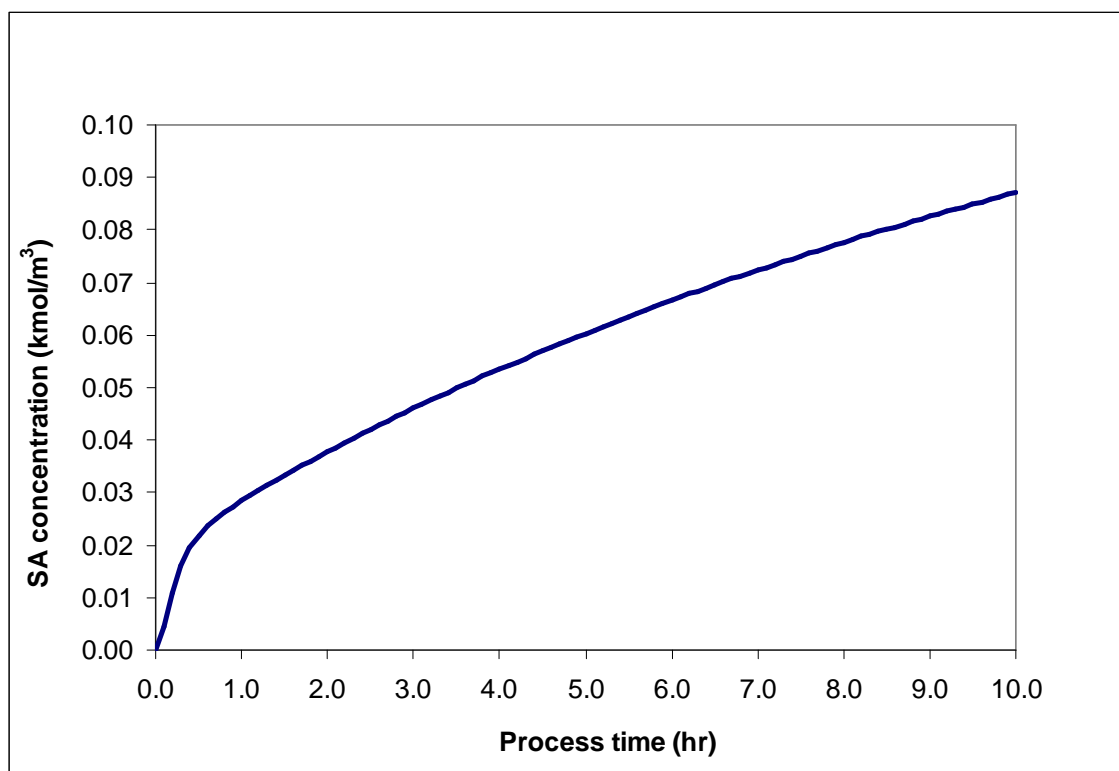


Figure 5.15 Simulated concentration profile of the aromatic sulfonic acid (—) (SA) with respect to process time at residence time θ : 1.0 hr, process temperature: 97 °C, process pressure: 364.7 psia, $F_{H_2}^0 / F_{sulfonyl}^0 = 8.0 \text{ mol/mol}$, $F_{H_2}^0 / F_{Ar}^0 = 3.0 \text{ mol/mol}$

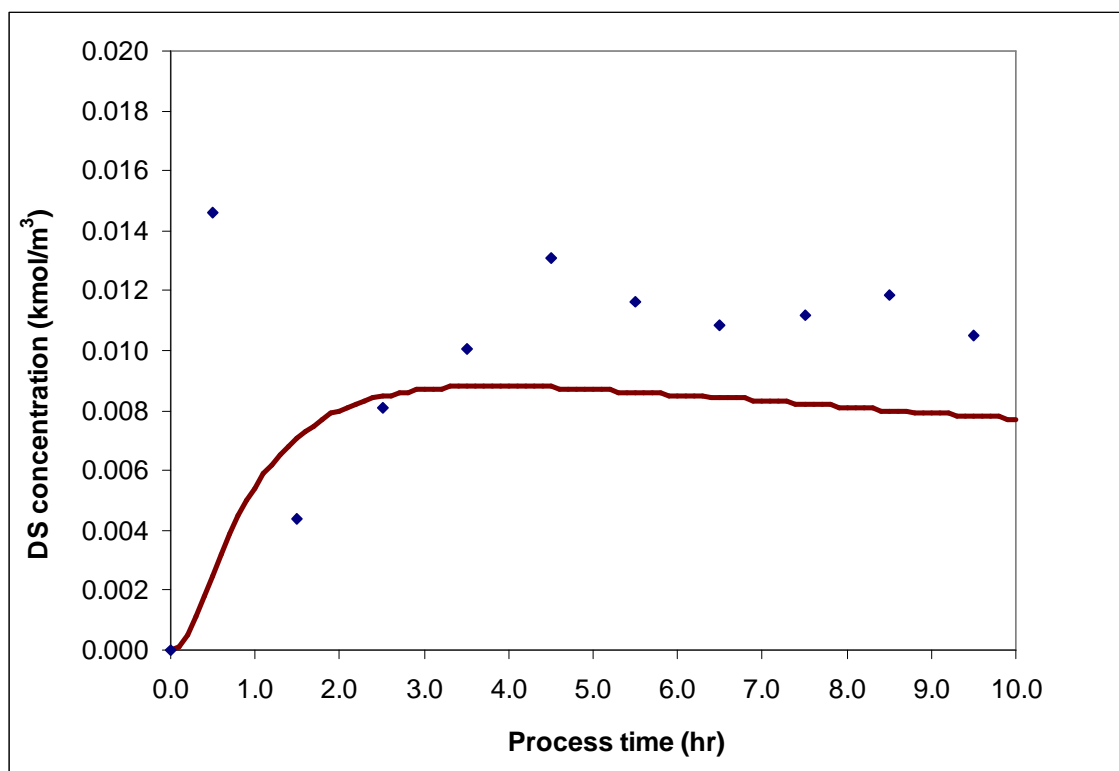


Figure 5.16 Comparison of simulated (—) and experimental (◆) concentration profiles of the aromatic disulfide (DS) with respect to process time at residence time θ : 1.0 hr, process temperature: 97 °C, process pressure: 364.7 psia,

$$F_{H_2}^0 / F_{sulfonyl}^0 = 8.0 \text{ mol/mol}, F_{H_2}^0 / F_{Ar}^0 = 3.0 \text{ mol/mol}$$

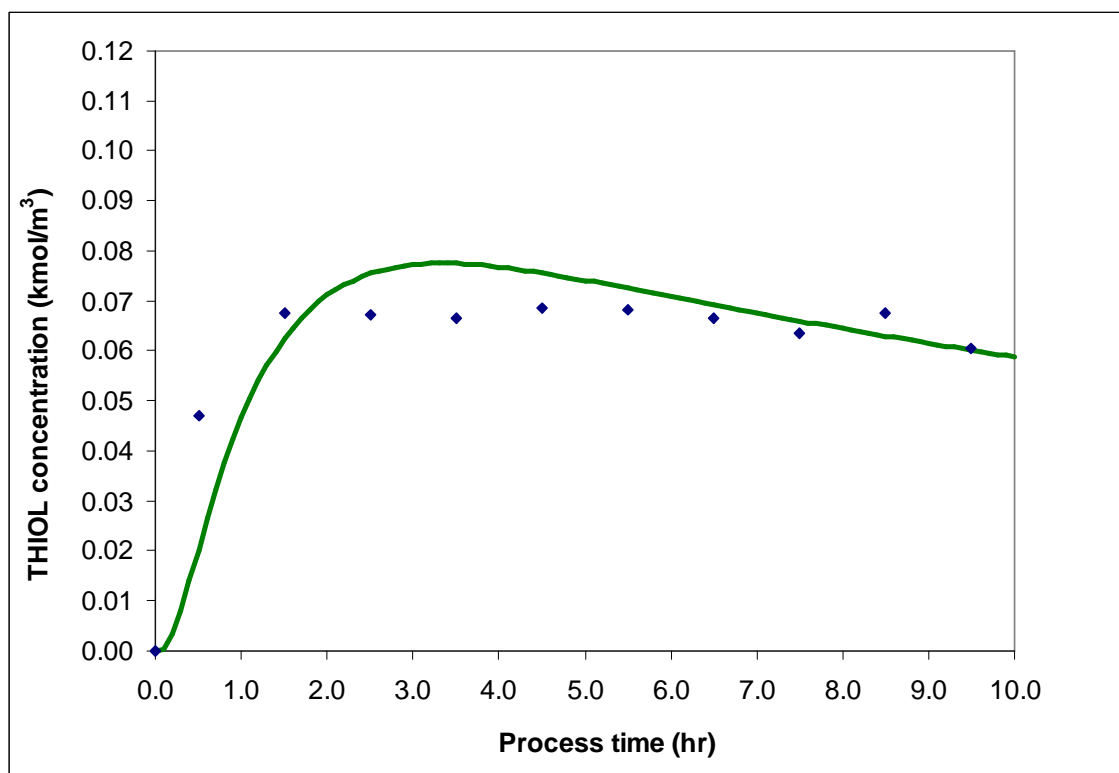


Figure 5.17 Comparison of simulated (—) and experimental (◆) concentration profiles of the aromatic thiol (THIOL) with respect to process time at residence time θ : 1.0 hr, process temperature: 97 °C, process pressure: 364.7 psia,

$$F_{H_2}^0 / F_{sulfonyl}^0 = 8.0 \text{ mol/mol}, F_{H_2}^0 / F_{Ar}^0 = 3.0 \text{ mol/mol}$$

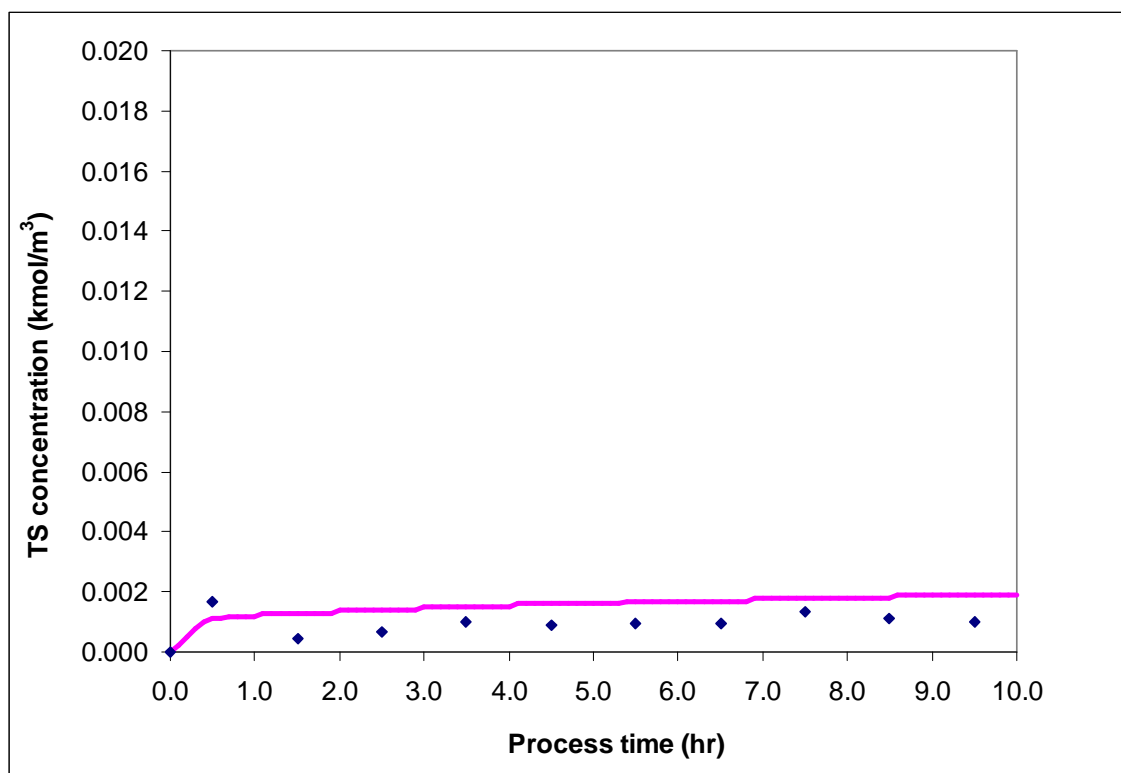


Figure 5.18 Comparison of simulated (—) and experimental (◆) concentration profiles of the aromatic thiosulfone (TS) with respect to process time at residence time θ : 1.0 hr, process temperature: 97 °C, process pressure: 364.7 psia,

$$F_{H_2}^0 / F_{sulfonyl}^0 = 8.0 \text{ mol/mol}, F_{H_2}^0 / F_{Ar}^0 = 3.0 \text{ mol/mol}$$

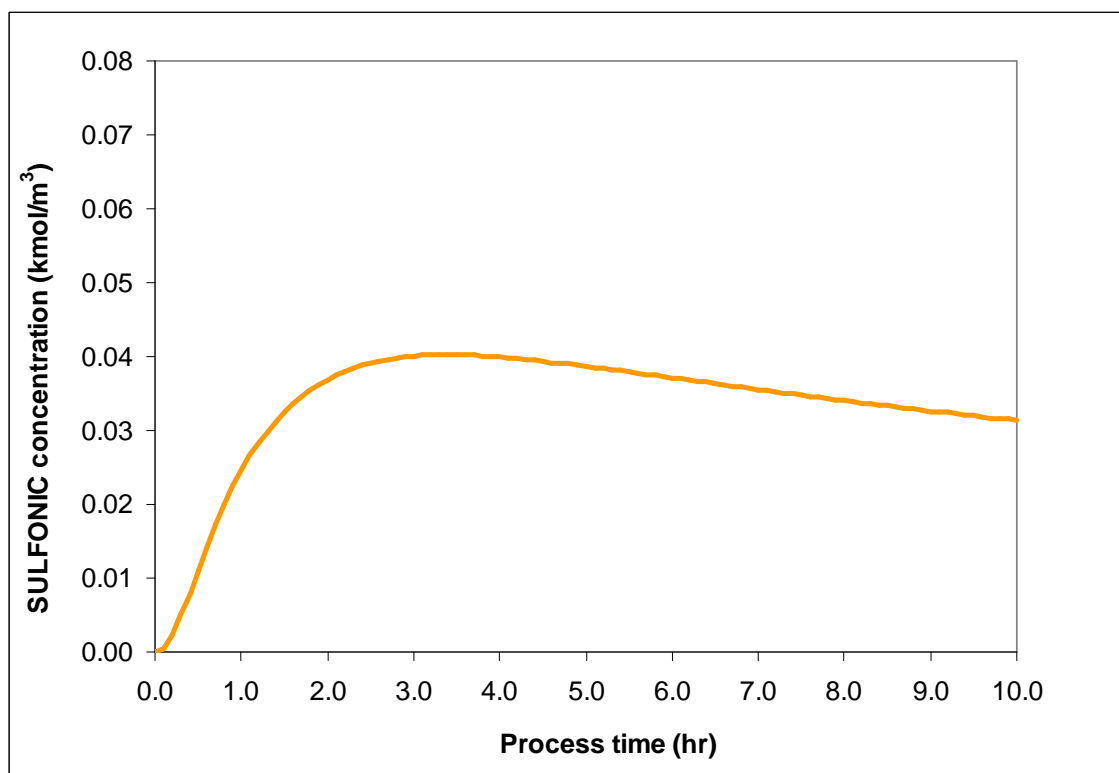


Figure 5.19 Simulated concentration profile of the aromatic sulfonic acid (—) (SULFONIC) with respect to process time at residence time θ : 1.0 hr, process temperature: 97 °C, process pressure: 364.7 psia, $F_{H_2}^0 / F_{sulfonyl}^0 = 8.0 \text{ mol/mol}$,

$$F_{H_2}^0 / F_{Ar}^0 = 3.0 \text{ mol/mol}$$

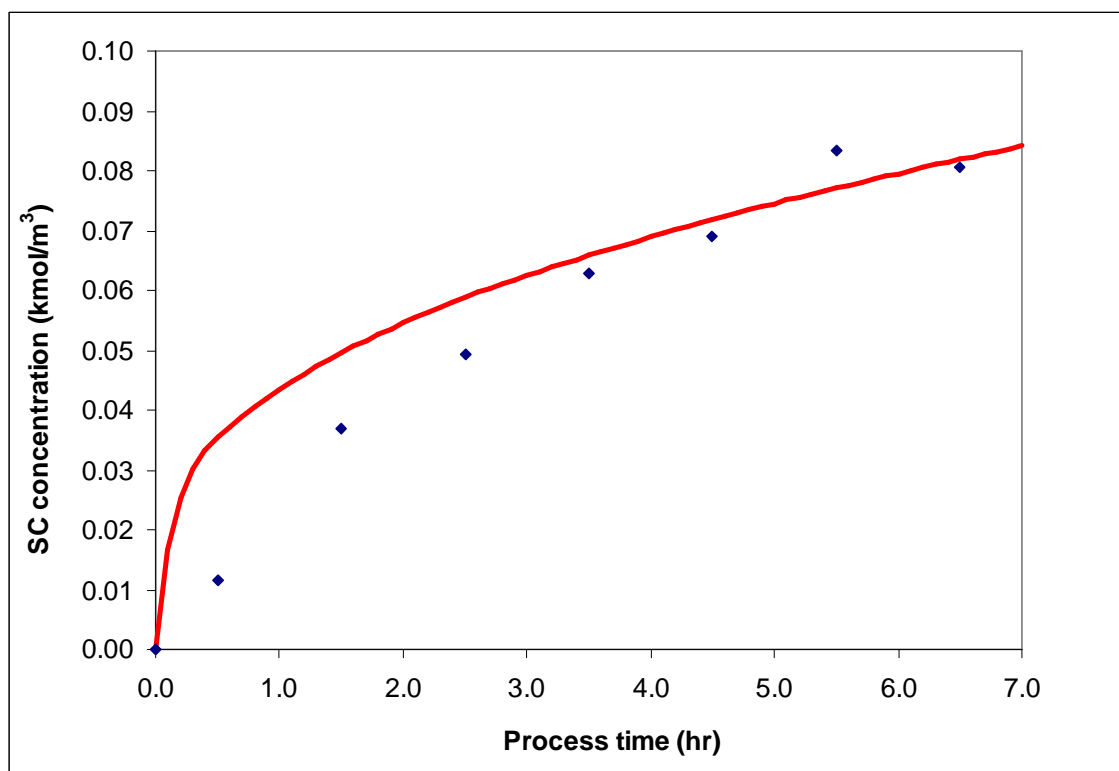


Figure 5.20 Comparison of simulated (—) and experimental (◆) concentration profiles of the aromatic sulfonyl chloride (SC) with respect to process time at residence time θ : 1.0 hr, process temperature: 110 °C, process pressure: 364.7 psia,

$$F_{H_2}^0 / F_{sulfonyl}^0 = 8.0 \text{ mol/mol}, F_{H_2}^0 / F_{Ar}^0 = 3.0 \text{ mol/mol}$$

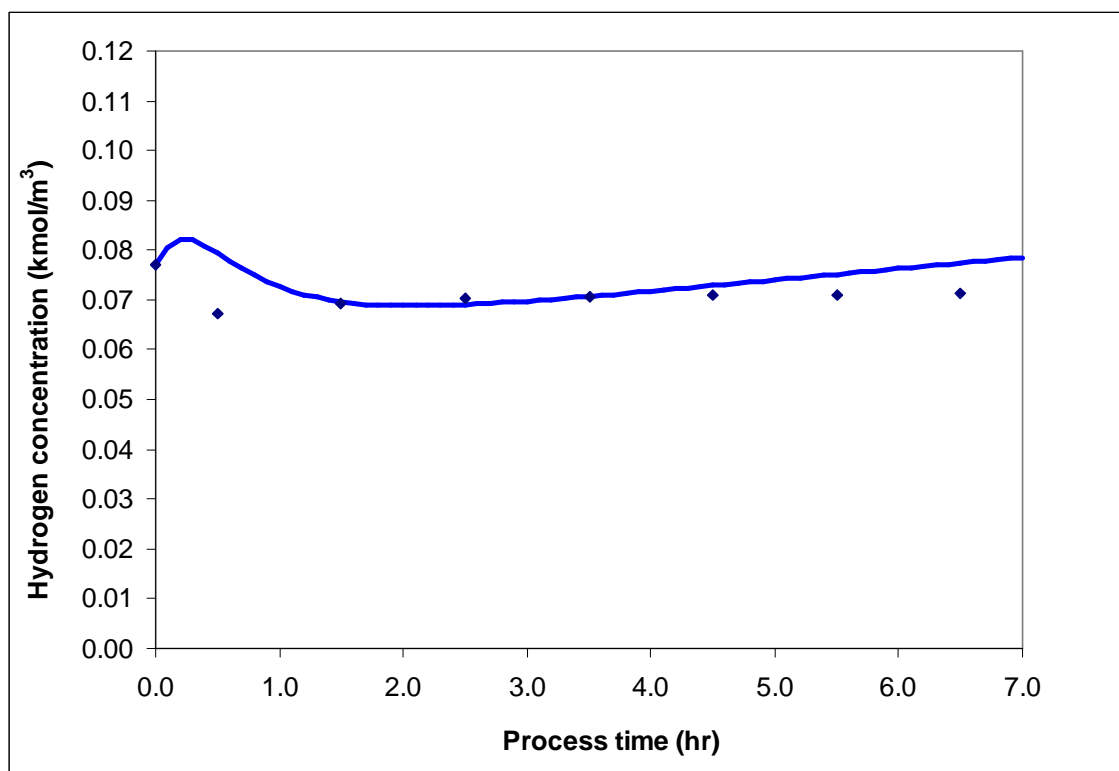


Figure 5.21 Comparison of simulated (—) and experimental (◆) concentration profiles of hydrogen with respect to process time at residence time θ : 1.0 hr, process temperature:

110 °C, process pressure: 364.7 psia, $F_{H_2}^0 / F_{sulfonyl}^0 = 8.0 \text{ mol/mol}$,

$F_{H_2}^0 / F_{Ar}^0 = 3.0 \text{ mol/mol}$

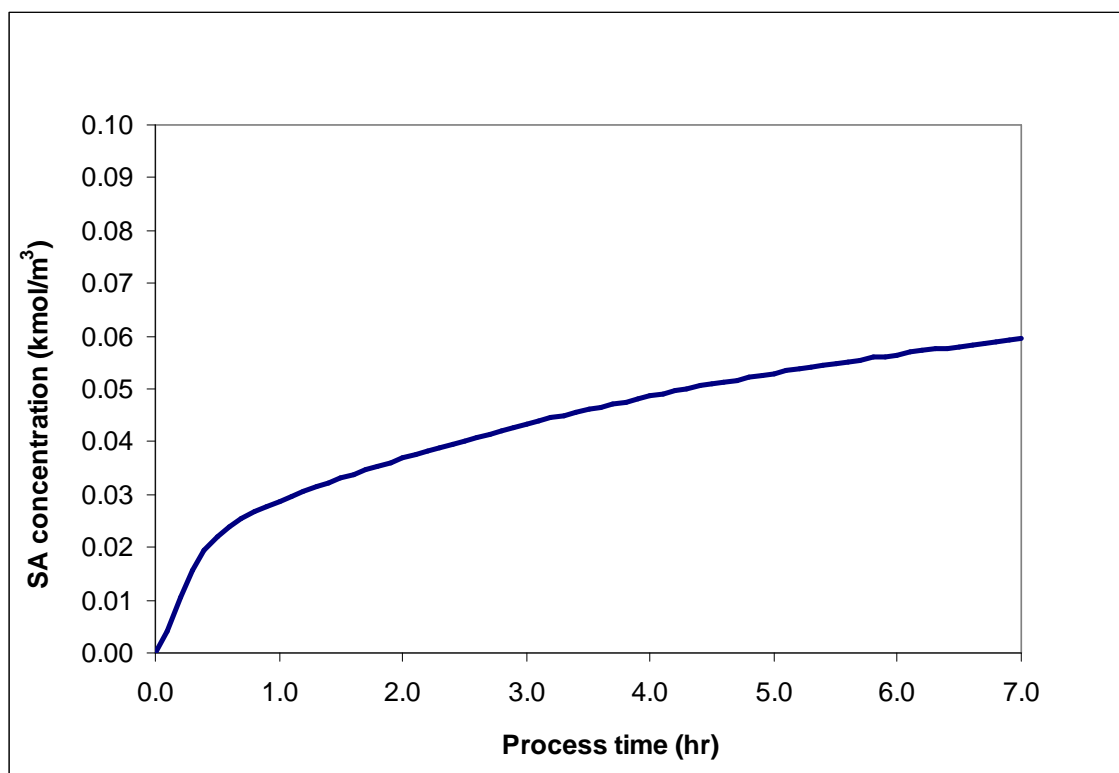


Figure 5.22 Simulated concentration profile of the aromatic sulfonic acid (—) (SA) with respect to process time at residence time θ : 1.0 hr, process temperature: 110 °C, process pressure: 364.7 psia, $F_{H_2}^0 / F_{sulfonyl}^0 = 8.0 \text{ mol/mol}$, $F_{H_2}^0 / F_{Ar}^0 = 3.0 \text{ mol/mol}$

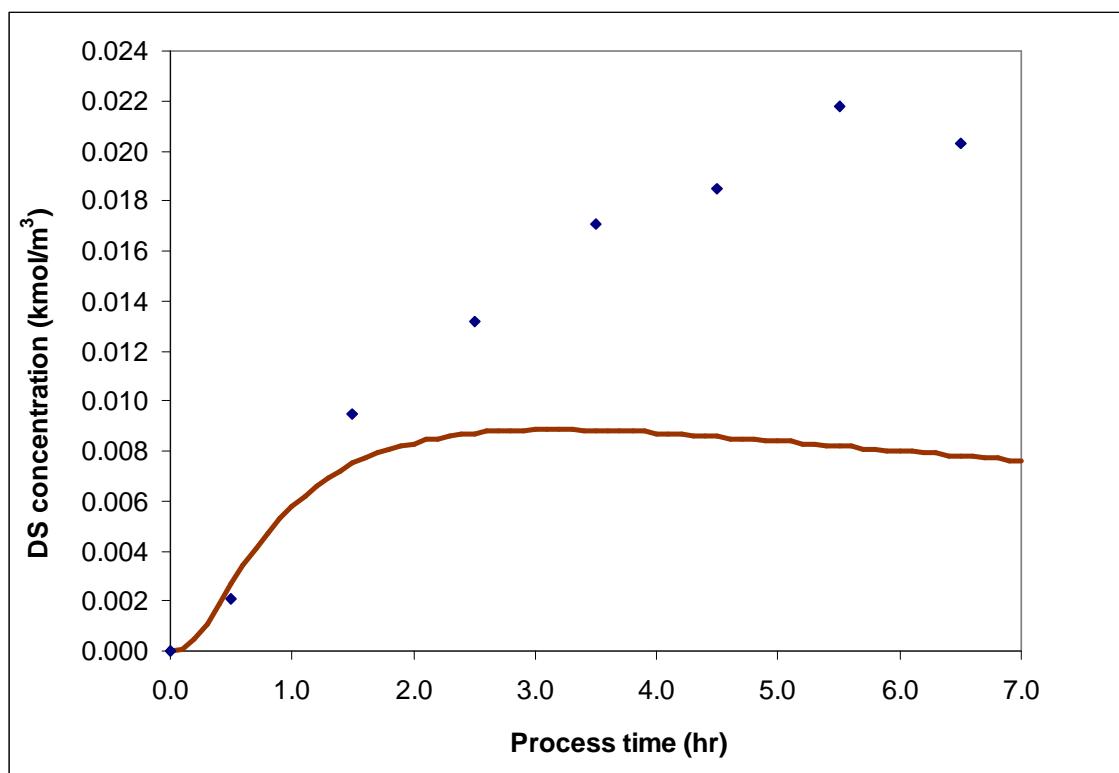


Figure 5.23 Comparison of simulated (—) and experimental (◆) concentration profiles of the aromatic disulfide (DS) with respect to process time at residence time θ : 1.0 hr, process temperature: 110 °C, process pressure: 364.7 psia,

$$F_{H_2}^0 / F_{sulfonyl}^0 = 8.0 \text{ mol/mol}, F_{H_2}^0 / F_{Ar}^0 = 3.0 \text{ mol/mol}$$

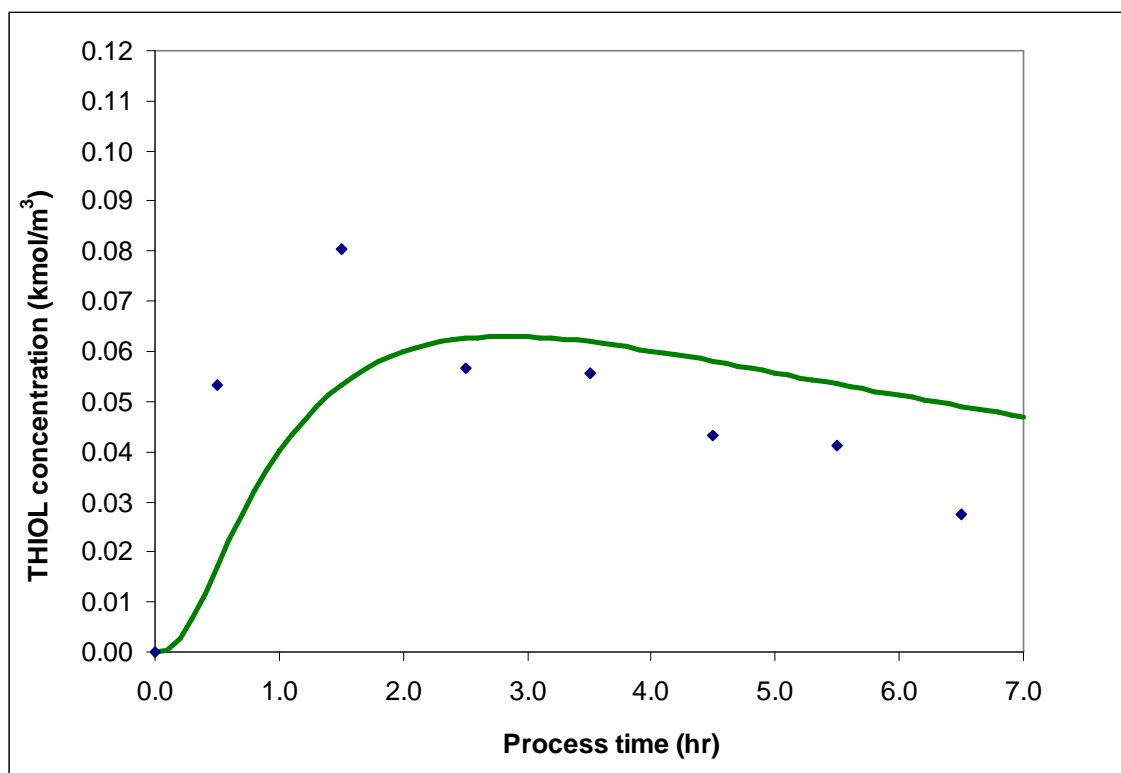


Figure 5.24 Comparison of simulated (—) and experimental (◆) concentration profiles of the aromatic thiol (THIOL) with respect to process time at residence time θ : 1.0 hr, process temperature: 110 °C, process pressure: 364.7 psia,

$$F_{H_2}^0 / F_{sulfonyl}^0 = 8.0 \text{ mol/mol}, F_{H_2}^0 / F_{Ar}^0 = 3.0 \text{ mol/mol}$$

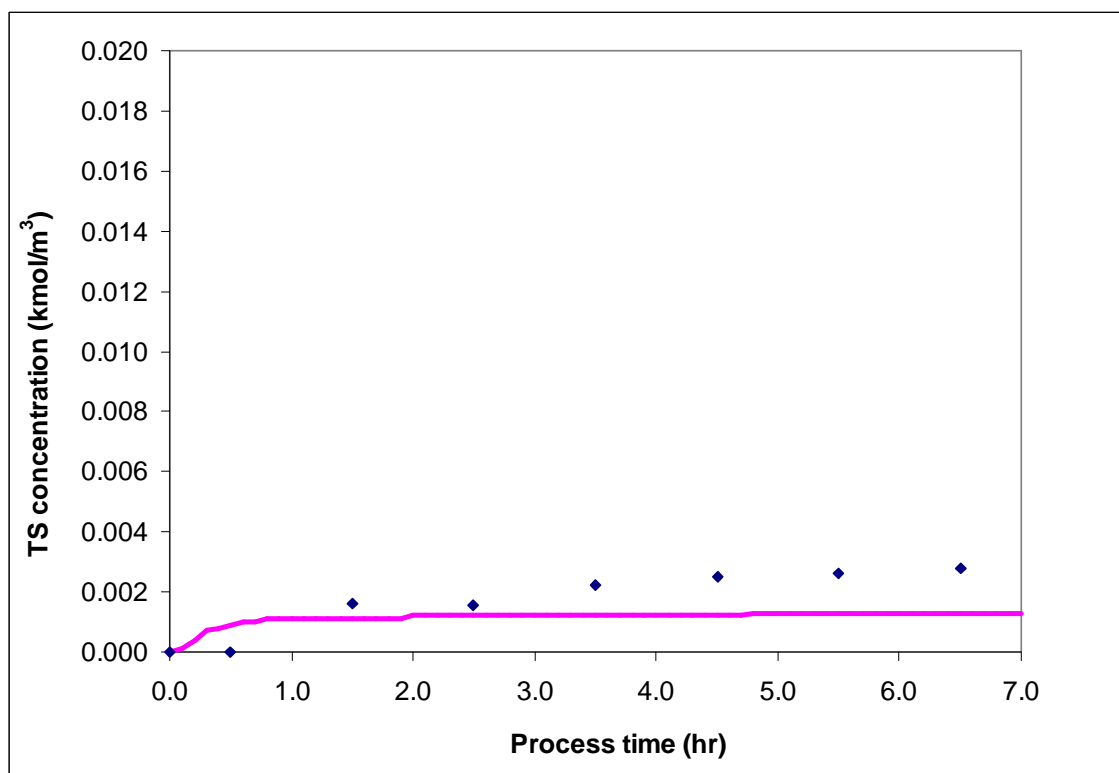


Figure 5.25 Comparison of simulated (—) and experimental (◆) concentration profiles of the aromatic thiosulfone (TS) with respect to process time at residence time θ : 1.0 hr, process temperature: 110 °C, process pressure: 364.7 psia,

$$F_{H_2}^0 / F_{sulfonyl}^0 = 8.0 \text{ mol/mol}, F_{H_2}^0 / F_{Ar}^0 = 3.0 \text{ mol/mol}$$

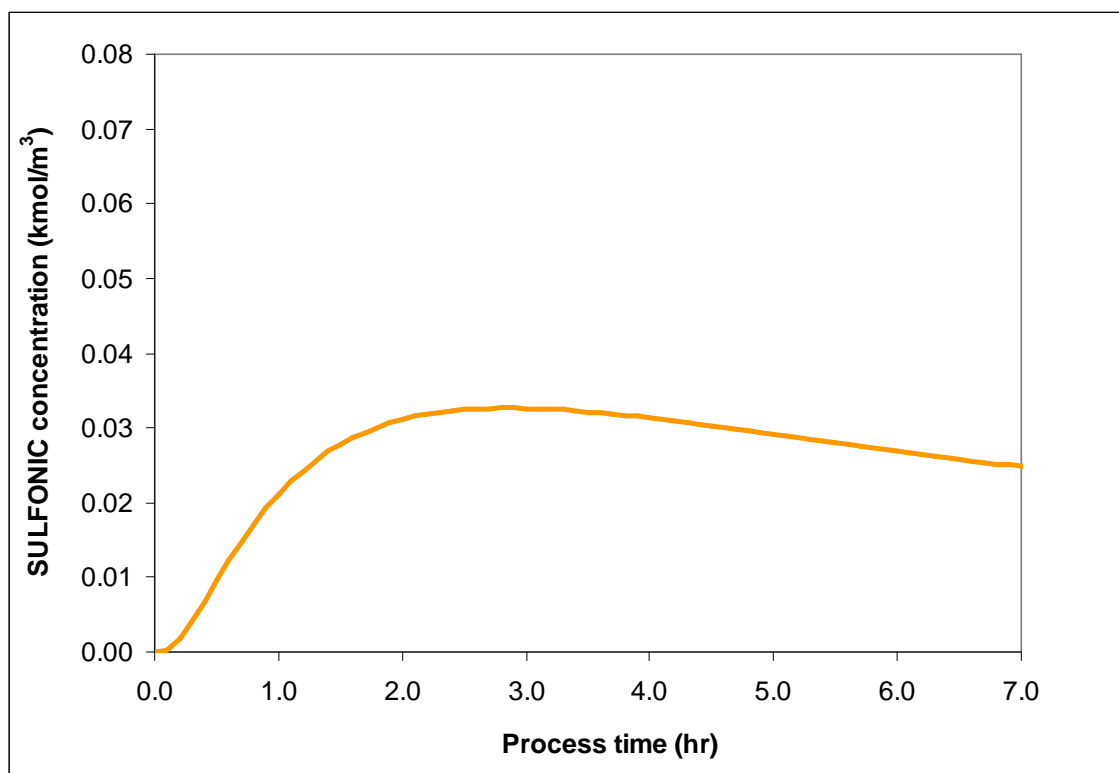


Figure 5.26 Simulated concentration profile of the aromatic sulfonic acid (—) (SULFONIC) with respect to process time at residence time θ : 1.0 hr, process temperature: 110 °C, process pressure: 364.7 psia, $F_{H_2}^0 / F_{sulfonyl}^0 = 8.0 \text{ mol/mol}$,

$$F_{H_2}^0 / F_{Ar}^0 = 3.0 \text{ mol/mol}$$

Figures 5.27 to 5.31 show the parity plots for each of the reacting species at all experimental conditions used for the parameter estimation.

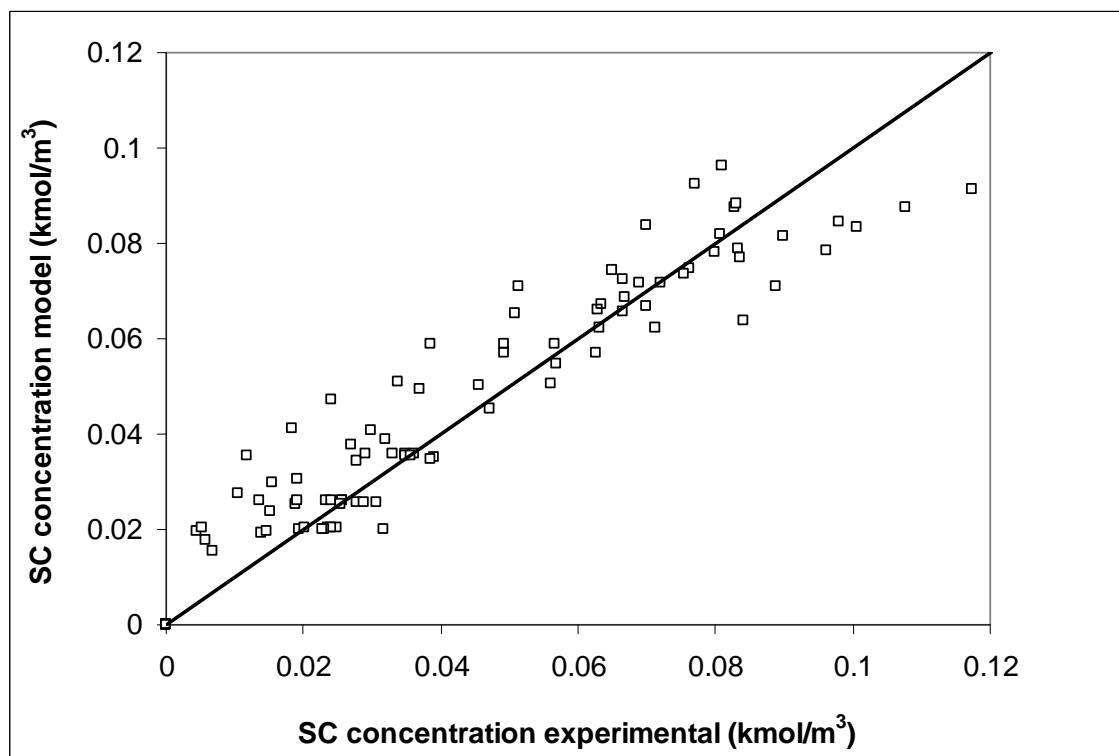


Figure 5.27 Parity plot for the comparison of experimental and simulated concentrations for the aromatic sulfonyl chloride (SC) at all experimental conditions

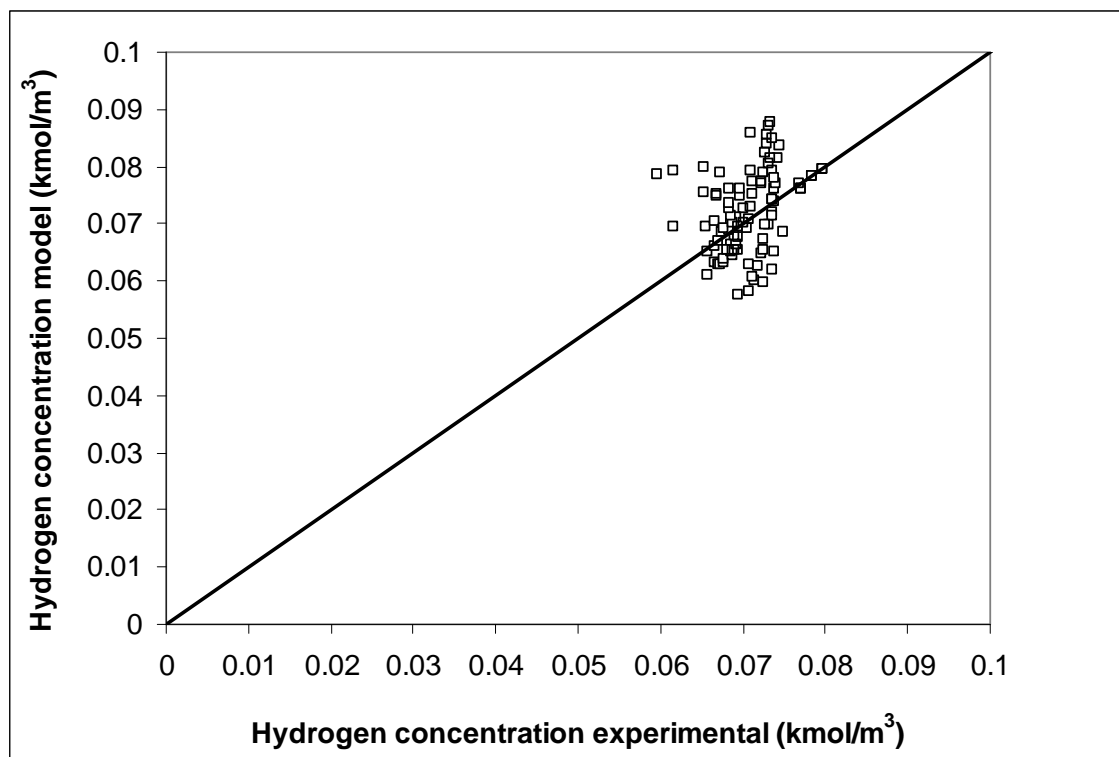


Figure 5.28 Parity plot for the comparison of experimental and simulated concentrations for hydrogen at all experimental conditions

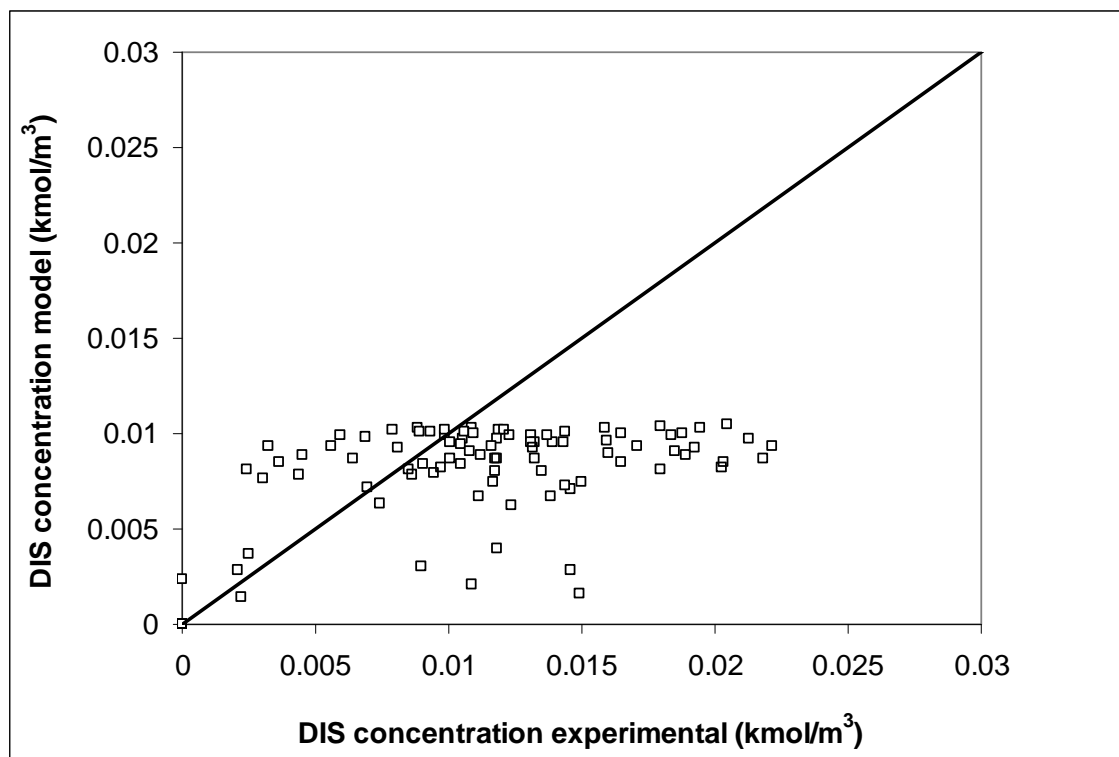


Figure 5.29 Parity plot for the comparison of experimental and simulated concentrations for the aromatic disulfide (DS) at all experimental conditions

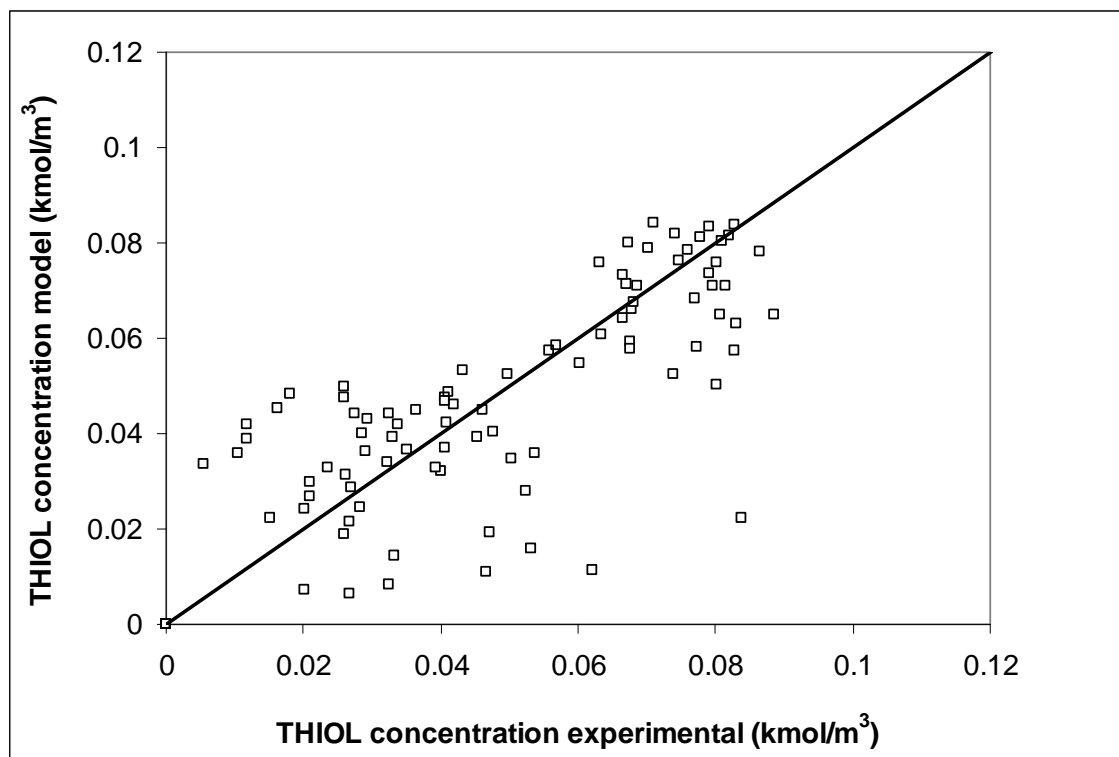


Figure 5.30 Parity plot for the comparison of experimental and simulated concentrations for the aromatic thiol (THIOL) at all experimental conditions

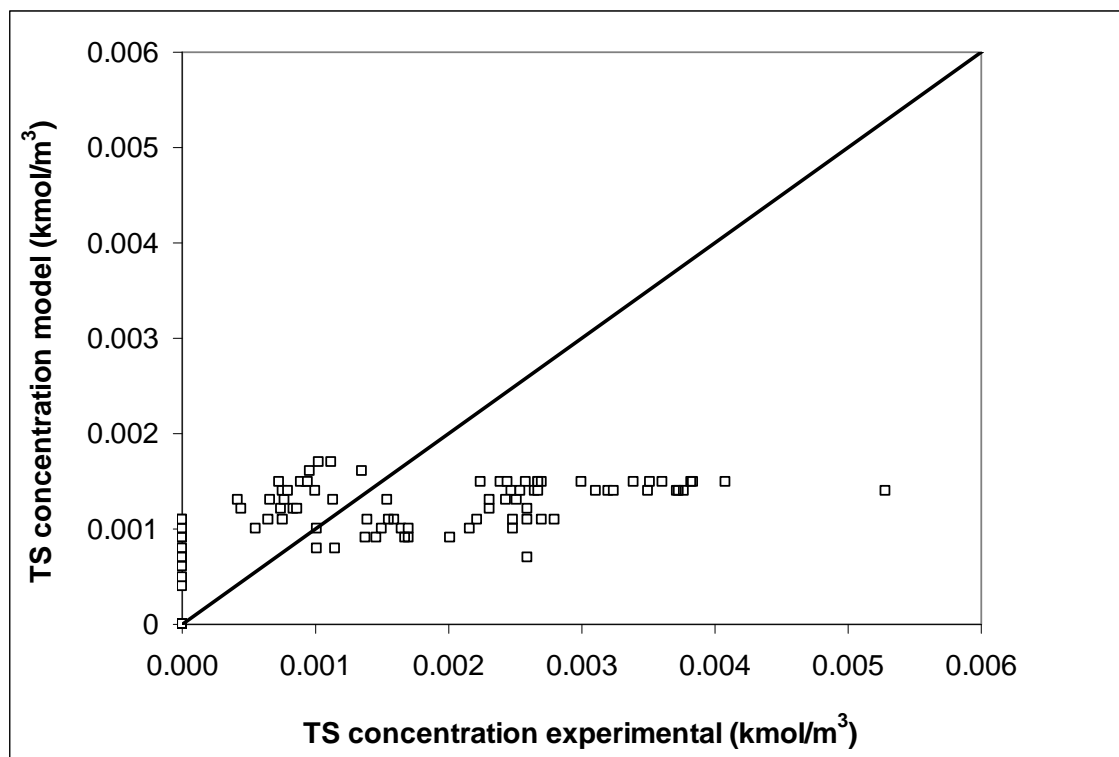


Figure 5.31 Parity plot for the comparison of experimental and simulated concentrations for the aromatic thiosulfone (TS) at all experimental conditions

The kinetic model show a good fit of the experimental data for the aromatic sulfonyl chloride, hydrogen and the aromatic thiol, as shown in the parity plots and the comparison of the simulated and experimental concentration profiles for these compounds. The kinetic model predicts higher values of concentration for the aromatic sulfonyl chloride at early process time, as shown in the concentration profiles in Figures 5.6, 5.13 and 5.20. Based on the parity plots shown in Figures 5.29 and 5.31, there is a lack of fit between the estimated concentrations with the experimental data for the aromatic disulfide and the aromatic thiosulfone. It is principally due to the absence of experimental data for the aromatic sulfinic acid.

At a process temperature of 97 °C, a maximum in the concentration of the aromatic disulfide has been observed experimentally at early process time and at all the residence times investigated. This maximum is not reproduced by the kinetic model as shown in Figure 5.16 for a residence time of 1.0 hr. It is probably caused by the initial value given before minimization of the objective function for the set of parameters as well as the large 95 % confidence interval obtained for the parameter estimates. Therefore, further improvements in the initial value of the set of parameters need to be conducted to represent fully the behavior of the intermediates with respect to process time. The same conclusion can be made considering the maximum obtained at early process time with the simulated concentration profile of hydrogen, which is not observed experimentally.

CHAPTER VI

CONCLUSION AND RECOMMENDATION

The catalytic hydrogenation of an aromatic sulfonyl chloride was investigated in continuous and semi-batch mode processes using a Robinson-Mahoney stationary basket reactor. Intrinsic reaction rates of the reacting species were obtained on the surface of a commercial 1 wt% palladium on charcoal catalyst. Kinetic data collected in continuous process show that the catalyst is deactivated during an experiment. The lost of catalyst activity was displayed by a continuous decrease of the molar yield Y_2 of the aromatic thiol from the aromatic sulfonyl chloride when the process time equal to 2-3 times the residence time θ of the liquid within the reactor. Beyond 3θ , the surface of catalyst accumulates more of the aromatic sulfonyl chloride, which continually deactivates the catalyst. It leads to the conclusion that the aromatic sulfonyl chloride is the deactivating agent, which is adsorbed irreversibly on the surface of the catalyst. XRD analysis shows that the active sites are blocked and an amorphous layer was formed on the surface of the palladium catalyst. Similar studies on the hydrogenation of sulfur-based compounds using a palladium catalyst show that the sulfur atom covers four metal active sites to form an inactive phase Pd_4S .

A heterogeneous kinetic model has been developed for the hydrogenation of the aromatic sulfonyl chloride using the Hougen-Watson type of reaction equation rate with a hyperbolic deactivation function expressed in term of process time. The mathematical model consists of non-linear and simultaneous differential equations with multiple variables. The kinetic parameters, which include the adsorption equilibrium constants for the reacting species, the kinetic constants for each catalytic step of the reaction scheme and the parameter alpha of the empirical hyperbolic deactivation function, were estimated from the minimization of a multi-response objective function using a sequential quadratic program. The program includes a quasi-Newton nonlinear multi-variable algorithm. The kinetic model with the set of estimated parameters led to a

fairly good fit of the experimental data for the aromatic sulfonyl chloride, hydrogen and the aromatic thiol. A lack of fit with the experimental data for the aromatic disulfide and the aromatic thiosulfone was observed. Large standard deviations and 95 % confidence intervals were obtained for each of the parameters of the kinetic model, which result in a high uncertainty in the values of the kinetic parameters obtained from the estimation work. Therefore, no conclusions can be made regarding the major route for the production of the aromatic thiol and the values of the kinetic parameters.

More research efforts need to be conducted with the following recommendations for future work:

- Characterization and quantitation of the white particles in suspension in the effluent liquid organic mixture
- Improvement of the gas phase analysis with investigations on the possible formation of hydrogen sulfide (H_2S) during the hydrogenation of the aromatic sulfonyl chloride
- Sampling of the reactor should be modified in the thiol production unit to avoid back-calculating the content of each reacting specie in the effluent organic mixture leaving the reactor from the content obtained by the analysis of the same liquid organic mixture after draining the liquid collector. The sampling of the content of the reactor should also include a method to determine experimentally the concentration of hydrogen dissolved in the organic liquid mixture within the reactor. In this respect, the concentration hydrogen, calculated and used in the kinetic model, was estimated from the solubility of hydrogen in pure toluene and not in the effluent liquid organic mixture
- Improvement in the values of the kinetic parameters and fit of the simulated and experimental data

NOMENCLATURE

a	Gas-liquid interfacial area (m_i^2 / m_r^3)
b_j	Estimated kinetic parameters
C_j	Concentration of sulfur-based compound j in the liquid mixture ($kmol / m^3$)
$C_{H_2,liq}$	Concentration of hydrogen in the liquid phase ($kmol / m^3$)
C_L	Concentration of a vacant active site
C_{jL}	Concentration of a chemisorbed species j
$C_{S,total}$	Molar density of the effluent liquid mixture containing toluene and the aromatic sulfur-based compounds ($kmol / m^3$)
C_P	Concentration of the poison ($kmol / m^3$)
C_t	Concentration of the total active sites
d_b	Bubble diameter (m)
D_L	Gas diffusion coefficient in the liquid phase (m^2 / s)
D_I	Impeller blade diameter (m)
d_P	Mean spherical diameter of the catalyst particle (m)
D_S	Diffusion coefficient into the solid phase (m^2 / s)
D_T	Reactor diameter (m)
e	Energy supplied per unit mass of slurry (m^2 / s^3)

F_C	Calculated F-value
F	Tabulated F-value
$F_{sulfonyl}^0$	Inlet molar flowrate of the aromatic sulfonyl chloride ($kmol/hr$)
$F_{H_2}^0$	Inlet molar flowrate of hydrogen ($kmol/hr$)
F_{Ar}^0	Inlet molar flowrate of argon ($kmol/hr$)
$F_{sulfonyl}$	Outlet molar flowrate of the aromatic sulfonyl chloride ($kmol/hr$)
$F_{disulfide}$	Outlet molar flowrate of the aromatic disulfide ($kmol/hr$)
$F_{thiosulfone}$	Outlet molar flowrate of the aromatic thiosulfone ($kmol/hr$)
F_{thiol}	Outlet molar flowrate of the aromatic thiol ($kmol/hr$)
F_{H_2}	Outlet molar flowrate of hydrogen ($kmol/hr$)
F_{Ar}	Outlet molar flowrate of argon ($kmol/hr$)
F_t	Outlet molar flowrate of the aromatic sulfur-based compounds ($kmol/hr$)
$F_{t_{mix}}$	Outlet molar flowrate of the gas mixture ($kmol/hr$)
g	Gravity acceleration (m/s^2)
G	Superficial gas mass flow velocity (kg/m_r^2s)
h	Calibration constant of sulfur-based compounds $mol/mol_{toluene}$
hp	Horsepower at a certain stirrer agitation speed
K	Solubility constant of hydrogen in toluene (Pa^{-1})

K_j	Adsorption equilibrium coefficient of an aromatic sulfur-based compound j ($m^3 / kmol$)
k_i	Kinetic constant for the catalytic step i ($m^3 / kg_{cat} hr$)
L	Free active site on the surface of the catalyst
\dot{m}_i	Mass flowrate of the liquid mixture (kg / hr)
$Mw_{toluene}$	Molecular weight of toluene ($kg / kmol$)
Mw_j	Molecular weight of each aromatic sulfur-based compound j ($kg / kmol$)
n	Number of responses
p	Number of parameters of the kinetic model
N	Agitation speed of the stirrer (RPM)
P/V	Power dissipated by the agitator per unit volume of the liquid (W / m^3)
$P_{reactor}$	Total pressure measured within the reactor (Pa)
P_{H_2}	Partial pressure measured within the reactor (Pa)
R	Gas constant ($8314 m^3 Pa / kmol \cdot K$)
r_i	Hougen-Watson reaction rates for reaction i ($kmol / m^3 \cdot hr$)
$s(b_j)$	Standard deviation of each estimated parameter
t_C	Calculated t-value
t	Tabulated t-value
t_{span}	Process time at the end of an experiment
T	Process temperature (K)
T_o	Average static torque of the stirrer ($N - m$)

V	True volume of the liquid corrected from the volume occupied by the basket V_{basket} and the volume occupied by the catalyst $V_{catalyst}$ (m^3)
V_{basket}	Volume occupied by the basket in the reactor (m^3)
$V_{catalyst}$	Volume occupied by the catalyst in the reactor (m^3)
V_L	Liquid holdup within the reactor (m^3)
$V_{reactor}$	Volume of the reactor (m^3)
V_S	Superficial gas velocity ($m^3 / m_r^2 s$)
V_t	Terminal gas-bubble velocity in free rise ($m^3 / m_r^2 s$)
$V_{T,liq}$	Outlet liquid volumetric flowrate (m^3 / hr)
$V_{T,gas}$	Outlet gas volumetric flowrate (m^3 / hr)
w	Mass of catalyst (kg_{cat})
X	Overall conversion of the aromatic sulfonyl chloride
X_{H_2}	Overall conversion of hydrogen
$x_{toluene}$	Mole fraction of toluene
x_j	Mole fraction of an aromatic sulfur-based compound j
$x_{H_2,liq}$	Mole fraction of hydrogen dissolved in toluene
Y_1	Molar yield of the aromatic sulfonyl chloride into the aromatic disulfide
Y_2	Molar yield of the aromatic sulfonyl chloride into the aromatic thiol

Y_3 Molar yield of the aromatic sulfonyl chloride into the aromatic thiosulfone

y_i Experimental point

\hat{y}_i Calculated value of y_i from the kinetic model

y_{H_2} Mole fraction of hydrogen in the gas phase

y_{Ar} Mole fraction of argon in the gas phase

Greek letters

α_i Hyperbolic deactivation parameter for the catalytic step i

β Percentage point of the t-distribution

δ_k Step length in the quasi-Newton method

ε Gas hold-up (m^3 / m_r^3)

Φ_i Deactivation function

ν Slip velocity (m/s)

ρ_L Density of the liquid (kg/m^3)

$\rho_{toluene}$ Density of toluene (kg/m^3)

ρ_G Density of the gas (kg/m^3)

μ_L Viscosity of the fluid surrounding the gas bubbles ($Pa.s$)

μ_G Viscosity of gas ($Pa.s$)

$\sigma^2(b_j)$	Experimental error variance
σ_L	Surface tension of the liquid (kg/s^2)
θ	Residence time of the liquid within the reactor (hr)
v	Slip velocity (m/s)

LITERATURE CITED

- [1] Wikipedia, the Free Encyclopedia: <http://en.wikipedia.org/wiki/Thiol>. Accessed: 12/07.
- [2] International Union of Pure and Applied Chemistry. *Nomenclature of Organic Chemistry*, Section C 5.1, Pergamon Press: New York, 1979.
- [3] Roy, K. *Thiols and Organic Sulfides*, Ullmann's Encyclopedia of Industrial Chemistry, 6th edition, Wiley-VCH, Weinheim, 2003.
- [4] Marcinkowski, M.; Clemens, J. *Estimation of the Fair Market Value of the Catalytic Hydrogenation Technology*, DuPont Internal Communication Report, Wilmington, DE, 2003.
- [5] Rase, H. *Handbook of Commercial Catalysts*, Chapter 12, CRC Press: Boca Raton, 2000.
- [6] Jacobson, S. *MT 484 Process Development, Hydrogen Reduction Route to BW732, MT553 Carbonylation to MJ673*, DuPont Internal Communication Report, Wilmington, DE, 1997.
- [7] Field, F.; Grunwald, F. Lithium Aluminum Hydride Reduction of Certain Sulfonic Acid and Derivatives, *J. Am. Chem. Soc.* **1951**, *16*, 946.
- [8] Oae, S. *Organic Sulfur Chemistry: Structure and Mechanism*, Chapter 7, CRC Press, Boca Raton, 1991.

- [9] Wong, W.; Kurzweil, E.; Jacobson, S. *MT 484 Process development, MR342 to BW 732 Steps, Laboratory Study*, Technology Transfer Report, DuPont Internal Communication Report, Wilmington, DE, 1998.
- [10] Jacobson, S. Hydrogen Reduction of Sulfonyl Chloride, US Patent # 6,667,421 B2, 2003.
- [11] Mylroie, V.; Doles, J. Reduction of Sulfonyl Chlorides, *Catalysis of Organic Reactions*, 40, 189, Marcel Dekker: New York, 1990.
- [12] Makar'ev, S.; Navalikhina, M.; Yulin, M. The Hydrogenation Treatment of Toluene, *Solid Fuel Chemistry*. **1977**, 11(5), 125-131.
- [13] Goodwin, R. Toluene Thermophysical Properties from 178 to 800 K at Pressures to 1000 bar, *J. Phys. Chem. Ref. Data*. **1989**, 18(4), 1565-1636.
- [14] Froba, A.; Leipertz, A. Viscosity and Surface Tension of Saturated Toluene From Surface Light Scattering, Paper Presented at the Fourteenth *Symposium on Thermophysical Properties*, June 25-30, 2000, Boulder, CO.
- [15] Wong, W.; Jacobson, S. *MT 484 Synthesis, Catalytic hydrogenation of MR342 to BW 732*, Technology Transfer Report, DuPont Internal Communication Report, Wilmington, DE, 1998.
- [16] International Union of Pure and Applied Chemistry. *Hydrogen and Deuterium*, Solubility Data Series, 5/6, Pergamon Press: New York, 1981.
- [17] Brunner, E. Solubility of Hydrogen in 10 Organic Solvents at 298.15, 323.15, and 373.15 K, *J. Chem. Eng. Data*. **1985**, 30, 269-273.

- [18] Barker, J.; Treybal, R. Mass Transfer Coefficient for Solids Suspended in Agitated Liquid, *AIChE J*, **1960**, *6*, 289-295.
- [19] Ahmed, T.; Semmens, M. Gas Transfer from Small Spherical Bubbles in Natural and Industrial Systems, *J. Env. Syst.* **2002**, *29(2)*, 101-123.
- [20] Griffith, R. Mass Transfer from Drops and Bubbles, *Chem. Eng. Sci.* **1960**, *12*, 198-213.
- [21] Yoshida, F.; Miura, Y. Interfacial, Gas Holdup, Liquid Phase Mass Transfer Coefficient, and Reaction Factor, *Ind. Eng. Chem. Proc. Des. Dev.* **1963**, *2(4)*, 263-268.
- [22] Prasher, B.; Wills, G. Mass Transfer in Agitated Vessel, *Ind. Eng. Chem. Process. Des. Dev.* **1973**, *12 (3)*, 351- 354.
- [23] Davies, J.; Kilmer, A.; Ratcliff, G. The Effect of Diffusivities and Surface Films on Rates of Gas Adsorption, *Chem. Eng. Sci.* **1964**, *19*, 583-590.
- [24] Calderbank, P.; Moo-Young, M. The Continuous Phase Heat and Mass Transfer Properties of Dispersions, *Chem. Eng. Sci.* **1961**, *16*, 39-54.
- [25] Calderbank, P. Physical Rate Process in Industrial Fermentation. Part I: The Interfacial Area in Gas-Liquid Contacting with Mechanical Agitation, *Trans. Instn. Chem. Engrs.* **1958**, *36*, 443-463.
- [26] Calderbank, P. Physical Rate Process in Industrial Fermentation. Part II: Mass Transfer Coefficients in Gas-Liquid Contacting with and without Mechanical Agitation, *Trans. Instn. Chem. Engrs.* **1959**, *37*, 173-189.

- [27] Sridhar, T.; Potter, O. Gas Holdup and Bubble Diameters in Pressurized Gas-Liquid Stirred Vessels, *Ind. Eng. Chem. Fundam.* **1980**, *19*, 21-26.
- [28] Froment, G.; Bischoff, K. *Chemical Reactors Analysis and Design*, Chapter 14, 2nd Edition, John Wiley & Sons: New York, 1990.
- [29] Sano, Y.; Yamagushi, N; Adachi, T. Mass Transfer Coefficient for Suspended Particles in Agitated Vessels and Bubble Columns, *J. Chem. Eng. Japan.* **1974**, *7*, 255.
- [30] Levins, D.; Glastonbury, J. Particle-Liquid Hydrodynamics and Mass Transfer in a Stirred Vessel. Part II: Mass transfer, *Trans. Instn. Chem. Engrs*, **1972**, *50*, 132-146.
- [31] Goto, S.; Saito, T. Liquid-Solid Mass Transfer in Basket Type Three-Phase Reactors, *J. Chem. Eng. Japan*, **1984**, *17*, 324-327.
- [32] Weekman, V. Laboratory Reactors and their Limitations, *AIChE J.* **1974**, *20(5)*, 833-840.
- [33] Shah, Y. *Gas-Liquid-Solid Reactor Design*, Chapter 5, McGraw-Hill: New York, 1979.
- [34] Ramachandran, P.; Chaudhari, R. *Three-phase Catalytic Reactors*, Chapter 12, Gordon and Breach Publishers: New York, 1983.
- [35] Myers, E.; Robinson, K. Multiphase Kinetic Studies with a Spinning Basket Reactor, *ACS Symposium Series.* **1978**, *65*, 447-458.
- [36] Mahoney, J.; Robinson, K.; Myers E. Catalyst Evaluation with Gradientless Reactor, *Chemtech*, **1978**, *8(12)*, 758.

- [37] Mahoney, J. The Use of a Gradientless Reactor in Petroleum Reaction Engineering Studies, *J. Catal.* **1974**, 32, 247-253.
- [38] Carberry, J. Designing Laboratory Catalytic Reactors, *Ind. Eng. Chem*, **1964**, 56, 11.
- [39] Berty, J. *Experiments in Catalytic Reaction Engineering*, Studies in Surface Science and Catalysis, Elsevier: Amsterdam, 124, 1999.
- [40] Mahoney, J. Laboratory Reactors for Mixed Phase Catalytic Studies, Amoco Oil Co., NATO Advanced Study Institutes Series, Series E, *Appl. Sci*, **1981**, 52, 487-513.
- [41] National Association of Corrosion Engineers. *Corrosion Data Survey*, Metals Section, Sixth Edition, NACE publication: Houston, 1985.
- [42] Schweitzer, P. *Corrosion Resistance Tables, Metals, Nonmetals, Coatings, Mortars, Plastics, Elastomers and Linings, and Fabrics*, Fifth edition, Revised and Expanded, Part B, CHR-IOD, Marcel Dekker: New York, 2004.
- [43] Haynes International: <http://www.haynesintl.com/mini/B2s/B2>. Accessed: 08/04.
- [44] Haynes International: <http://www.haynesintl.com/mini/C276s/C276>. Accessed: 08/04.
- [45] Haynes International: <http://www.haynesintl.com/C2000alloy/C2000folder>. Accessed: 08/04.
- [46] Haynes International: <http://www.haynesintl.com/mini/C22s/C22>. Accessed: 08/04.

- [47] Cabot Performance Material: <http://w1.cabot-corp.com>. Accessed: 02/08
- [48] Institution of Chemical Engineer: <http://ed.icheme.org/costmats>. Accessed: 08/04
- [49] Patei, S. *The Chemistry of the Thiol Group, Part I*, Chapter 4, John Wiley & Sons: New York, 1974.
- [50] Davis, F.; Jenkins, L.; Billmers, R. Chemistry of Sulfenic Acids. Reason for the High Reactivity of Sulfenic Acids. Stabilization by Intermolecular Hydrogen Bonding and Electronegativity Effects, *J. Org. Chem.* **1986**, *51*, 1033-1040.
- [51] Benson, S. Thermochemistry and Kinetics of Sulfur-Containing Molecules and Radicals, *Chem. Rev.* **1978**, *78(1)*, 23-35.
- [52] Burkhard, R.; Sellers, D.; DeCou, F.; Lambert, J. The pKa's of Aromatic Sulfinic Acids, *J. Org. Chem.* **1959**, *24(6)*, 767-769.
- [53] Kice, J.; Hampton, D.; Fitzgerald, A. The Effect of Structure on the Rate of Disproportionation of Aromatic Sulfinic Acids, *J. Org. Chem.* **1965**, *30(3)*, 882-885.
- [54] Senning, A. *Sulfur in Organic and Inorganic Chemistry*, Chapter 6, Marcel Dekker: New York, 1971.
- [55] Oae, S. *Organic Sulfur Chemistry: Structure and Mechanism*, Chapter 1, CRC Press: Boca Raton, 1991.
- [56] Pryor, W. *Mechanisms of Sulfur Reaction*, Chapter 3, McGraw-Hill: New York, 1962.

- [57] Jacobson, S.; Cobranchi, D.; Tong, W. *MT484 Process Development, Hydrogenation of MR342 to BW732, Accelerating Rate Calorimeter (ARC) Studies, Heat of Reaction and Reaction Kinetics*, DuPont internal Communication Report, Wilmington, DE, 1998.
- [58] Oudar, J.; Wise, H. Deactivation and Poisoning of Catalysts, *Chemical Industries*, 20, Chapter 3, Marcel Dekker: New York, 1985.
- [59] Hughes, R. *Deactivation of Catalysts*, Chapter 1, Academic Press: Orlando, 1984.
- [60] Bartholomew, C. *Mechanisms of Catalyst Deactivation*, *Appl. Catal. A.* **2001**, *212*, 17-60.
- [61] Radovic, L.; Vannice, A. Sulfur Tolerance of Methanol Synthesis Catalysts: Modelling of Catalyst Deactivation, *Appl. Catal.* **1987**, *29*, 1-20.
- [62] Novakova, E.; McLaughlin, L.; Burch, R.; Crawford, P.; Griffin, K.; Hardacre, C.; Hu, P.; Rooney, D. Palladium-Catalysed Liquid-Phase Hydrogenation/Hydrogenolysis of Disulfides, *J. Catal.* **2007**, *249*, 93-101.
- [63] Taylor, J. Phase Relationships and Thermodynamic Properties of the Pd-S System, *Metall. Mater. Trans B.* **1985**, *16 B*, 143-148.
- [64] Oudar, J.; Wise, H. Deactivation and Poisoning of Catalysts, *Chemical Industries*, 20, Chapter 1, Marcel Dekker: New York, 1985.
- [65] Hoyos, L.; Primet, M.; Praliaud, H. Sulfur Poisoning and Regeneration of Palladium-Based Catalyst Part I.-Dehydrogenation of Cyclohexane on Pd/Al₂O₃ and Pd/SiO₂-Al₂O₃ Catalysts, *J. Chem. Soc. Faraday. Trans.* **1992**, *88(1)*, 113-119.

[66] Holland C. D.; Anthony R. G. *Fundamentals of Chemical Reaction Engineering*, 2nd Edition, Chapter 2, McGraw-Hill: New York, 1989.

[67] Autoclave Engineers, Documentation Catalog, *Reactors-Vessels-Instrumentation & Systems*: Erie, 2004.

[68] International Union of Pure and Applied Chemistry, *Hydrocarbon with Water and Seawater, Part I: Hydrocarbons C₅ to C₇*, Solubility Data Series, 37, Pergamon Press: New York 1989.

[69] Froment, G.; Bischoff, K. *Chemical Reactors Analysis and Design*, Chapter 5, 2nd Edition, John Wiley & Sons: New York, 1990.

[70] Brad Atkinson, A Novel, Green Technology for the Production of Aromatic Thiol from Aromatic Sulfonyl Chloride, Ph D Dissertation, Texas A&M University, College Station, 2008.

[71] Holland C. D.; Anthony R. G. *Fundamentals of Chemical Reaction Engineering*, 2nd Edition, Chapter 1, McGraw-Hill: New York, 1989.

[72] Mathworks: <http://www.mathworks.com> Accessed: 03/08.

[73] Wikipedia, the Free Encyclopedia: http://en.wikipedia.org/wiki/BFGS_method Accessed: 03/08

[74] Froment, G.; Bischoff, K. *Chemical Reactors Analysis and Design*, Chapter 2, 2nd Edition, John Wiley & Sons: New York, 1990.

APPENDIX A

```
Function sulfonyl_2007  
  
p_init = [p_init0(1), p_init0(2),...p_init0(p)] % initial value of the parameters  
  
X0 = [X0(1), X0(2),...X0(j)] % initial value for the concentrations of the reacting species  
  
p_est = fmincon(@obj_fn, p_init) % Sequential quadratic programming with quasi-Newton  
non-linear multi-variable method  
  
p_est = [p_est(1), p_est(2),...p_est(p)] % Estimated value of the parameters after  
minimization of the objective function  
  
end
```

Figure A.1. Structure of *sulfonyl_2007* function to estimate the parameters of the kinetic model

```

Function e = obj_fn (p_var)

p_var = [p_var(1), p_var(2),...p_var(p)]    % Change of the value of the parameters during
                                          % minimization of the objective function

t_span = [t_span(t1), t_span(t2),...t_span(tf)]    % Process time span vector

X_exp(1) = [X_exp(t1), X_exp(t2),...X_exp(tf)]
      ⋮
      ⋮
      ⋮
      ⋮
X_exp(j) = [X_exp(t1), X_exp(t2),...X_exp(tf)]    % Experimental concentrations of
                                                    % reacting species 1 to n from process time
                                                    % t_span(t1) to t_span(tf)

[t, X_model] = ode45(@sul_ode, tspan, X0, p_var)    % Numerical solution of the set ode's defined
                                                    % in sul_ode function with the appropriate
                                                    % kinetic model. ODE 45 includes Runge-Kunta
                                                    % method to solve numerically the set of ODE's

e = (X_exp(1)-X_model(1))^2 + (X_exp(2)-X_model(2))^2    % Objective function defined as the sum
      +...+(X_exp(j)-X_model(j))^2                    % of the square of the residual between
                                                    % experimental data and data obtained from
                                                    % the kinetic model

end

```

Figure A.2. Structure of *obj_fn* function to define the objective function


```

Function X_model = sul_ode(tspan, X0, p_var)

ri =  $\frac{(\text{kinetic constant}) \times (\text{driving - force group})}{(\text{adsorption group})} \times \text{deactivation function}$ 
% Hougen-Watson equation rates derived for each step i of the reaction scheme

 $\frac{dX\_model(1)}{dt} = \dots$ 
 $\vdots$ 
% Unsteady state continuity equations derived for a continuous stirred tank reactor (CSTR) and for each reacting specie 1 to j
 $\frac{dX\_model(j)}{dt} = \dots$ 

% sul_ode returned the data obtained from the kinetic model by solving numerically the set of ODE's for the reacting species 1 to j

end

```

Figure A.3. Structure of *sul_ode* function to solve numerically the set of unsteady state continuity equations for a continuous stirred tank reactor with the appropriate Hougen-Watson equation rates

VITA

Nicolas Julien Rouckout was born in Suresnes, the son of Dany Gerard Rouckout and Daniele Nicole Slezak. He entered Universite Pierre et Marie Curie in September, 1997 and received his Bachelor of Science degree in chemistry in July, 2001. He received from the same University his Master of Science degree in Chemical Engineering in September, 2002. The title of the thesis is: "Modeling of the recombination of atomic oxygen on ceramic and metallic surfaces". He enrolled in the graduate program in the Department of Chemical Engineering at Texas A&M University in January 2003 and started working on his research in January 2004.

Address:

Texas A&M University
Department of Chemical Engineering
TAMU MS 3122
College Station, TX 77843